

UNDERSTANDING CARBON METABOLISM IN HYDROGEN PRODUCTION
BY PNS BACTERIA

A THESIS SUBMITTED TO
THE GRADUATE SCHOOL OF NATURAL AND APPLIED SCIENCES
OF
MIDDLE EAST TECHNICAL UNIVERSITY

BY

EZGİ MELİS DOĞAN

IN PARTIAL FULFILLMENT OF THE REQUIREMENTS
FOR
THE DEGREE OF MASTER OF SCIENCE
IN
CHEMICAL ENGINEERING

AUGUST 2016

Approval of the Thesis;

**UNDERSTANDING CARBON METABOLISM IN HYDROGEN
PRODUCTION BY PNS BACTERIA**

submitted by **EZGİ MELİS DOĞAN** in partial fulfillment of the requirements for
the degree of **Master of Science in Chemical Engineering Department, Middle
East Technical University** by,

Prof. Dr. Gülbin Dural Ünver
Dean, Graduate School of **Natural and Applied Sciences**

Prof. Dr. Halil Kalıpçılar
Head of the Department, **Chemical Engineering**

Asst. Prof. Dr. Harun Koku
Supervisor, **Chemical Engineering Dept., METU**

Examining Committee Members:

Prof. Dr. Ufuk Bölükbaşı
Chemical Engineering Dept., METU

Asst. Prof. Dr. Harun Koku
Chemical Engineering Dept., METU

Assoc. Prof. Dr. Serkan Kıncal
Chemical Engineering Dept., METU

Assoc. Prof. Dr. Demet Çetin
Department of Primary Education, Gazi University

Asst. Prof. Dr. Eda Çelik Akdur
Chemical Engineering Dept., Hacettepe University

Date: 17.08.2016

I hereby declare that all information in this document has been obtained and presented in accordance with academic rules and ethical conduct. I also declare that, as required by these rules and conduct, I have fully cited and referenced all material and results that are not original to this work.

Name, Last name: Ezgi Melis Dođan

Signature :

ABSTRACT

UNDERSTANDING CARBON METABOLISM IN HYDROGEN PRODUCTION BY PNS BACTERIA

Doğan, Ezgi Melis

M.Sc., Chemical Engineering Department

Supervisor: Asst. Prof. Dr. Harun Koku

August 2016, 164 pages

In biological hydrogen production systems using purple non-sulfur bacteria (PNS bacteria), a thorough understanding of the metabolism of these microorganisms plays a vital role in assessing and improving efficiency and productivity. This metabolism is very complex, and the result of the interplay of several systems and components such as the photosystems, carbon flow and enzymatic reactions. Mathematical models are sought to represent the complex metabolism of these bacteria, which in turn can be used to interpret and enhance the phenomenological equations obtained from experiment, and ultimately aid the design of large-scale bioreactors. The aim of this study is to analyze the metabolism of PNS bacteria using contemporary tools and techniques (Flux Balance Analysis), with emphasis on carbon flow. The thesis mainly concerns the modeling of the metabolism of PNS bacteria, focusing on *Rhodospseudomonas palustris* which utilizes sucrose as a carbon source and glutamate

as a nitrogen source in a growth medium with a low N/C ratio. For this purpose, the metabolic model in the present work was verified with the experimental results which were previously performed based on the same conditions considered by the model. Two objective functions, namely, the maximal growth rate of biomass and maximum hydrogen production rate were investigated in particular. The distribution of fluxes in *R. palustris* showed a linear increase in the specific growth rate of biomass with increasing glutamate uptake rate. The biomass growth was found constant when initial sucrose concentration was changed and a strong function of glutamate uptake rate. A decrease in H₂ production was observed at higher photon fluxes and PHB was antagonistically produced to H₂ production. Acetic acid and formic acid were found the most and least effective organic acid for H₂ production, respectively. The distribution of modeled fluxes will help explain the capability of the hydrogen production and growth on sucrose of *R. palustris*.

Keywords: Metabolic Engineering, Purple Non-Sulphur Bacteria, Biological Hydrogen Production, Sucrose, Mathematical Model

ÖZ

MOR KÜKÜRTSÜZ BAKTERİLERİN HİDROJEN ÜRETİMİNDEKİ KARBON METABOLİZMASININ ANLAŞILMASI

Doğan, Ezgi Melis

Yüksek Lisans, Kimya Mühendisliği Bölümü

Tez Yöneticisi : Y. Doç. Dr. Harun Koku

Ağustos 2016, 164 sayfa

Mor kükürtsüz bakterilerle biyolojik hidrojen üretiminin verimi ve üretilebilirliğini artırmak için bu bakterilerin metabolik faaliyetlerini anlamak çok büyük bir öneme sahiptir. Bu metabolizma oldukça karmaşıktır ve birden fazla metabolizma ögesinin ortak faaliyeti sonucu oluşur. Bu ögeler genel olarak fotosistem, karbon akışı ve enzimatik reaksiyonlardan oluşmaktadır. Bu metabolizmayı ve elemanlarını yorumlamak için matematiksel modeller kullanılmaktadır. Matematiksel modeller, deneyler aracılığıyla elde edilen olgusal denklemleri yansıtır ve karmaşık bir metabolizmanın daha basit bir şekilde ifade edilmesini sağlar. Böylelikle büyük ölçekli fotobiyoreaktor tasarımı süreçleri kolaylaştırılabilir. Bu tezin asıl amacı çağdaş yöntemler ve teknikler kullanarak ve karbon akışına odaklanarak, mor kükürtsüz bakterilerin metabolizmalarını analiz etmektir. Bu tez genel olarak mor kükürtsüz bakterilerden *Rhodopseudomonas palustris* bakteri türü üzerine

odaklanarak bir metabolizma modeli ortaya çıkarmayı hedeflemektedir. Karbon kaynağı olarak sukroz ve azot kaynağı olarak glutamat esas alınmıştır. Bakteri koşulları için ortamda bulunan karbon miktarının nitrojen miktarına oranı düşük kabul edilmiştir. Bu nedenle, bu araştırma konusu daha önce model için ifade edilen koşullarda sukroz ile yapılan deney sonuçları ile test edilerek, sonuçları yorumlamak amacıyla metabolik akı analizinin uygulanmasını içerir. Metabolik akı analizi, bakterinin maksimum büyüme hızı ve maksimum hidrojen üretme hızı olmak üzere, iki farklı amaç fonksiyonunu incelemektedir. *R. palustris* in elde edilen akı dağılımından, bakteri büyüme hızının glutamat alım hızına paralel bir şekilde değiştiği gözlemlenmiştir. Ortamdaki sukroz konsantrasyonu değiştirildiğinde, bakteri büyüme hızı değişiklik göstermemiştir. Yüksek foton akılarında, hidrojen üretim hızında azalma, PHB üretim hızında artma görülmüştür. Asetik asit ve formik asit, sırasıyla, hidrojen üretimini artırmak için en çok ve en az etkili organik asitler olarak belirlenmiştir. Yapılan metabolik akı analizinin sonuçları olarak elde edilen akı dağılımı, *R. palustris*'in sukroz ile hidrojen üretim kapasitesini çalışmak için kullanılabilir.

Anahtar Kelimeler: Metabolizma Mühendisliği, Mor Kükürtsüz Bakteriler, Biyolojik Hidrojen Üretimi, Sukroz, Matematik Model

To my family,

ACKNOWLEDGEMENTS

I would like to thank sincerely to my supervisor Asst. Prof. Dr. Harun Koku and I would like to express my gratitude to Prof. Dr. İnci Erođlu for their guidance, support, suggestions and more importantly, motivation throughout this study.

I would like to give my special thanks to Prof. Dr. Meral Yücel and Prof. Dr. Ufuk Gündüz for their valuable ideas, aids and support.

I am thankful to Emrah Sađır who provided experimental data used in the evaluation of this present work. I also thank to Muazzez Gürgan from Biology department for her advices in this study.

I am grateful deeply to my fiancé, Feyyaz Güner who gave motivation and encouragement to me during my thesis with his endless support and love.

Lastly, I sincerely thank all members of my family, especially my parents for their encouragement, support and love throughout my thesis.

This study was supported by the Scientific and Technological Research Council of Turkey (TUBITAK) as project numbered '114M436'.

TABLE OF CONTENTS

ABSTRACT.....	v
ÖZ.....	vii
ACKNOWLEDGEMENTS.....	x
TABLE OF CONTENTS.....	xi
LIST OF TABLES	xiv
LIST OF FIGURES	xvi
LIST OF ABBREVIATIONS	xix
CHAPTERS	
1. INTRODUCTION.....	1
1.1 Hydrogen Production Techniques.....	2
1.2 Techniques of Bio-hydrogen Production.....	5
1.2.1 Bio-photolysis.....	6
1.2.2 Dark Fermentation.....	6
1.2.3 Photo Fermentation.....	7
1.2.4 Integrated systems.....	8
1.3 The Role of Metabolic Engineering for Hydrogen Production.....	9
1.4 Objective and Scope.....	10
2. LITERATURE SURVEY.....	13
2.1 Characteristics of Purple Non-Sulfur Bacteria.....	13
2.2 Overview of the Metabolism in Hydrogen Production by PNS Bacteria.....	16
2.2.1 Carbon Flow.....	18
2.2.2 Enzyme Systems.....	20
2.2.3 Photosynthetic Unit.....	24
2.3 Sucrose Metabolism in PNS Bacteria.....	27
2.4 Metabolic Modeling and its Application to PNS Bacteria.....	31

3. METHODOLOGY.....	35
3.1 Metabolic Flux Analysis.....	35
3.2 Classification of Metabolic Flux Analysis.....	37
3.2.1 Flux Balance Analysis.....	38
3.2.2 Fluxomics.....	40
3.3 Construction of the Metabolic Network.....	41
3.4 Construction of the Metabolic Model.....	43
3.4.1 Mass Balance and Stoichiometric Reduction.....	45
3.4.2 Steady State Assumption.....	48
3.4.3 Optimization in Linear Programming.....	50
3.4.3.1 Objective Functions and Constraints.....	50
3.4.3.2 Optimization Algorithm.....	52
3.5 Overall Modeling Procedure.....	54
4. RESULTS AND DISCUSSION.....	57
4.1 Verification of the Simulation Script.....	57
4.2 Metabolic Network.....	61
4.3 Descriptions of cases and Results for the Base Case.....	65
4.3.1 Inputs and List of Cases.....	65
4.3.2 Base Case Results.....	68
4.3.3 Sensitivity Analysis.....	75
4.4 Comparison with Experimental Results.....	77
4.5 Effect of Individual Parameters.....	80
4.5.1 Initial Glutamate Uptake Rate.....	80
4.5.2 Initial Sucrose Concentration.....	87
4.5.3 Effect of Illumination.....	92
4.5.4 Organic Acids in the Growth Media.....	99
4.6 Applicability of the Model.....	100
5. CONCLUSIONS.....	101
REFERENCES	105
APPENDICES	

A. TEST CASE.....	113
A.1 Test Case Details.....	113
A.2 Matlab Script for the Test Case.....	117
B. COMPONENTS OF THE METABOLIC NETWORK.....	119
B.1 List of Metabolites.....	119
B.2 List of Enzymes.....	123
B.3 List of Reactions with their Enzymes.....	125
C. PART OF THE STOICHIOMETRIC MATRIX	135
D. GROWTH REACTION COEFFICIENTS OF <i>R. palustris</i>	137
E. SAMPLE CALCULATIONS	139
E.1 Calculation of Initial Sucrose Flux.....	139
E.2 Calculation of Initial Glutamate Flux.....	139
E.3 Calculation of Photon Flux.....	140
E.4 Calculation of Sucrose Conversion Efficiency.....	141
F. MATLAB SCRIPTS.....	143
F.1 Objective Function: Maximum Biomass Growth Rate.....	143
F.2 Objective Function: Maximum Hydrogen Production Rate.....	146
G. FLUX DISTRIBUTIONS.....	149
H. TABULATED RAW DATA OF THE PLOTS.....	159

LIST OF TABLES

TABLES

Table 2.1: Comparison of individually expressed nitrogenase types and resulted H ₂ productivity <i>in vivo</i> (Oda <i>et al.</i> , 2015).....	21
Table 2.2: Comparison of enzymes responsible for H ₂ production in PNSB.....	23
Table 4.1: Comparison of flux distribution of test case to published data.....	58
Table 4.2: Control parameters of stoichiometric model.....	66
Table 4.3: List of model cases.....	67
Table 4.4: The resulting fluxes of all reactions in the metabolic network (Obj 1: Maximization of biomass growth, Obj 2: Maximization of hydrogen production).....	70
Table 4.5: Photosynthetic reactions and their resultant fluxes.....	73
Table 4.6: Reactions for hydrogen production with their resulted fluxes.....	74
Table 4.7: Results of sensitivity analysis based on slight changes in initial glutamate uptake rate.....	76
Table 4.8: Experimental and computed output parameters for the base case.....	78
Table 4.9: Individual effects of organic acids on H ₂ production.....	99
Table A.1: Definitions of enzymes used in the test case with the related reaction number.....	113
Table A.2: List of metabolites used in reactions of the test case.....	115
Table A.3: Coefficients of metabolites in the objective function used in the test case (Table A.2 can be referred for definitions of the metabolite abbreviations).....	116
Table B.1: Definitions of enzymes used in the construction of the metabolic network of <i>R. palustris</i>	123
Table B.2: Definitions of the reactions on the metabolic network.....	126

Table C.1: Partly tabulated form of the stoichiometric matrix.....	135
Table D.1: Coefficients of biomass growth reaction (148 th reaction) per g dry cell weight (Appendix B1 can be referred for abbreviations of the metabolites).....	137
Table G.1: Flux distribution of different cases for the objective function of maximum biomass growth rate.....	149
Table G.2: Flux distribution of different cases for the objective function of maximum hydrogen production rate.....	154
Table H.1: Effect of initial glutamate flux in the case of maximum biomass growth rate (Raw data of Figure 4.3-4.8)	159
Table H.2: Effect of initial glutamate flux in the case of maximum hydrogen production rate (Raw data of Figure 4.3-4.8)	160
Table H.3: Effect of initial sucrose flux in the case of maximum biomass growth rate (Raw data of Figure 4.9-4.13).....	161
Table H.4: Effect of initial sucrose flux in the case of maximum hydrogen production rate (Raw data of Figure 4.9-4.13)	162
Table H.5: Effect of photon flux in the case of maximum biomass growth rate (Raw data of Figure 4.14-4.19).....	163
Table H.6: Effect of photon flux in the case of maximum hydrogen production rate (Raw data of Figure 4.14-4.19).....	164

LIST OF FIGURES

FIGURES

Figure 2.1: Overview of growth modes for PNSB (Larimer <i>et al.</i> , 2004).....	14
Figure 2.2: The overall scheme for hydrogen production (Koku <i>et al.</i> , 2002).....	17
Figure 2.3: Simplified overall scheme of carbon flow in PNSB.....	19
Figure 2.4: Processes for components of photosynthetic unit in PNSB; solid arrows: electron flow, dotted arrows: proton (hydrogen ion, H ⁺) flow (Klamt <i>et al.</i> , 2008)....	24
Figure 2.5: Pathway map of sucrose and starch metabolism in <i>R. palustris</i> (Kanehisa <i>et al.</i> , 2015).....	29
Figure 3.1: Annual number of publications involving MFA with respect to years; a. general trend, b. distribution of organism studied for MFA (Crown <i>et al.</i> , 2013).....	36
Figure 3.2: Example of a metabolic map; Fluxes distributed over different metabolic pathways (Stephanopoulos <i>et al.</i> , 1998).....	38
Figure 3.3: Geometric representation of; a. all possible solutions before limitations, b. a specific solution space considering flux limitations (Tanis, 2006).....	39
Figure 3.4: General representation of a metabolic network (Tanis, 2006).....	42
Figure 3.5: A general scheme for Flux Balance Analysis (Orth <i>et al.</i> , 2010).....	44
Figure 3.6: a. Simple reaction network to form mass balance, b. An example of a set of mass balance equations.....	45
Figure 3.7: Example representation for linear combination of pathways.....	47
Figure 3.8: Graphical analysis of the iteration approach; a. Simplex method b. Interior point method (Hillier <i>et al.</i> , 2001).....	53
Figure 3.9: Schematic representation of modeling procedure.....	55
Figure 4.1: Graphical comparison between test fluxes and published fluxes.....	59

Figure 4.2: Linear optimization results for the test case using network of <i>E. coli</i> aerobic respiration (Varma and Palsson, 1992); partially dashed arrows represent reversible reactions, with the solid portion of the arrow indicating the direction of the calculated flux.....	60
Figure 4.3: Central carbon flow in <i>R. palustris</i> for growth on sucrose (A:Sucrose pathway, B:Glycolysis, C:Penrose phosphate pathway, D: Calvin cycle, E: TCA cycle, F: PHB synthesis).....	63
Figure 4.4: Specific growth rate of biomass as a function of glutamate uptake rate for two objective functions (● : Maximum biomass growth, ◇ : Maximum hydrogen production).....	81
Figure 4.5: Sucrose uptake rate of biomass as a function of glutamate uptake rate for two objective functions (● : Maximum biomass growth, ◇ : Maximum hydrogen production).....	82
Figure 4.6: Hydrogen production rate as a function of glutamate uptake rate for two objective functions (● : Maximum biomass growth, ◇ : Maximum hydrogen production).....	82
Figure 4.7: PHB production rate as a function of glutamate uptake rate for two objective functions (● : Maximum biomass growth, ◇ : Maximum hydrogen production).....	84
Figure 4.8: CO ₂ production rate as a function of glutamate uptake rate for two objective functions (● : Maximum biomass growth, ◇ : Maximum hydrogen production).....	84
Figure 4.9: Organic acid production rates as a function of glutamate uptake rate for two objective functions (● : Maximum biomass growth, ◇ : Maximum hydrogen production).....	86
Figure 4.10: Specific growth rate (a) and Sucrose uptake rate (b) as a function of initial sucrose concentration for two objective functions (● : Maximum biomass growth, ◇ : Maximum hydrogen production).....	88

Figure 4.11: H₂ production rate as a function of initial sucrose concentration for two objective functions (● : Maximum biomass growth, ◇ : Maximum hydrogen production).....89

Figure 4.12: PHB production rate as a function of initial sucrose concentration for two objective functions (● : Maximum biomass growth, ◇ : Maximum hydrogen production).....89

Figure 4.13: CO₂ production rate as a function of initial sucrose concentration for two objective functions (● : Maximum biomass growth, ◇ : Maximum hydrogen production).....90

Figure 4.14: Production rate of acetic acid (a), lactic acid (b) and formic acid (c) as a function of initial sucrose concentration for two objective functions (● : Maximum biomass growth, ◇ : Maximum hydrogen production).....91

Figure 4.15: Specific growth rate as a function of photon flux for two objective functions (● : Maximum biomass growth, ◇ : Maximum hydrogen production)..93

Figure 4.16: Sucrose uptake rate as a function of photon flux for two objective functions (● : Maximum biomass growth, ◇ : Maximum hydrogen production)..93

Figure 4.17: H₂ production rate as a function of photon flux for two objective functions (● : Maximum biomass growth, ◇ : Maximum hydrogen production)..94

Figure 4.18: PHB production rate as a function of photon flux for two objective functions (● : Maximum biomass growth, ◇ : Maximum hydrogen production)..95

Figure 4.19: CO₂ production rate as a function of photon flux for two objective functions (● : Maximum biomass growth, ◇ : Maximum hydrogen production)..96

Figure 4.20: Organic acid production rates as a function of photon flux.....97

LIST OF SYMBOLS AND ABBREVIATIONS

Acetyl-CoA	Acetyl Coenzyme A
CoA	Coenzyme A
ADP	Adenosine diphosphate
ATP	Adenosine triphosphate
C	Carbon
gdcw	Gram dry cell weight of bacteria
H ₂	Hydrogen
h	hours
l	liter
mM	millimolar
mmol	millimole
N ₂	Nitrogen
NAD	Nicotineamid Adenine Dinucleotide
FAD	Flavin Adenine Dinucleotide
PBR	Photobioreactor
PHB	Poly-β- hydroxybutyrate
P _i	Inorganic Phosphate
PNS	Purple Non-Sulphur
PNSB	Purple Non-Sulphur Bacteria
TCA	Tricarboxylic acid
EMCoA	Ethylmanoyl-CoA
CM	Citramalate cycle
RC	Reaction Center
PSU	Photosynthetic unit
bchl	Bacteriochlorophyll
Fd	Ferredoxins

c ₂	Cytochrome c ₂ complex
bc ₁	Cytochrome bc ₁ complex
Q	Ubiquinone
QH ₂	Ubiquinol
LHC	Light Harvesting Complexes
e ⁻	Electrons
H _i ⁺	Intracytoplasmic protons
H _p ⁺	Periplasmic proton
MFA	Metabolic Flux Analysis
FBA	Flux Balance Analysis
CFA	Carbon Flux Analysis
CPF	Corner Point Feasible
S	Stoichiometric matrix
v	Unknown flux vector
Obj 1	Maximum biomass growth rate
Obj 2	Maximum hydrogen production rate
<i>R. capsulatus</i>	<i>Rhodobacter capsulatus</i>
<i>R. palustris</i>	<i>Rhodospseudomonas palustris</i>
<i>R. sphaeroides</i>	<i>Rhodobacter sphaeroid</i>

CHAPTER 1

INTRODUCTION

Energy consumption has been dramatically rising because of increasing world population and rapid urbanization. In the project of International Energy Outlook 2016, The U.S. Energy Information Administration estimated a 48% increase in the world energy consumption between 2012 and 2040 (Doman *et al.*, 2016). Almost all of the current consumption depends on fossil fuels which are sources of non-renewable energy in limited reserves. In addition, the use of fossil fuels is not environmentally friendly because of pollutant greenhouse gas emissions resulting from combustion of these fuels (Das & Veziroglu, 2001). To overcome this problem, researchers have been attempting to find renewable energy sources that can be substituted for fossil fuels. Hydrogen (H₂) is one of the best prospective renewable energy sources as a future energy carrier. Its energy content (122 kJ/g) is 2.4, 2.8 and 4 times as high as the content of methane, gasoline and coal, respectively (Argun *et al.*, 2008 & Marbán *et al.*, 2007). Moreover, hydrogen only evolves water instead of greenhouse gases in combustion. Therefore, hydrogen is a clean, sustainable and environmentally friendly fuel for energy demand in the future (Kotay *et al.*, 2008). Although studies that focus on hydrogen as a potential resource to address the problem of rising energy demand are relatively recent, its production is already available for industrial uses such as oil refining, metal treatment, ammonia production, and hydrogenation in food production. The annual hydrogen production in the US is approximately 10-11 million metric tons (Energy Information Administration, 2008). Hydrogen can be obtained from various sources, from fossil fuels as well as renewable sources such as water and biomass.

Furthermore, it can be obtained as a secondary energy source via conversion processes involving renewable energy sources such as solar, wind and thermal energy. Biological hydrogen production from microorganism (biomass) has been considered as one of the most promising methods for future energy requirement because it has low cost and low energy consumption (operation at ambient conditions) resulting long term production (Azwar *et al.*, 2013). The following sections of this chapter will briefly explain various hydrogen production techniques and then, focus on techniques of bio-hydrogen production.

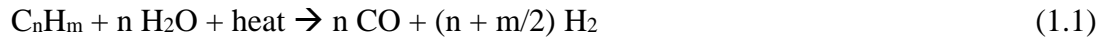
1.1 Hydrogen Production Techniques

A variety of techniques using fossil fuels (natural gas and coal) or renewable sources (biomass, water, sunlight and wind) is available in literature for hydrogen production. These techniques are mainly natural gas reforming, gasification of coal, splitting of water and thermochemical /biological processing of biomass. Hydrogen is currently produced industrially from natural gas (40%), oil (30%), coal (18%) and water electrolysis (4%) (Brentner *et al.*, 2010). Electrolysis of water was the first commercial technique used to obtain pure hydrogen. Fossil fuel-based hydrogen production has become the most commonly used production method in the industry since 1960s (Riis *et al.*, 2006).

Natural gas reforming

Steam reforming, partial oxidation and auto-thermal reforming are three different chemical processes used to produce hydrogen from natural gas. Approximately 90% of the hydrogen in the world is obtained via steam reforming of natural gas (Haryanto *et al.*, 2005). In a typical steam reforming process, hydrogen and carbon monoxide are obtained via endothermic reaction of natural gas and water vapor at pressures of 3-25 bar and temperatures of 700- 850 °C.

To eliminate the resulting carbon monoxide in the product gas (approximately 12%), the water-gas shift reaction is carried out (Riis *et al.*, 2006). Equations (1.1) and (1.2) show steam reforming and water gas shift reactions, respectively.



In partial oxidation of natural gas, hydrogen and carbon monoxide are yielded by the partial combustion of natural gas with oxygen gas in an exothermic reaction as shown in Equation (1.3). (Riis *et al.*, 2006).



Auto-thermal reforming can be defined as a combination of reactions in steam reforming (1.1) and partial oxidation (1.3). It has an exothermic reaction releasing gas at temperatures of 950 - 1100 °C (Riis *et al.*, 2006).

Gasification of coal

A typical reactor in gasification of coal converts carbon to hydrogen and carbon monoxide in an endothermic reaction as seen in Equation (1.4). Similar to the water gas shift reaction in the end of steam reforming, carbon monoxide can be converted to hydrogen and carbon dioxide with the same reaction (1.2) in this process (Riis *et al.*, 2006).



Splitting of water

As shown in Equation (1.5), electrical energy is used to split water into hydrogen and oxygen in an electrolyzer device. Alkaline with potassium hydroxide electrolyte and PEM (polymer electrolyte membrane) are two common types of electrolyzers utilized in splitting of water (Limpan, 2011).

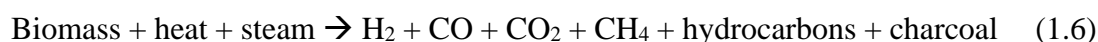
The electrical energy required for water electrolysis decreases with increasing temperature, but the total energy required increases. Therefore, using waste heat released by other processes is important to save the energy. However, water electrolysis is a process that is approximately 25% efficient, based on the comparison in energy content of the required electricity to electrolyze water and the energy content of the produced hydrogen (Miller *et al.*, 2004). Future costs of hydrogen obtained via water electrolysis should be investigated because of dependency on the use of electricity. Therefore, low-cost electricity should be available for this technique to compete with other commercial hydrogen production methods.



Thermochemical and biological process of biomass

Hydrogen can be obtained using biomass in either thermochemical or biological processes. For thermochemical production of hydrogen from biomass, gasification and pyrolysis are the most promising methods to commercialize this technique of hydrogen production. Pyrolysis or gasification is a process converting biomass into hydrogen into other gaseous compounds (depending on the biomass used) with charcoal and liquid oils in the absence of air. Its range of operation pressures is 0.1-0.5 MPa at temperatures of 650-800 K (Ni *et al.*, 2005).

However, the aim of the gasification process is to obtain gaseous products whereas pyrolysis is carried out to produce charcoal and liquid oils. Overall reactions of gasification and pyrolysis are shown in equation (1.6) and (1.7), respectively. Steam reforming can be applied to product gases to obtain further hydrogen (Ni *et al.*, 2005).



Biological hydrogen production from biomass mainly involves enzyme-based processes. Two enzymes in particular, nitrogenase and hydrogenase, have the ability to produce hydrogen in microorganisms such as algae, cyanobacteria and photosynthetic bacteria. Bio-hydrogen production seems as a potential alternative to the commercially used techniques of hydrogen production. It requires less energy due to operation at ambient conditions (Azwar *et al.*, 2013). To explain further, the next section will summarize the techniques of bio-hydrogen production.

1.2 Techniques of Bio-hydrogen Production

Bio-hydrogen can be obtained in a variety of processes including biophotolysis using algae and cyanobacteria, dark fermentation with fermentative bacteria, photo fermentation by photosynthetic bacteria and integrated systems using both photosynthetic and fermentative bacteria (Das *et al.*, 2001). In bio-hydrogen production systems, parameters such as substrate conversion efficiency, hydrogen productivity and light conversion efficiency are defined to evaluate and compare different processes.

Substrate conversion efficiency is the ratio of mole of theoretical hydrogen production on the substrate to the mole of experimental hydrogen production.

Hydrogen productivity represents the rate of hydrogen production defined as the concentration of the produced hydrogen per unit time at the end of the process.

Light conversion efficiency is the energy content of produced hydrogen divided by the total energy content directed to the photo bioreactor from a light source.

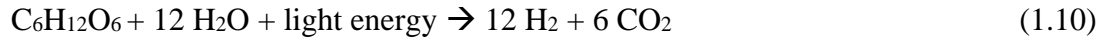
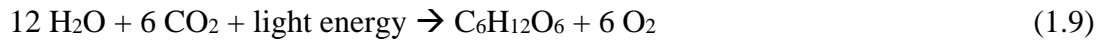
In the following subsections, four different techniques of bio hydrogen production are summarized.

1.2.1 Biophotolysis

Green algae and cyanobacteria are utilized in anaerobic conditions to produce hydrogen via biophotolysis. Sunlight is directly converted into stored chemical energy (H₂) using water via equation (1.8) which is the reaction of direct photolysis (Levin *et al.*, 2004).



The main challenge for direct biophotolysis is the sensitivity of hydrogenase in cyanobacteria and green micro algae to oxygen (Hallenbeck *et al.*, 2009). Therefore, the amount of oxygen should be maintained below 0.1 % to obtain maximum hydrogen yield (Hallenbeck *et al.*, 2002). On the other hand, hydrogen can also be produced by photosynthesis of cyanobacteria or algae capable of utilizing CO₂ as carbon source (Levin *et al.*, 2004). This process is called indirect biophotolysis. The reactions of cyanobacteria/algae producing hydrogen through photosynthesis are shown by equation (1.9) and (1.10).



1.2.2 Dark Fermentation

Dark fermentation is performed by fermentative bacteria at heterotrophic growth. In this process, bio-hydrogen is produced with conversion of organic substrates without presence of light (Shin *et al.*, 2004). Carbohydrates are the most commonly used substrates for dark fermentation (Levin *et al.*, 2004). However, low yields were observed in the process of dark fermentation resulting in hydrogen with low purity (Hallenbeck, 2014).

In addition, it is difficult to control the pH level of hydrogen production media, organic acid productions and nutrition feed rate. Especially, the pH is an important factor for the hydrogen production (Venkata *et al.*, 2007). Short-chain organic acids are obtained as a result of incomplete utilization of organic substrates. These organic acids can be converted to hydrogen and CO₂ using photo-heterotrophic bacteria. This brings the idea of using combinations of dark and photo fermentations to obtain high yield of hydrogen (Kapdan *et al.*, 2006).

1.2.3 Photofermentation

Purple non-sulfur bacteria (PNSB) in photoheterotrophic growth can evolve hydrogen using their hydrogen-producing enzymes (nitrogenase and hydrogenase). For hydrogen production in their metabolism, organic substances are reduced using light energy in a nitrogen-limited environment (Levin *et al.*, 2004).

When photoheterotrophic bacteria are compared with cyanobacteria and green algae, they are accepted as the more promising hydrogen producers (Zhang *et al.*, 2015). More detailed information about the characteristics of purple non-sulfur bacteria and their metabolism for hydrogen production will be given in Chapter 2. Although organic acids obtained from the end products of dark fermentation can be utilized to produce hydrogen by photoheterotrophic bacteria, the volume of hydrogen production is not still high enough (Azwar *et al.*, 2013). Therefore, integration of dark and photo fermentation systems has been suggested to achieve the highest hydrogen yield close to theoretical one (Tao *et al.*, 2007).

1.2.4 Integrated Systems

An integrated system sequentially combines the processes of dark and photo fermentation in two stages to enhance the hydrogen production yields. Nearly complete conversion of organic substrates to hydrogen is aimed in the integrated systems. Dark fermentation effluent including short chain organic acids (acetate, lactate, formate, propionate, etc.) is used by photosynthetic bacteria to produce additional hydrogen in photo fermenter as the second stage (Azwar *et al.*, 2013).

However, the major drawback of these systems is the difficulty of their operation and optimization because of the different natures of two microorganisms used in a sequential system. To obtain a non-inhibitory substrate for the second stage, a substantial treatment might have to be applied to the effluent of dark fermentation. Therefore, complex and costly design of bioreactor systems can be required for integrated systems (Hallenbeck *et al.*, 2015). A recent study in which such a system has been designed is the Hyvolution project performed for the EU 6th Framework Program (2006 – 2010). This project used thermophilic bacteria in the dark stage and photofermentative bacteria in the second (photo) stage to produce more hydrogen.

Moving bed and trickling bed reactors were combined to optimize the dark fermentation stage whereas a bioreactor with low density polyethylene tubes and a flat panel reactor having transparent plastic walls was used for the photo fermentation stage (Urbaniec & Grabarczyk, 2014; Boran *et al.*, 2012a).

In addition to integrated systems, metabolic engineering can be applied to obtain higher yields of hydrogen in the light of results obtained from metabolic modeling. As is the objective of the present work, metabolic modeling can provide to understand the metabolism of the bacteria (Hallenbeck *et al.*, 2015).

1.3 The Role of Metabolic Engineering for Hydrogen Production

Metabolic engineering is a multi-disciplinary field which aims to design and implement favorable manipulation of cellular properties in metabolism of an organism. Genetic engineering, molecular genetics, biochemistry and bioinformatics are the roots of this field (Koffas *et al.*, 1999). Metabolic engineering can be applied for a variety of purposes such as modifying cell properties, enhancing production of chemicals naturally obtained from the host organism, improving the capacity of substrate utilization, providing novel catabolic activities degrading toxic compounds and obtaining novel compounds from the host organism (Cameron *et al.*, 1993).

Examples of metabolic engineering are available in biological hydrogen production systems. To improve hydrogen yields, various strategies such as the overexpression of hydrogen producing genes, elimination of competitive pathways and implementation of new hydrogen production pathways have been employed (Goyal *et al.*, 2013). Furthermore, metabolic engineering has a potential to redirect and optimize electron flow towards hydrogen production.

Photosynthetic bacteria, algae and cyanobacteria are targeted microorganisms for metabolic engineering in photosynthetic bio-hydrogen production (Sparling *et al.*, 2012). Purple non-sulfur bacteria have higher conversion efficiency of substrate to H₂ compared to other photosynthetic bacteria (Basak *et al.*, 2007) and hence, they are powerful candidates for metabolic engineering among other photosynthetic bacteria. Oh *et al.* (2011) summarized various metabolic engineering studies on purple non-sulfur bacteria for better bio-hydrogen production. The genes of nitrogenase and hydrogenase have been engineered, in particular (Ozturk *et al.*, 2006).

Genome scale metabolic models are predictive tools used for metabolic engineering applications. The main objective of using these metabolic models is to examine the effects of modifications via metabolic engineering on the host organism.

The potential pathway for metabolic engineering can be predicted based on the model results. Additionally, the reaction network of the organism can be analyzed to calculate the maximum theoretical efficiency of a new pathway (Durot *et al.*, 2009).

1.4 Objective and Scope

The objective of this work was to investigate carbon utilization patterns in purple non-sulfur bacteria (PNSB) by formulating a metabolic framework. A thorough understanding of the complex metabolism of PNSB plays a vital role in assessing and improving efficiency and productivity of hydrogen production. The carbon metabolism of PNSB was modeled and the results were investigated, specifically focusing on the species *Rhodospseudomonas palustris*. This species of PNSB was selected as a model bacteria for two reasons: First, *R. palustris* was experimentally observed to result in maximum hydrogen productivity from sucrose compared to the other PNS species *Rhodobacter capsulatus*, *Rhodobacter capsulatus* YO3 (hup-) and *Rhodobacter sphaeroides* (Sagir, 2012). Second, the full genome sequence of *R. palustris* was first released in 2004.

In the present study, sucrose and glutamate were considered as the carbon and nitrogen sources, respectively, to emulate typical conditions for hydrogen production. Flux Balance Analysis (FBA) was implemented as a practical tool to study the network of biochemical reactions. This metabolic model consists of 148 reconstructed biochemical reactions with 128 compounds within the reaction network from substrate to product. Pseudo steady-state was assumed for the entire reaction network and the fluxes were assumed to depend on maximal growth of biomass or maximum hydrogen production as the objective functions. Therefore, an optimal solution for each objective function was obtained.

The flux distribution obtained in this model will help explain the capability of the hydrogen production on sucrose by *Rhodospseudomonas palustris* as well as the effects of changes in the growth conditions of the bacteria on biomass production and hydrogen production, in particular.

Understanding carbon metabolism of PNSB on sucrose plays a major role in metabolic engineering studies pursued to enhance hydrogen production from photosynthetic bacteria. In addition, sucrose is a cheap feedstock compared to other organic substrates and wastes from sugar industry contains high amounts of sucrose, resulting a lower cost process for hydrogen production (Keskin *et al.*, 2012). To the best of our knowledge, until now no one has attempted to model metabolic network of PNSB to understand their carbon utilization patterns on sucrose.

The rest of this manuscript is organized as follows: in the next chapter (Chapter 2), characteristics of purple non-sulfur bacteria and their metabolism in hydrogen production are explained in detail. The functions of carbon flow, enzyme systems and photosynthetic unit of PNSB during hydrogen production are clarified. The sucrose metabolism of PNSB is also mentioned. In addition, metabolic modeling is defined and its application to PNS bacteria in literature is reviewed.

Chapter 3 describes the methodology followed for the metabolic modeling in the present work. The objective of metabolic flux analysis as a mathematical tool used in this study is covered and the application of this mathematical framework is described. Important aspects in the construction of this model, namely, mass balances, stoichiometric reductions, the pseudo steady-state assumption, optimization in linear programming, objective functions and constraints used in the study and optimization algorithm are explained in detail. Lastly, the overall modeling procedure is presented to conclude the chapter.

In chapter 4, which presents the results, first metabolic parameters are defined and the verification of simulation script is shown. Then, the verification and simulation results of the model is presented and discussed. Model results are compared with experimental data previously obtained in other studies. The resulting metabolic flux network is evaluated in detail. Furthermore, the effect of various environmental growth conditions such as glutamate uptake rate, initial sucrose concentration, illumination and organic acids on the control parameters of the model is evaluated and discussed.

The final chapter (Chapter 5) summarizes the main conclusions and offers further recommendations.

CHAPTER 2

LITERATURE SURVEY

2.1 Characteristics of Purple Non-Sulphur Bacteria

Purple Non-Sulfur Bacteria (PNSB) are an important group of photosynthetic organisms enriched in an anaerobic or facultative environment (Madigan *et al.*, 2009). PNSB are named as ‘non-sulfur’ because they do not consume hydrogen sulfide as an electron donor. Moreover, purple to deep red pigments are observed when PNSB are present in facultative anaerobic conditions rather than aerobic conditions (Basak *et al.*, 2007). Their optimum pH and temperature range are 6-9 and 25-35°C, respectively (Sasikala *et al.*, 1991).

PNSB are capable of growing as photo-heterotrophs, photoautotrophs or chemoheterotrophs depending on the presence of light, oxygen, and organic or inorganic sources of carbon. Inorganic compounds (CO₂) are used in autotrophic growth and organic compounds are used in heterotrophic growth. Figure 2.1 (Larimer *et al.*, 2004) summarizes the modes by which PNSB are able to grow. It shows that PNSB are metabolically versatile organisms because they have a metabolism supporting photoautotrophic (energy from light and carbon from carbon dioxide), photoheterotrophic (energy from light and carbon from organic compounds), chemoheterotrophic (carbon and energy from organic compounds) and chemoautotrophic (energy from inorganic compounds and carbon from carbon dioxide) growth modes.

In an anaerobic environment, photosynthesis occurs by PNSB using energy from light whereas chemosynthesis takes place with energy from organic or inorganic compounds. Hydrogen production is favorable under anaerobic conditions where no oxygen exists. Hydrogen-producing enzymes (hydrogenase and nitrogenase) become active in the bacterial membrane in the absence of oxygen.

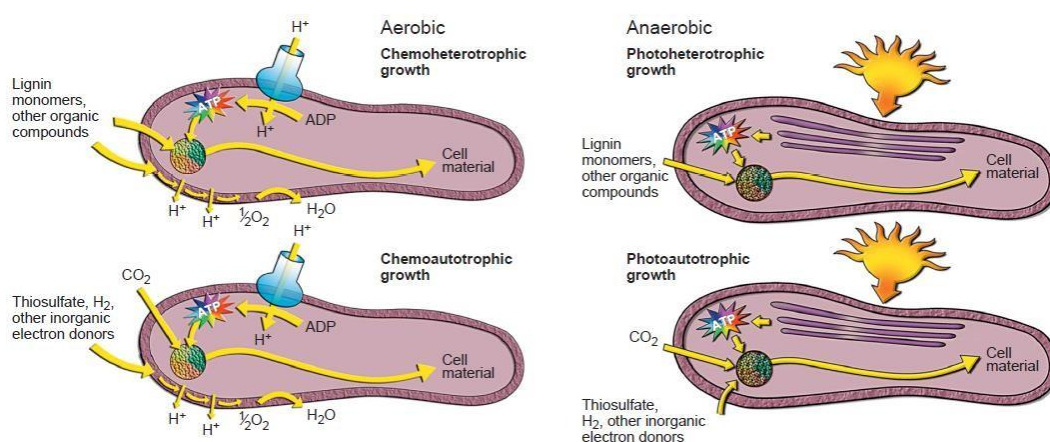


Figure 2.1: Overview of growth modes for PNSB (Larimer *et al.*, 2004)

PNSB are promising candidates for biological hydrogen production compared to algae and cyanobacteria (Basak *et al.*, 2007). For example, the energy desired for hydrogen production by PNSB with complete decomposition of organic compounds has been compared to the energy required for water splitting by algae and PNSB were found to require much less energy. This is because they have high efficiency to convert organic compounds (carbon source) to hydrogen. PNSB have the ability to utilize organic substrates (sugars and short chain organic acids) typically found in agricultural and industrial wastes for hydrogen production (Eroglu *et al.*, 2014).

In addition, a large portion of the solar spectrum can be utilized by PNSB to obtain energy (Basak *et al.*, 2007). PNSB includes various species such as *Rhodobacter capsulatus*, *Rhodobacter sulfidophilus*, *Rhodobacter sphaeroides*, *Rhodopseudomonas palustris*, *Rhodospirillum rubrum*, all capable of producing hydrogen using energy from a light source. The model species of the present work is *Rhodopseudomonas palustris* because good yields of hydrogen were obtained in the photoheterotrophic growth mode of bacteria on cheap sugar substrates (Sagir, 2012, Zhang *et al.*, 2015). In addition, the genome sequence of *R. palustris* was made available in 2004 as the first PNS bacteria that exhibit the complex metabolism (Larimer *et al.*, 2004). This genome sequence is a starting point to use *R. palustris* as a model to explore its metabolism resulting maximum hydrogen productivity compared to other PNSB. Its genome sequence shows that *R. palustris* has additional metabolic capabilities (Larimer *et al.*, 2004), not in common with other PNSB such as *R. sphaeroides* or *R. rubrum*. *R. palustris* is capable of modulating photosynthesis according to light quality. This is because its photosynthetic membrane has multiple light harvesting complexes differing in the wavelengths of light absorbed. Therefore, it can harvest light of differing qualities and intensities.

Moreover, it undergoes asymmetric cell division and produces a cell surface adhesion at one end of the cell that causes cells to stick to solid substrates resulting good yields in the hydrogen production. On the other hand, Sagir (2012) experimentally observed *R. palustris* having maximum hydrogen productivity (0.78 mmol/h) from sucrose compared to the other PNS species *Rhodobacter capsulatus*, *Rhodobacter capsulatus* YO3 (hup-) and *Rhodobacter sphaeroides*. PNSB have been noted for their hydrogen production capabilities from a wide selection of substrates. Enhancing the hydrogen yields and productivities still remains a challenge due to their complex metabolism. The metabolic activities of the PNSB that drive hydrogen production are discussed in the next section.

2.2 Overview of the Metabolism in Hydrogen Production by PNS bacteria

A thorough understanding of the metabolism plays a vital role in assessing and improving efficiency and productivity in biological hydrogen production systems. This is especially the case for purple non-sulfur (PNS) bacteria, in which the hydrogen production metabolism is the result of the complex interplay of several systems and components such as the photosystems, carbon flow and enzymatic reactions (Figure 2.2). The overall scheme of hydrogen production is illustrated in the form of a flow chart in Figure 2.2. The distribution of protons and electrons over the components of bacteria are shown as streams in the block diagram.

Substrate (sucrose in this work) is broken down and oxidized through the sucrose pathway, glycolysis and TCA cycle. Electrons from the oxidation of the substrate are carried by NAD (Nicotinamide adenine dinucleotide) and Fd (Ferredoxin) to the Calvin cycle, biosynthetic reactions, and the Nitrogenase and Hydrogenase enzymes (Vignais *et al.*, 1985). At the same time, light energy is converted into ATP in the Photosynthetic unit (PSU). Nitrogenase receives ATP along with the protons and electrons. Protons are supplied in part by the TCA cycle and the remainder by ATP-synthase, the latter working as a part of the photosynthetic apparatus. Nitrogenase reduces protons to molecular hydrogen whereas Hydrogenase functions bi-directionally in general, both producing and consuming hydrogen. The detailed explanation of each component in Figure 2.2 will be given in the following sections.

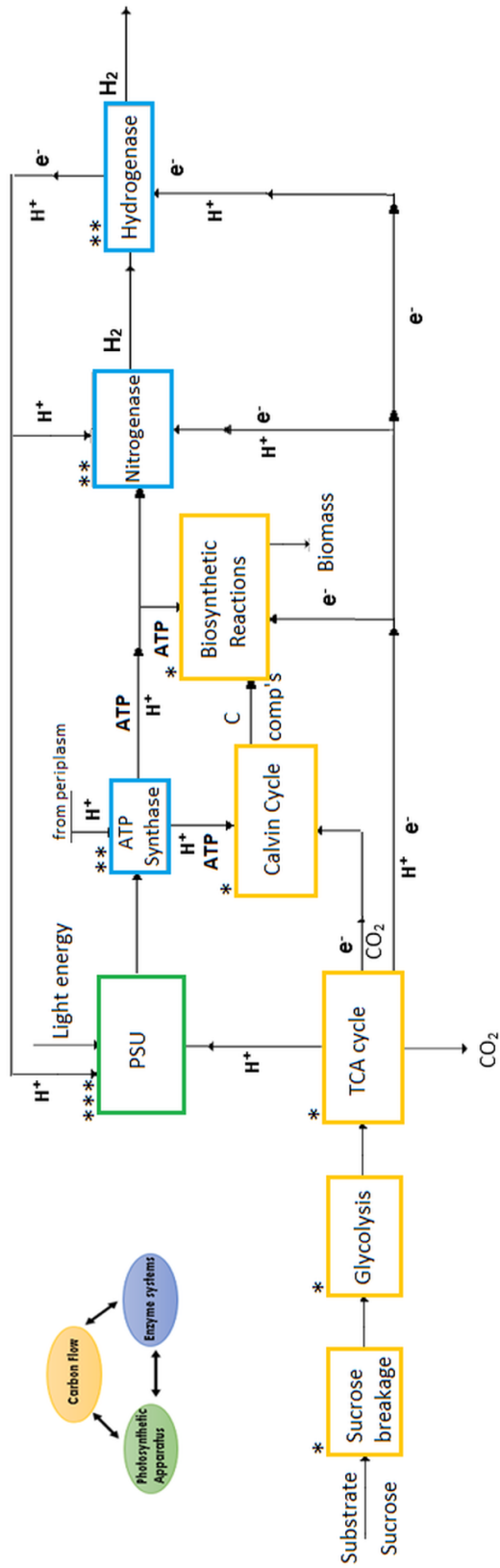


Figure 2.2: The overall scheme for hydrogen production.

Boxes: (*) Carbon flow, (**): Enzyme Systems, (**): The photosynthetic unit (PSU)

2.2.1 Carbon flow

The hydrogen productivities and conversion efficiencies of even simple substrates such as sugars and small organic acids can vary due to the differences in the utilization manner of different substrates. Accordingly, more insight is needed into the carbon utilization patterns of these species. Figure 2.3 shows the simplified scheme of carbon metabolism of PNSB (Koku *et al.*, 2002). Sucrose is broken down to glucose and fructose in the sucrose pathway. The glycolysis pathway (Embden Meyerhoff Pathway), Entner Doudorof pathway and Pentose Phosphate pathway can differ with respect to the species of the PNSB (Hädicke *et al.*, 2011). For example, the pentose phosphate pathway has only been observed in *R. palustris* whereas the Entner Doudorof pathway is present in only *R. sphaeroides*. Moreover, *R. rubrum* does not have either of the Entner Doudorof pentose phosphate pathways (Hädicke *et al.*, 2011). In Figure 2.3 (Koku *et al.*, 2002), Glucose and Fructose are converted into Glyceraldehyde 3-P in the Entner Doudorof pathway and Embden Meyerhoff Pathways, respectively. CO₂ is fixed and Glyceraldehyde 3-P is converted into pyruvate in the Calvin cycle. Acetyl CoA is produced from pyruvate while electrons and CO₂ are produced in the TCA cycle (tricarboxylic acid cycle). *R. palustris* encodes a complete tricarboxylic acid cycle. However, it also uses the glyoxylate shunt which is a direct pathway from isocitrate to malate (McKinlay *et al.*, 2011).

The genome sequence that encodes the carbon cycle also indicates the synthesis of glycogen and poly β -hydroxyalkanoates as carbon storage polymers (Adessi *et al.*, 2012). Poly- β -hydroxybutyrate (PHB) is synthesized to eliminate excess electron carriers in the carbon flow. PHB production increases with excess carbon and energy sources in a nitrogen deficient environment where limited cell growth can occur. However, the stored PHB is degraded when bacteria is transferred to the environment convenient for cell growth.

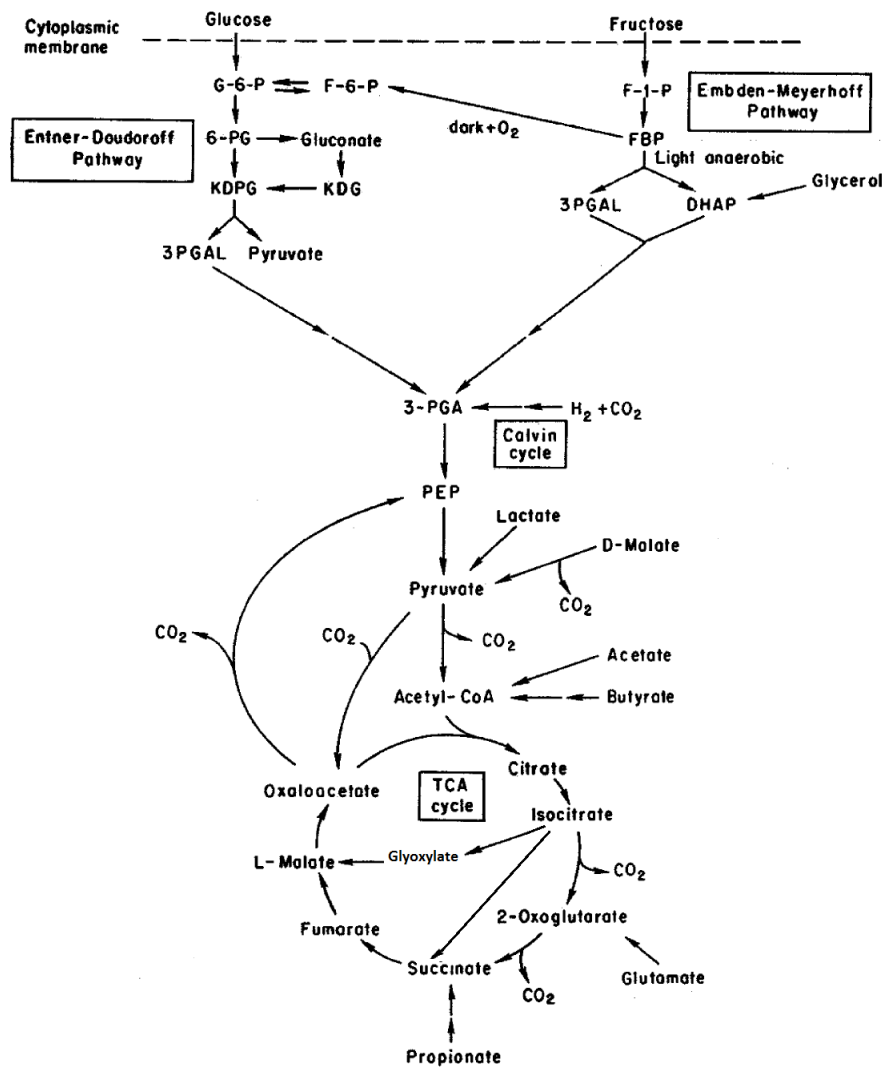
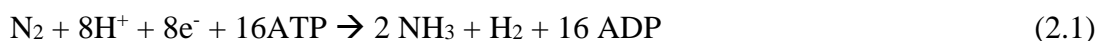


Figure 2.3: Simplified overall scheme of carbon flow in PNSB (Koku *et al.*, 2002)

Conditions of growth media of bacteria (pH and substrate) can affect the rate of PHB production (Chen *et al.*, 2011). Pathway of PHB production may compete with the pathway of hydrogen production for electrons because both pathways are favorable with unbalanced growth (Vincenzini *et al.*, 1997).

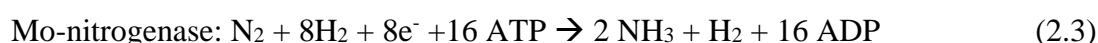
2.2.2 Enzyme Systems

In biological hydrogen production of PNSB, nitrogenase and hydrogenase are the two most important enzymes that result in hydrogen production. Both enzymes produce hydrogen from protons and electrons either in the presence or absence of a nitrogen source. However, depending on the type and amount of the nitrogen source, nitrogenase functions in different ways to produce hydrogen. Equation (2.1) shows the reaction of nitrogenase when fixing nitrogen (N₂) to ammonia (NH₃), whereas (2.2) is the hydrogen production reaction of nitrogenase in low amounts or total absence of the nitrogen source. In the absence of molecular nitrogen, nitrogenase still produces H₂ using only protons, electrons and ATP (Equation 2.2), without nitrogen fixation (McKinlay, 2014).



Hydrogen production by Nitrogenase is an irreversible reaction. In addition to molecular nitrogen, oxygen and ammonium present in hydrogen production medium can repress the activity of nitrogenase (Koku *et al.*, 2002). For this reason, limited amounts of the nitrogen source are provided to PNSB for hydrogen production to prevent low nitrogenase activity; this condition is typically referred to as a high carbon-to-nitrogen (C/N) ratio. This results in the absence of significant growth (Keskin, Abo-Hashesh and Hallenbeck, 2011). When limited molecular nitrogen is supplied to bacteria, one mole of molecular hydrogen requires 4 moles of ATP as seen in (2.2).

Most PNSB carry molybdenum in the center of their nitrogenase enzyme, which is called the Mo-nitrogenase for this reason. However, two other nitrogenases have also been identified for some PNSB, with vanadium (V – nitrogenase) or iron (Fe – nitrogenase) in the center of the enzyme (Basak *et al.*, 2007). Nitrogenases are named for the metals present in their active sites. *R. palustris* is a unique example of PNSB encoding all three nitrogenase isozymes (McKinlay, 2014). The reactions of these isoenzymes are given in (2.3), (2.4) and (2.5).



As seen from the reactions, H₂ production is performed more efficiently by alternative nitrogenases in the presence of molecular nitrogen. PNSB encoding V-nitrogenase and Fe-nitrogenases theoretically catalyze three and nine times as much hydrogen as do Mo- nitrogenases, respectively. Oda *et al.* (2005) compared *in vivo* rates of H₂ production by strains using each nitrogenase individually under nitrogen fixing environment.

Table 2.1: Comparison of individually expressed nitrogenase types and resulted H₂ productivity *in vivo* (Oda *et al.*, 2005)

Nitrogenase expressed	Growth rate (h⁻¹)	H₂ production (μmol/mg protein)	Specific H₂ productivity (μmol/(mg protein)h⁻¹)
Mo- only	0.048	30	1.44
V- only	0.036	51	1.84
Fe- only	0.028	140	3.92

Table 2.1 shows the comparison in terms of growth rate, H₂ production and specific H₂ productivity. To obtain the data in this table, Oda *et al.*(2005) experimentally observed growth rates and H₂ production in the presence of nitrogen, but calculated specific H₂ productivities based on the Monod model. Strains expressing V and Fe-nitrogenases grow more slowly, but they have higher specific H₂ productivities.

On the other hand, when no nitrogen or a limited nitrogen source is available, the reactions of all nitrogenase isozymes for H₂ production are identical. Therefore, in such a situation, V – nitrogenase and Fe – nitrogenase have the same reaction as Mo-nitrogenase (McKinlay, 2014).

Hydrogenase, which is the other enzyme responsible for H₂ production has the reaction shown in (2.6).



This is similar to the reaction of nitrogenase in the case of a limited nitrogen source in terms of producing H₂ from protons and electrons (McKinlay *et al.*, 2010). However, no ATP is utilized for H₂ production. The reaction is reversible under certain conditions, with hydrogen being either produced or consumed (McKinlay *et al.*, 2010).

Similar to the case of alternative nitrogenases, [Fe]-hydrogenase, [NiFe]-hydrogenase, and [FeFe]-hydrogenase have been classified based on the type of metal in the active site of the enzymes, so far. [Fe]-hydrogenase and [FeFe]-hydrogenase have reactions exclusively in the direction of H₂ production whereas the other catalyze H₂ consumption or uptake (Cammack 1999).

The hydrogen uptake of hydrogenase ([NiFe]-hydrogenase) can be defined as the metabolic antagonist of nitrogenase and the term uptake hydrogenase is used when hydrogenase catalyzes H₂ consumption instead of production. Some studies have reported higher hydrogen yields by modifying or completely eliminating the hydrogenase activity of PNSB. Ooshima *et al.* (1998) obtained mutants of *R. capsulatus* without hydrogen uptake enzyme and observed a significant increase in substrate (60 mM malate) conversion efficiency to 68% in the mutant type from 25% in the wild type. Öztürk *et al.* (2006) eliminated the gene of uptake hydrogenase in *Rhodobacter capsulatus* to have higher hydrogen productivity and obtained 70% hydrogen production efficiency. However, this deletion is probably unnecessary or even detrimental for hydrogen production in *R. palustris*, because its genome sequence reveals an inactive uptake hydrogenase and other hydrogenase(s) that produce hydrogen (Rey *et al.* 2006).

R. palustris was reported to encode [FeFe]-hydrogenase and [NiFe]-hydrogenase (Androga *et al.*, 2012) where [NiFe]-hydrogenase was inactivated by a regulatory mechanism explained by Rey *et al.* (2006) The main characteristics of nitrogenase and hydrogenase are compared in Table 2.2 (Basak *et al.*, 2007).

Table 2.2: Comparison of enzymes responsible for H₂ production in PNSB

Characteristics	Nitrogenase	Hydrogenase
H ₂ production	Yes	Yes
H ₂ uptake	No	Yes
Oxygen sensitivity	Yes	Yes
ATP dependency	Yes	No
Catalytic rate	Low	High
Subunits	6	1-3

2.2.3 Photosynthetic Unit

The photosynthetic unit (PSU) of PNSB is located in the cell membrane. During photosynthesis of bacteria, functions of light-harvesting vesicular, photosynthetic pigments (bacteriochlorophyll, carotenoids etc.) and an electron transport chain are observed in this unit. Light energy is converted to ATP as a result of a set of equations driven by the membrane-based components of the PSU. Figure 2.4 (Klamt *et al.*, 2008) illustrates these components and their functions for ATP production.

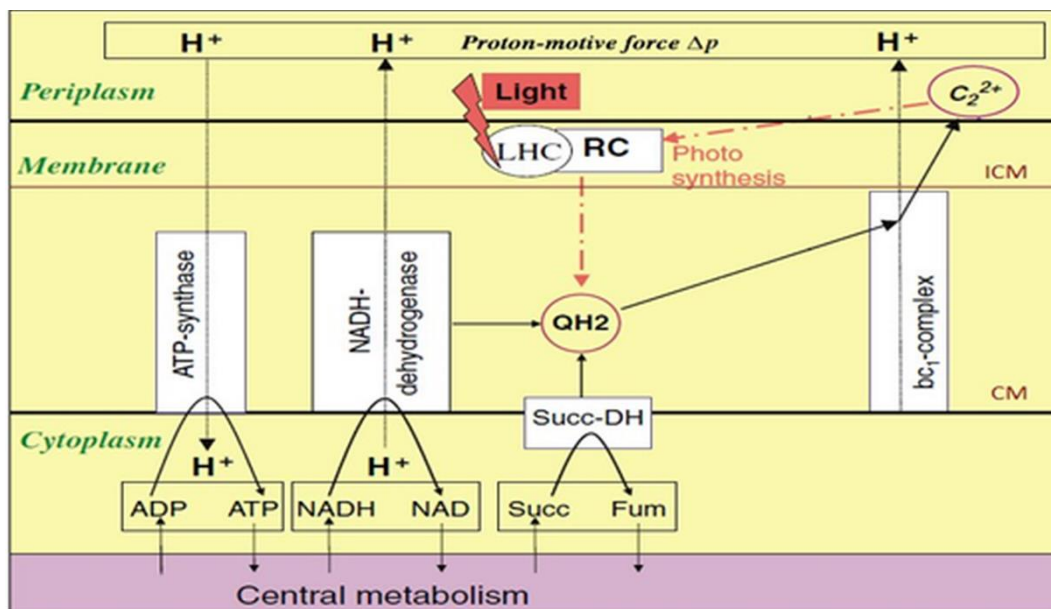
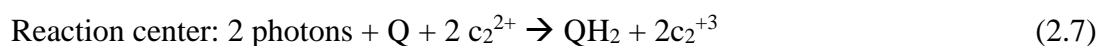


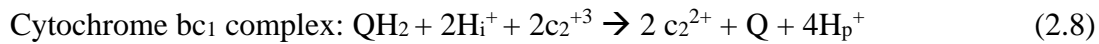
Figure 2.4: Processes for components of photosynthetic unit in PNSB; solid arrows: electron flow, dotted arrows: proton (hydrogen ion, H^+) flow (Klamt *et al.*, 2008)

The membrane closer to periplasm is defined as intracytoplasmic membrane (ICM) whereas the rest of the membrane is known as cytoplasmic membrane (CM). In the intracytoplasmic membrane, the reaction center (RC), light harvesting complexes (LHC) and photosynthetic pigments play the important roles of absorbing photons from the light source and starting the cyclic ATP production (red arrows in Figure 2.4). Cytoplasmic membrane includes the components of electron transport chain of PSU. The components of electron transfer chain are NADH dehydrogenase, succinate dehydrogenase, cytochrome bc_1 , cytochrome c_2^{2+} , ubiquinone (Q) / ubiquinol (QH₂) and ATP synthase. In the membrane, ubiquinone (Q), cytochrome c_2^{2+} and NADH are electron carriers. NADH bridges the membrane and central metabolism by interchanging electrons, whereas the others diffuse only in the membrane. The 5 important reactions taking place in the photosynthetic unit are listed below as equations (2.7)-(2.11) where H_i^+ and H_p^+ represent protons (hydrogen ions) in the cytoplasm and periplasm, respectively.

In the photosynthetic unit, light harvesting complexes including chlorophyll and carotenoids pigments surround the reaction center (integral membrane protein complex) and harvest light energy from the light source. Therefore, photons are absorbed by the light harvesting complexes in the form of excitation energy in chlorophylls. Bacteriochlorophyll (bchl) plays the important role of charge separation and the initiation of a cyclic electron flow with electron carriers, acting as the primary electron donor and final electron acceptor. The excitation energy is exchanged with electrons in the reaction center by reducing Q to QH₂ and oxidizing c_2^{2+} to c_2^{3+} .



The reaction by the cytochrome bc_1 complex occurs in the opposite direction of the reaction center. Reduced QH₂ is converted back into Q and electrons are transferred to cytochrome c_2 to be reduced. The cytochrome bc_1 complex takes electrons from the Q pool to cytochrome c_2 and protons are pumped to periplasm.



NADH Dehydrogenase reversibly transfers two electrons for reduction of Q to QH₂ and pumps only four protons towards periplasm.



Succinate Dehydrogenase does not pump protons to periplasm, only reversibly reduces Q to QH₂ by transferring succinate to fumarate. In that way, central metabolism and the components of PSU based on ubiquinone (Q).



The final and critical component of PSU in PNSB is ATP synthase. Protons accumulated in the periplasm are used by ATP synthase to produce ATP. NADH dehydrogenase and Succinate dehydrogenase donate protons in opposite directions of other components to maintain the redox balance of Q pool. In this way, a proton gradient between periplasm and cytoplasm forms for ATP synthesis during photosynthesis. ATP synthase converts the generated proton gradient to chemical energy in the form of ATP. This conversion is called cyclic photophosphorylation because the process is continuous as long as the bacteria uses energy from a light source.



2.3 Sucrose Metabolism in PNS Bacteria

Sugar industry wastes containing high amounts of sucrose have been used as main substrates for PNSB (Keskin *et al.*, 2012). Beet molasses, sugar cane and wastewater are typical wastes obtained during sugar manufacturing. In earlier studies, hydrogen production was performed using two different stages. In the so-called, two-stage processes, the first stage is the conversion of fermentative sugar to organic acids and hydrogen whereas in the second stage only organic acids are utilized for H₂ production. Lo *et al.* (2010) obtained a yield of 5.8 mole H₂ per mole of sucrose using microorganisms of *Clostridium butyricum* CGS55 and *Rhodospseudomonas palustris* WP3-5. However, recent studies have aimed to perform hydrogen production in a single-stage batch process, in order to reduce the cost and complexity of the overall process. Keskin *et al.* (2011) achieved hydrogen production using beet molasses, black strap and pure sucrose with *Rhodobacter capsulatus* in a single stage photo-fermentation process for the first time. Yields of 10.5 mole, 8 mole and 14 mole H₂ per mole of sucrose are obtained, respectively. This result seems to be very promising when compared to two stage photo-fermentation processes.

Independently, Sagir (2012) studied single stage photo-fermentation on molasses using *Rhodobacter capsulatus* YO3 and observed a productivity of 0.41 mole H₂/(m³.h). However, in single stage photo fermentation, significant decreases in pH values of hydrogen production medium was observed due to organic acid released by bacteria. Hydrogen production was found to be negatively affected because of decreasing pH in the bacterial culture (Sagir *et al.*, 2012). Indeed, both single and two stage processes have some disadvantages such as dependence on a light source and the difficulty in designing photo-bioreactors. To overcome these drawbacks and to obtain higher H₂ yields, the use of metabolic engineering and process control techniques is required (Hallenbeck *et al.*, 2015).

PNSB are organisms with very versatile metabolic pathways (Larimer *et al.*, 2004). Unlike metabolism of other carbon sources such as simple sugars and organic acids, sucrose metabolism is not well-understood in these bacteria. Although their genome sequences are available in the literature, the enzymes in sucrose metabolism have not been identified in terms of their activity during sucrose utilization. Figure 2.5 shows the pathway map of sucrose and starch metabolism in *R. palustris*. This metabolic pathway is primarily responsible for the conversion of sucrose into glucose and fructose. Some enzymes are known via genomic studies (Kanehisa *et al.*, 2015) to be active in *R. palustris*. On the other hand, experimental studies resulting in biomass growth and H₂ production on sucrose by PNSB (Hallenbeck *et al.*, 2015 and Sagir, 2012), lend support to the presence of additional enzymes not identified within the genome. Therefore, in modeling the metabolism, it is possible to use an overall, hypothesized pathway of sucrose utilization for the bacteria, marked by red in Figure 2.5. The boxes circled in red represent the enzymes assumed to be present. Of these, the green boxes correspond to confirmed enzymes in *R. palustris* whereas the white boxes correspond to enzymes that have not been verified but hypothesized to be present in the current study. The pathway where maltose is utilized was ignored because the bacterial culture does not have extracellular maltose to be consumed. In addition, glycogen, cellulose and pectin pathways were not included in the model because there is no experimental observation about synthesis of these metabolites by *R. palustris*. In particular, enzymes for transportation and breakdown of extracellular sucrose (2.7.1.69 and 3.2.1.26) are assumed to be present in the metabolic network. The list of enzymes with their EC number and names can be found in Appendix B.2.

As seen from Figure 2.5, sucrose is also synthesized within the metabolism from the phosphorylated intermediate sucrose-6'-phosphate by enzymes of sucrose-phosphate synthase (SPS-2.4.1.13) and sucrose-phosphatase (SPP-3.1.3.24). Both external and produced sucrose are broken down by the enzymes of invertase or sucrose synthase (3.2.1.26) into glucose and fructose to be used in glycolysis pathways as mentioned in section 2.2

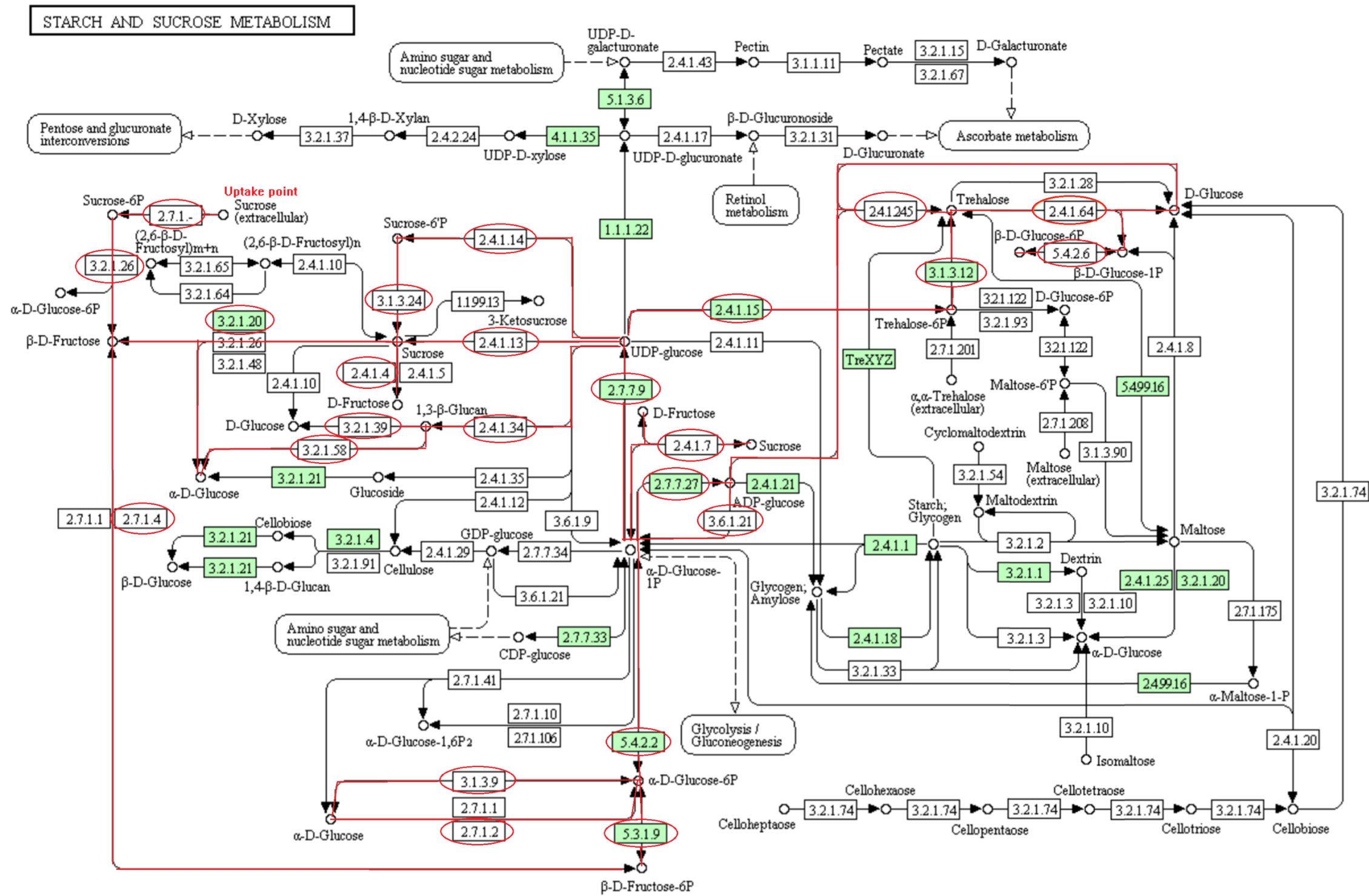


Figure 2.5: Pathway map of sucrose and starch metabolism in *R. palustris* (Kanehisa *et al.*, 2015)

2.4 Metabolic Modeling and its Application to PNS Bacteria

The metabolism can be defined as the rate of biochemical reactions of chemical compounds (metabolites) taking place in the organism. Complex molecules are either formed or broken down in the metabolism. Energy is also required or produced in some of these processes. An organism should have a balanced metabolism in terms of the reactions to be alive. The metabolism of a microorganism can be used to increase the yield of a desired product obtained from the microorganism. For this purpose, a research area of metabolic engineering has been studied by especially, pharmaceutical companies for drug development and industrial companies for product development to understand the metabolism of organisms. For this purpose, a quantification of the metabolism is required. Metabolic models have been developed from networks of chemical reactions representing the metabolism of the organism. To construct the network, the genome sequence and biochemical information of the organism are used.

Therefore, the objective of metabolic engineering is to obtain the optimum metabolic network resulting maximum product synthesis. An optimum metabolic network shows the biochemical paths that a substrate should follow to obtain the desired productivity of the process. This network is estimated from the flux distribution (the rate of each biochemical reaction) obtained from metabolic models.

There are different techniques to model metabolic networks. Dynamic flux analyses and metabolic flux analysis are the main categories for metabolic modeling. Dynamic flux analysis requires detailed, reliable kinetic data for the metabolism of the organism of interest (Gao *et al.*, 2007). Though more rigorous in principle, the amount of experimental data needed to be amassed prohibits the applicability of such an approach, especially for the metabolically versatile PNSB.

Klamt *et al.* (2008) constructed a mathematical model of electron transport chain of PNSB to predict changes in fluxes of the reactions with respect to different environmental conditions. However, only 10 out of 33 time dependent variables were kinetically defined. The whole metabolism of PNSB has not been dynamically modeled so far because detailed kinetic data is not available in literature. The other modeling technique is metabolic flux analysis which is the method used in the present work. The methodology chapter will present a more extensive overview of metabolic flux analyses. The process of hydrogen production by PNSB has some drawbacks such as low light conversion efficiency, low enzyme activity of nitrogenase and the presence of pathways competing with hydrogen production for electrons (Ghosh *et al.*, 2015). In this work, the objective of the metabolic modeling is to increase hydrogen production capacities of PNSB. This capacity depends on carbon and nitrogen sources utilized and activities of hydrogen producing enzymes, light source and the components of photosynthetic unit of the bacteria. Metabolic modeling has also been applied in other studies to improve the process of hydrogen production by PNSB so far. Recently, most of the studies have been focusing on the metabolic flux analysis in carbon metabolism of PNSB.

Klamt *et al.* (2002) first attempted to apply flux balance analysis for the central metabolism of PNSB. The photoheterotrophic growth of the bacteria was quantitatively analyzed. This study showed that important metabolic constraints can be identified from the stoichiometric analysis performed.

Golomysova *et al.* (2010) constructed the first comprehensive mathematical model of the metabolism of PNSB in a condition of photoheterotrophic growth. 314 metabolic reactions and 287 compounds in *R. sphaeroides* were modeled using flux balance analysis. Computed metabolic fluxes were compared with some experimental values previously studied.

McKinlay and Harwood (2010) used ^{13}C -metabolic flux analysis (^{13}C -MFA) to assess the significance of the Calvin cycle in PNSB producing hydrogen. *R. palustris* was analyzed with acetate as substrate in photoheterotrophic growth. The Calvin cycle was quantified, with CO_2 fixation resulting from the analysis. 22% of the carbon in acetate was found to be oxidized to CO_2 and 68% of this CO_2 was observed to be reused by the bacteria in Calvin cycle. Therefore, this result showed Calvin cycle has an important role to recycle electron carriers by CO_2 fixation because it re-oxidized nearly half of the reduced cofactors when the acetate was utilized to produce CO_2 .

Imam *et al.* (2011) constructed a genome-scale metabolic model with 796 metabolites and 1158 reactions of *R. sphaeroides* under photoheterotrophic growth conditions. The model results were found close to experimental observations. The model reported that maximum yield of H_2 can be achieved as much as ~50% higher than the yield experimentally determined. The presence of competing pathways was indicated to prevent low yields of H_2 production.

McKinlay and Harwood (2011) obtained metabolic fluxes resulted from metabolic flux analysis in *R. palustris* grown on a range of organic compounds (fumarate, succinate, acetate and butyrate). Metabolic fluxes were determined using two different strains of *R. palustris*; wild type and a NifA strain which is a mutated strain to grow photoheterotrophically in the presence of NH_4^+ as the nitrogen source. Nitrogenase was active in NifA strain (hydrogen producing strain) as opposed to wild type (non-hydrogen producing strain) because mineral medium containing NH_4^+ was used in their study. The contribution of Calvin cycle in the metabolism of the bacteria was determined by comparing the fluxes obtained from these strains. Since the active metabolic routes change depending on the substrate input, the hydrogen yield changes, accordingly. In addition, H_2 yield was observed to increase with all substrates studied when the Calvin cycle was blocked.

Hädicke *et al.* (2011) developed a stoichiometric model using metabolic flux analysis for three main representatives of PNSB (*Rhodospirillum rubrum*, *Rhodobacter sphaeroides* and *Rhodopseudomonas palustris*) grown on different substrates (succinate, malate, propionate, acetate and fructose). Their central metabolism was modeled to understand and compare the redox mechanism behind their metabolism in either photoheterotrophic or photoautotrophic growth. Different pathways were observed in central metabolism of three organisms studied. For example, *R. palustris* was found to assimilate acetate using the enzyme of isocitrate lyase in a pathway named glyoxylate shunt whereas *R. sphaeroides* and *R. rubrum* use ethylmalonyl-CoA (EMCoA) pathway and citramalate cycle (CM), respectively. The resulted flux distribution showed that *R. sphaeroides* can grow on acetate without functional Calvin cycle because EMCoA pathway mimics the Calvin cycle consuming reducing equivalents.

Tao *et al.* (2011) studied glucose metabolism of *R. sphaeroides* in photoheterotrophic growth and presented its intracellular carbon fluxes using metabolic flux analysis. H₂ yield was found to increase due to significant increase in fluxes of tricarboxylic acid cycle (TCA cycle) corresponding to 82 to 88% of the increase in NADH formation when the enzymes of hydrogenase and poly- β -hydroxybutyrate (PHB) synthase were disrupted.

The present work models the carbon metabolism of *R. palustris* in bacterial culture with low nitrogen (glutamate) to carbon (sucrose) ratio to assess its capability of the hydrogen production on sucrose. Additionally, effects of changes in the growth conditions of the bacteria were analyzed on biomass production and hydrogen production, in particular. A distinctive feature of this study is that a metabolic model investigating carbon utilization patterns of *R. palustris* on sucrose in hydrogen production environment has not been studied previously, to the best of our knowledge.

CHAPTER 3

METHODOLOGY

3.1 Metabolic Flux Analysis

Metabolic flux analysis is a practical methodology to study the network of biochemical reactions and to predict fluxes of metabolic pathways. In this method, a single cell of the organism is treated as a system that exchanges mass with its surroundings, as well as carry out internal (intracellular) reactions. The set of reactions and transport streams are referred to as fluxes and collectively from the metabolic network of the system. The method enables the determination of these fluxes when proper conditions and assumptions are met. The knowledge of metabolic fluxes in a biological production system informs scientists of the degree of involvement of various pathways in the metabolic reaction network. Knowledge of the distribution of intracellular fluxes on metabolic pathways plays a critical role on metabolic engineering design, as it helps identify specific targets for genetic manipulation in order to maximize the production of a desired metabolite. For the present study, the one of the objectives of the metabolic flux analysis is to determine the pathways that have the potential for genetic modification and may contribute to higher H₂ yield. One definitive aspect of metabolic engineering is the focus on a system of interacting biochemical reactions as a network instead of on individual enzymatic reactions. This metabolic network is an abstract representation of the cellular metabolism (Stephanopoulos *et al.*, 1998).

Metabolic Flux Analysis (MFA) has become a reliable and widely used technique to obtain accurate intracellular fluxes within the metabolism over the past 20 years. According to a literature study (Crown *et al.*, 2013), 700 published papers containing the term of ‘metabolic flux’ or ‘flux analysis’ or ‘fluxes’ were found. Among these, 70 papers were found to be about experimental MBA and approximately 50 of them were simulation based and theoretical studies. The number of publications related to MFA are shown in Figure 3.1-a and b.

Figure 3.1-a shows that the annual number of publications on the topic of metabolic flux analysis has had an increasing trend since 1995. The inspected papers consist of a diverse set of organisms such as bacteria, fungi, mammalian cells and plants. In Figure 3.1-b, the distribution of organisms studied for MFA is given with the annual number of publications. In recent years, the publications covering MFA on bacteria have constituted the majority of the total.

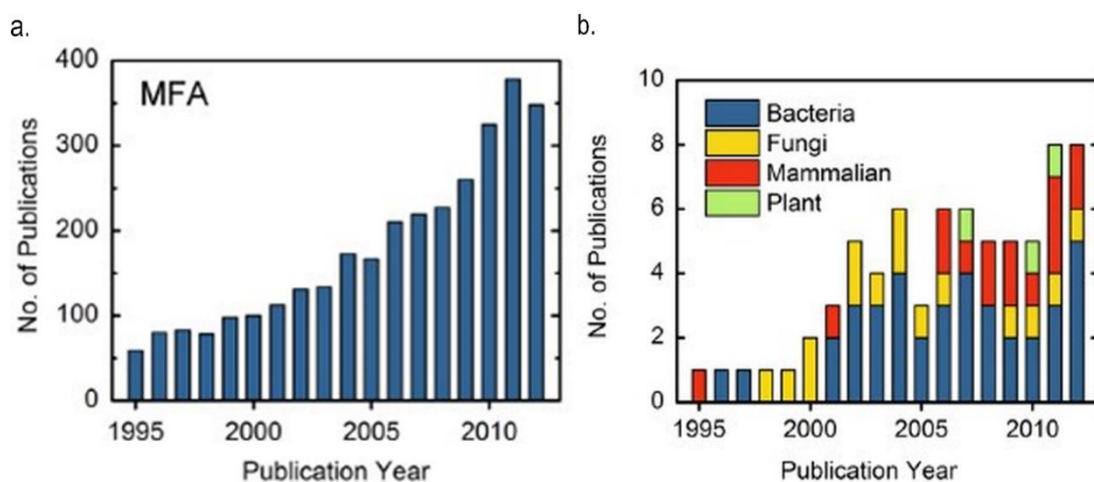


Figure 3.1: Annual number of publications involving MFA with respect to years; a. general trend, b. distribution of organism studied for MFA (Crown *et al.*, 2013)

To implement MFA in this study, a practical guideline present in the literature (Crown *et al.*, 2013) was followed. A summarized overview of good practices and a required checklist in MFA were also included in this guideline. As a good practice it is recommended that all reactions should be listed in table form in a concise manner by giving all substrates and products clearly. In addition, the metabolites and fluxes to be estimated should be listed. This is because the list of metabolites and fluxes will be connected to obtain a metabolic network model, which is basis for the entire analysis. It is also recommended that a table should list the experimental and estimated results for convenient comparison rather than a figure showing this comparison. In the present study, results were presented based on these recommendations.

3.2 Classification of Metabolic Flux Analysis

For MFA, a stoichiometric model is needed in the form of metabolic pathway map where the intracellular reactions are represented in order to determine the intracellular fluxes by applying mass balances around intracellular metabolites. Mass balances utilize a set of experimental extracellular fluxes as input to the flux calculations. These extracellular fluxes are the experimentally determined cellular uptake and excretion rates of metabolites. The result of the analysis is a metabolic flux map shown as a diagram of the biochemical reactions included in the calculations along with an estimate of the steady-state rates (i.e., the flux) for each reaction. Figure 3.2 shows an example of such a diagram called a metabolic flux map (Stephanopoulos *et al.*, 1998). In general, MFA evaluates intracellular fluxes considering the stoichiometry of the metabolism reactions and other mass balances that result in an extensive understanding of metabolic network. However, metabolic flux analysis can be divided into two categories based on the techniques used in the estimation of fluxes. These are flux balance analysis (MFA with a metabolite balance technique) and fluxomics (MFA with a tracer based technique), as will be explained in the following sections.

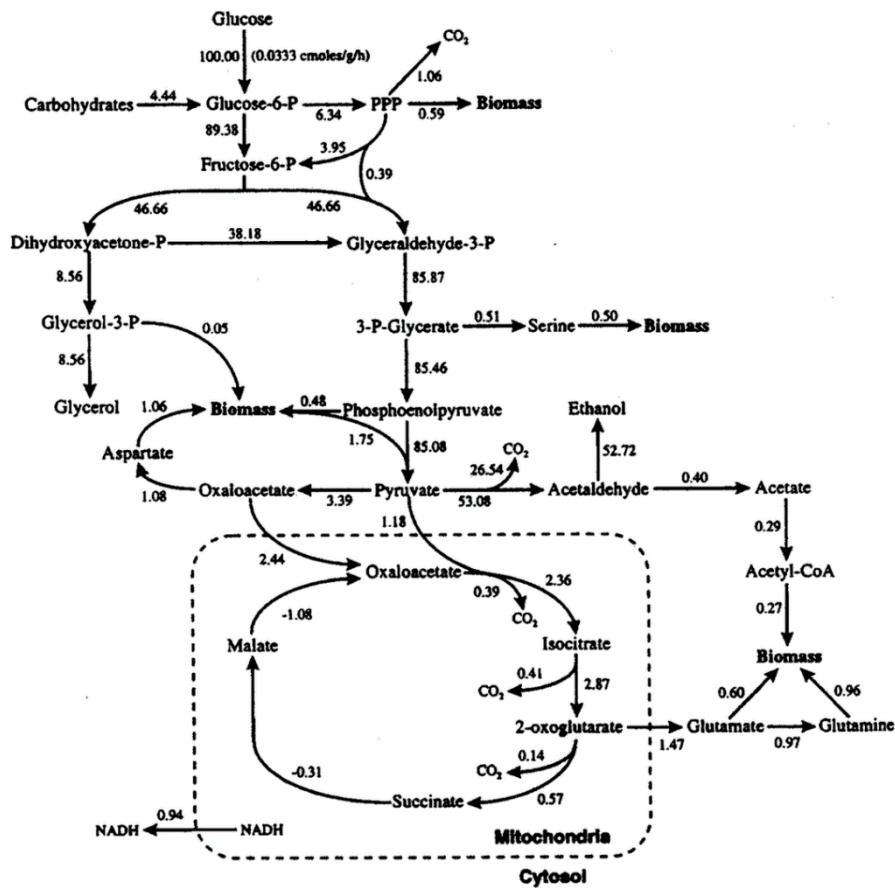


Figure 3.2: Example of a metabolic map; Fluxes distributed over different metabolic pathways (Stephanopoulos *et al.*, 1998).

3.2.1 Flux Balance Analysis

Flux balance analysis (FBA) depends on the constraints of a metabolic model based on a stoichiometric matrix. This stoichiometric matrix shows the reactions taking place in the metabolic network. The matrix is analogous to the one used in reaction engineering to find the reaction rates of complex multiple reactions that occur simultaneously in a reactor.

In this study, FBA was performed as modelling approach where bacterial metabolism is analogous to a set of biochemical reactions occurring in a reactor. The stoichiometric matrix consists of the stoichiometric coefficients of metabolites formed and consumed in the metabolic reactions and can be constructed using pre-defined reactions in the metabolic network. This approach allows a metabolic network to adopt different constraints assumed to be obeyed by organisms. These constraints are expressed in mathematical form as a multi-dimensional geometric representation in which a single solution can be obtained as a result of FBA. This is because each metabolic flux represents a dimension (i.e., a vector) in the solution space and constraint fluxes determine the resulting solution space that corresponds to a specific metabolic network. An example of the geometric representation of constraint based solution space is shown in Figure 3.3a & b (Tanis, 2006).

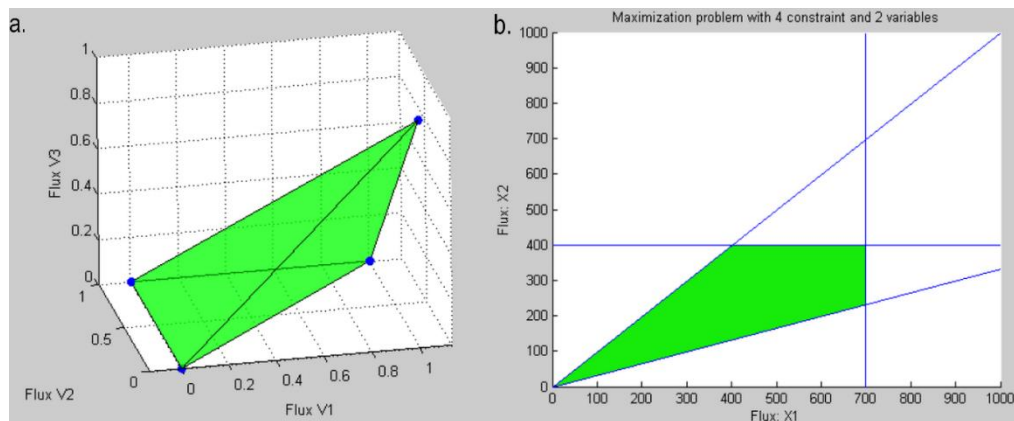


Figure 3.3: Geometric representation of; a. all possible solutions before limitations, b. a specific solution space considering flux limitations (Tanis, 2006)

The pyramid seen in Figure 3.3-a can be a solution space narrowed by three fluxes present in the metabolic network. However, this space includes many solutions that are possible to obtain from the constructed stoichiometric matrix without any limitation.

After the constraints are determined, the cone becomes a bounded solution space shown in Figure 3.3-b. These constraints could be mathematical statements converted from experimental measurements or an objective function used in the optimization of flux distribution. Optimization can be performed by linear programming, which allows to obtain the optimal flux distribution based on the constraints. Because this study uses FBA as a modeling approach, the theory behind this technique will be explained in more detail in the following sections.

3.2.2 Fluxomics

In the analysis of a metabolic network, fluxomics is a complementary method to overcome the shortcomings of constraint based MFA (FBA) by combining experimental and mathematical methods. Fluxomics, also named as Carbon Flux Analysis (CFA), is a tracer based technique. This technique uses ^{13}C isotopes to label the substrates, which are distributed from the source of the substrate within different metabolic pathways. Isotopic distributions in the steady state condition can be measured using nuclear magnetic resonance spectroscopy (NMR) and mass spectrometry including liquid chromatography–mass spectrometry (LC–MS), gas chromatography–mass spectrometry (GC–MS) and matrix assisted laser desorption ionization time-of-flight mass spectrometry (MALDI-TOF- MS)(Cai *et al.*, 2010). These measurements supplements the extracellular flux data used in FBA. An underlying assumption in this approach is that enzymes cannot differentiate between ordinary and ^{13}C -tagged carbon molecules.

This approach is applicable when all intracellular fluxes cannot be predicted by FBA. This is especially the case for too many bidirectional and cyclic fluxes present in the metabolic network. Therefore, the resulting data obtained from carbon labeling experiments helps to predict the intracellular fluxes. As the metabolic network and constraints in the present study were enough to quantitate the intracellular fluxes, the fluxomics approach was not necessary.

3.3 Construction of the Metabolic Network

The metabolic network of an organism shows how substrates are converted to products in the form of a diagram. Reactions physiologically active in the metabolism and metabolites in the metabolic network must be defined clearly to construct the metabolic models to be studied by FBA. To characterize the metabolic network of the organism, the fields of bioinformatics and theoretical biology help the construction of metabolic models. There are several important fields like genomics, proteomics, transcriptomics and metabolomics in biological studies to understand the phenotypic characteristics of an organism.

The starting point of all of these fields is the genomic sequence. Gene annotation is performed on the sequence to obtain gene functions which describe the metabolic enzymes. Therefore, all chemical reactions catalyzed by these enzymes can be defined. Figure 3.4 illustrates the resulting representation of a metabolic network.

In Figure 3.4, A, B and C are internal metabolite concentrations. v_1 , v_2 and v_3 represent internal fluxes in vector form whereas b_1 , b_2 and b_3 are the external fluxes which relate the substrates and products of the cell.

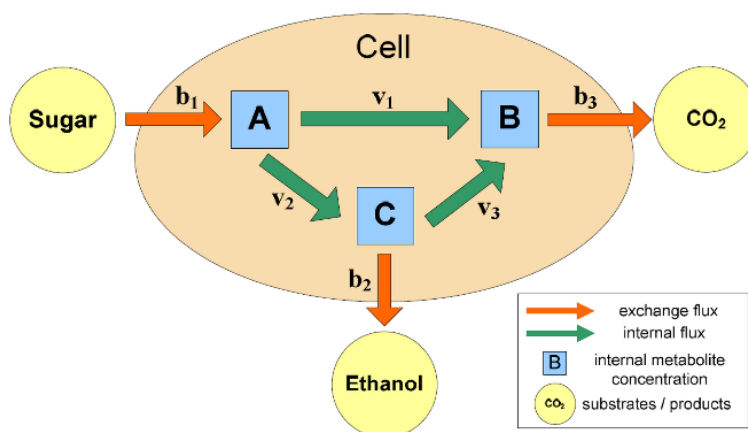


Figure 3.4: General representation of a metabolic network (Tanis, 2006)

It is difficult to determine the intracellular fluxes with only genomic data used as basis for the constructed metabolic network. The knowledge of external fluxes such as the sugar uptake rate or product (ethanol and CO₂) secretion rate from the cell is very valuable to estimate and interpret the internal fluxes. This is because the metabolic network in the cell is interrupted by external fluxes to affect a flux distribution of the network. However, this requires the use of mathematical modeling and computer simulation. Dynamic modeling and metabolic flux analysis are two existing methods of mathematical modeling.

Dynamic modeling was not selected as a mathematical method because it requires detailed kinetic data on the enzymes or cofactors and such data is not well-defined in the literature. In the present study, Flux Balance Analysis was used to model the constructed metabolic network by overcoming lack of these kinetic data. The next section will emphasize the methodology behind the model construction by Flux Balance Analysis.

3.4 Construction of the Mathematical Model

The metabolic network is the basis of model construction because it is a map of all metabolites and their reactions in the cellular metabolism. Internal and external fluxes defined in the metabolic network are used to form mass balance equations for each metabolite. Mass balance equations mathematically define the cellular information. Figure 3.5 summarizes the mathematical representation of the metabolic network and the rest of the procedure in FBA to obtain an optimal flux distribution.

The modeling approach does not need any kinetic information for enzymes and cofactors because it is a constraint based method which assumes the metabolites undergo steady state reaction rates (i.e., fluxes). Constraints are defined by mass balance equations, reversibility/irreversibility of the metabolic reactions and the knowledge of external fluxes. No other adjustable/estimated parameters are necessary. To estimate the fluxes in a reaction network, the pseudo steady-state condition is assumed.

In matrix notation (Figure 3.5-b) (Orth *et al.*, 2010), rows are metabolites (equations) and columns represent fluxes of reactions (unknowns). The number of rows is usually less than the number of columns in FBA. This is the case of underdetermined systems which exhibit many solutions in the feasible solution space.

An objective function is defined to narrow the solution space and to obtain a single optimal solution. Therefore, this general scheme emphasizes that the model construction requires mass balances, the steady-state assumption and an optimization process to obtain an optimal flux distribution over the metabolic network. Their implementation will be explained in the following sections.

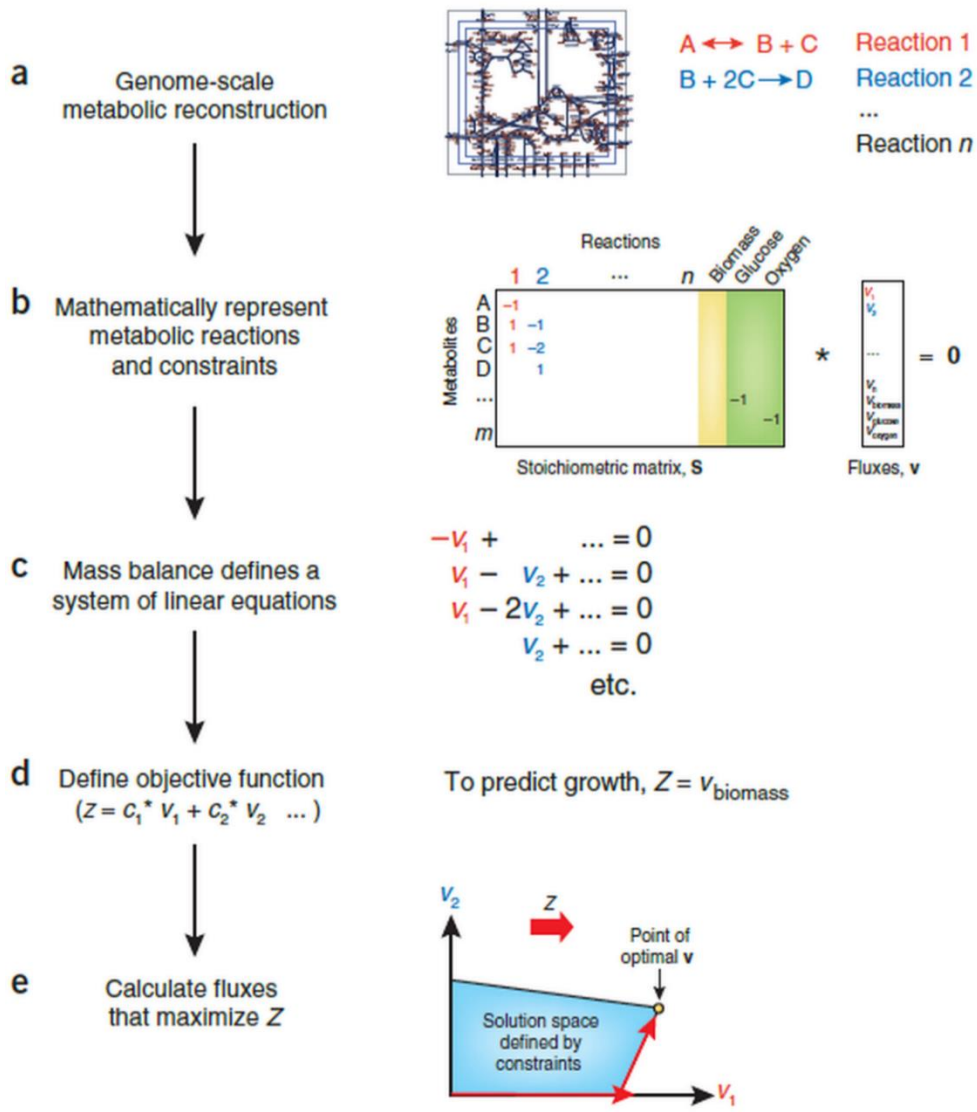


Figure 3.5: A general scheme for Flux Balance Analysis (Orth *et al.*, 2010)

3.4.1 Mass Balances and Stoichiometric Reduction

Mass balances are built up by all metabolites in the metabolic network. Mass balance equations for each metabolite depict the change of concentration of that metabolite over time. This change corresponds to the difference between production and consumption rates of that metabolite. Figure 3.6-a and b illustrate the formation of mass balance equations based on predefined metabolic network.

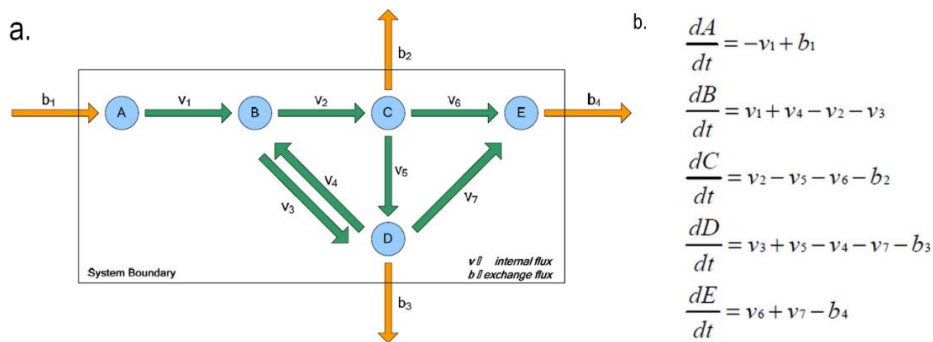


Figure 3.6: a. Simple reaction network to form mass balance, b. An example of a set of mass balance equations

In Figure 3.6, the v terms represent unknown internal fluxes whereas the b terms are the known external fluxes. Mass balance equations are presented in a matrix form with a stoichiometric matrix (S) and an unknown flux vector (v). The stoichiometric matrix is an $m \times n$ matrix and v is the vector of unknown fluxes, where m is the number of metabolites and n is the number of the reactions. The relation between internal and external fluxes is converted into a mathematical expression with these matrices. Equation (3.1) displays the system of equations in terms of S and v , and equation (3.2) is the full-form of equation (3.1) for an example stoichiometric matrix.

$$\begin{bmatrix} \frac{dA}{dt} \\ \vdots \\ \frac{dE}{dt} \end{bmatrix} = \mathbf{S} \cdot \mathbf{v} \quad (3.1)$$

$$\begin{bmatrix} \frac{dA}{dt} \\ \frac{dB}{dt} \\ \frac{dC}{dt} \\ \frac{dD}{dt} \\ \frac{dE}{dt} \end{bmatrix} = \begin{bmatrix} -1 & 0 & 0 & 0 & 0 & 0 & 0 & 1 & 0 & 0 & 0 \\ 1 & -1 & -1 & 1 & 0 & 0 & 0 & 0 & 0 & 0 & 0 \\ 0 & 1 & 0 & 0 & -1 & -1 & 0 & 0 & -1 & 0 & 0 \\ 0 & 0 & 1 & -1 & 1 & 0 & -1 & 0 & 0 & -1 & 0 \\ 0 & 0 & 0 & 0 & 0 & 1 & 1 & 0 & 0 & 0 & -1 \end{bmatrix} \begin{bmatrix} \mathbf{v}_1 \\ \vdots \\ \mathbf{v}_7 \\ \mathbf{b}_1 \\ \vdots \\ \mathbf{b}_4 \end{bmatrix} \quad (3.2)$$

The numbers in the stoichiometric matrix represent the stoichiometric coefficients of all metabolic reactions in the constructed network, including the growth reaction of biomass. A set of linear equations is obtained when steady state is assumed. However, these equations must be linearly independent to avoid trivial solutions.

To consolidate the equation system, stoichiometric reduction is performed on the metabolic network by analyzing the individual pathways. Figure 3.7 shows an example of this type of analysis for stoichiometric reduction; each pathway in Figure 3.7 can be seen individually in different section of databases as a part of metabolism. However, pathway 3 is a combination of Pathway 1 and 2. Therefore, only pathway 3 should be considered in the stoichiometric matrix (Papin *et al.*, 2004).

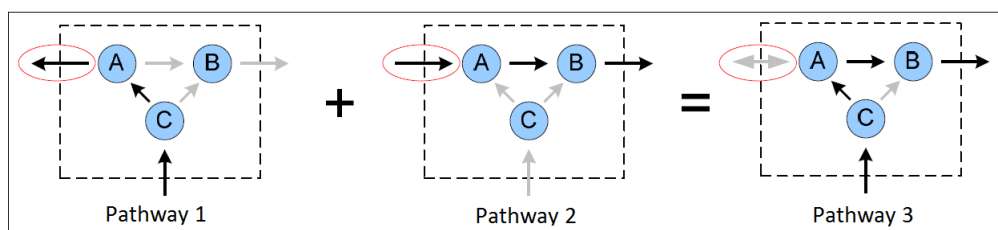


Figure 3.7: Example representation for linear combination of pathways

Moreover, intermediate metabolites reacting in a single direction can be neglected in the absence of branching (Varma *et al.*, 1993b). These metabolites can be named as a single metabolite. In addition, a reversible reaction has a single and unidirectional flux in the final solution even though chemically it is bi-directional. The sign of resulting flux will give the direction of that reversible reaction (Edwards *et al.*, 2000). Stoichiometric reductions also help to simplify the metabolic network. For this reason, some compounds that are not of interest in the studied metabolism are not included in the reaction network. For example, some biosynthetic reactions are lumped into one reaction because this study focuses on hydrogen production in *R. palustris* rather than the detailed synthesis of all products. Furthermore, cofactor molecules such as coenzyme A and NAD^+ , which are carriers for specific molecular species, have their fluxes intrinsically balanced and can therefore be ignored in the network. Inclusion of such metabolites only leads to the generation of dependent rows (Varma *et al.*, 1993b).

In this study, the dependent reactions were eliminated by hand and also using the ‘licols’ function in Matlab to make sure that all linearly-dependent rows were eliminated. As a result, the number of rows in the stoichiometric matrix was reduced from 128 to 121. To illustrate, a part of the stoichiometric matrix is shown in Appendix C.

3.4.2 Steady State Assumption

The steady-state assumption plays a key role in FBA because it simplifies the implementation of mass balances for each metabolite present in the metabolic network. In the previous section, mass balance equations are formed using equation (3.1). When the metabolites are also presented in a vector notation, equation (3.3) represents the reduced form of mass balance equation with steady state assumption used in this study where X is $m \times 1$ metabolite vector and t represents time.

$$\frac{dX}{dt} = S \cdot v = 0 \quad (3.3)$$

Equation (3.4) (Stephanopoulos *et al.*, 1998) shows the general form of mass balance of metabolites in the vector notation to reveal what reductions are made on this equation.

$$\frac{dX}{dt} = r - \mu X = S \cdot v \quad (3.4)$$

In Equation (3.4), X is the concentration vector of intracellular metabolites and r represents the net rates of formation of the metabolites in the metabolic network. The μX term shows the consumption rate of metabolites due to cell growth called dilution rate where μ is specific growth rate is constant. In addition, $\frac{dX}{dt}$ shows the change in concentrations of the metabolites over time. When the steady-state assumption is valid, this term is equal to zero because all metabolites have constant concentration over time. This assumption means that there is no metabolite accumulation within the metabolism. It is reasonable to make such an assumption in FBA because the reaction rates of intracellular metabolites is much higher than the dynamic changes outside of the cells due to the nature of enzymatic reactions in the cellular metabolism. It is accepted that enzymes present in organism have high turnover ratio and, therefore the metabolite pool can be conserved (Stephanopoulos *et al.*, 1998).

This results in a pseudo steady-state condition for cellular metabolism. In other words, the incoming fluxes of each intracellular metabolite pool balance the outgoing fluxes, which can be described as one linear equation for each intracellular metabolite shown in Figure 3.6-b. The rank theorem (Varma *et al.*, 1994), shown in equation (3.5), is used to determine the solution space of these linear equations where v is unknown flux vector to be solved.

$$F = n - \text{rank}(S) \quad (3.5)$$

In Equation (3.5), F represents the degree of freedom to show the solution space of stoichiometric matrix. Rank of the stoichiometric matrix determines the number of independent linear equations whereas n is the number of reactions within the metabolic network.

If n is equal to the rank of stoichiometric matrix (S), the system consisting of a set of independent linear equations is called determined and all unknown fluxes can be calculated in a unique solution.

However, the number of linearly independent equations (metabolites) is usually less than the number of unknown fluxes (reactions). This is the case of underdetermined systems which is also observed in this study. These systems imply infinitely many solutions because the degree of freedom (F) is greater than zero. In this work, n is equal to 148 and rank of the stoichiometric matrix is 121. The degree of freedom becomes 27 as seen in equation (6).

$$F = 148 - 121 = 27 \quad (3.6)$$

Therefore an optimization approach is preferred in order to estimate the unique solution. The optimization approach narrows the solution space using a specific objective function in the cell, hence a unique flux solution is obtained.

Maximal cell growth is mostly selected as a specific objective because it is presumably the most primary objective of a growing cell (Varma *et al.*, 1994). The implementation of the optimization approach will be detailed in the next section.

3.4.3 Optimization in Linear Programming

Optimization is incorporated into the mathematical representation of metabolic network constructed by FBA. The essentials of an optimization approach are constraints and a specific objective of the cell called an objective function expressed in mathematical form. This approach maximizes or minimizes the objective function subject to the constraints. The objective function and constraints are functions of some of the unknown fluxes in the v vector whereas constraints are additionally bounded by a lower and an upper value for a specific flux.

In this work, both objective function and constraints are linear with unknown flux variables; this approach is a problem of linear programming which solves optimization problem with linear algebraic equations. The most commonly used algorithm in linear optimization problems is the simplex method. However, the interior point method was used in this study instead of simplex method because of the structure of solution space. The following sections will explain the case of optimization problem in this study.

3.4.3.1 Objective Function and Constraints

The objective function is typically set to maximize the growth rate of the biomass since this is arguably the natural goal of the cell. However, the existence of other objective functions has been argued such as maximization of certain products, maximization of ATP production or minimization of substrate consumption.

Although the objective function can in principle be set to any condition possible in the metabolic network, it has been argued that this is not biologically realistic and the natural objective function is biomass growth (Feist *et al.*, 2010). Nevertheless, in this work, maximizing hydrogen production rate was also studied as an objective function in addition to maximizing the growth rate of *R. palustris*. However, the objective function of maximum hydrogen production is questionable and for this reason, with a few exceptions where stated, all the solutions in this work were obtained for the growth objective function. Appendix D shows the coefficients of metabolites related with the growth reaction of *R. palustris*.

In this work, the flux vector has a large range of initial solution space resulting in a large difference between its lower and upper bounds. This is because there is no well-defined rate limitation for a specific enzyme or a set of enzymes in the metabolic network of *R. palustris*. The lower and upper bounds in this work were chosen as -1000 and +1000, respectively.

These values are very high compared to the values of model inputs; here, the upper and lower bounds do not have a physical meaning for the biomass but rather, they are introduced to achieve convergence and obtain proper finite values. No solutions were found when unconstrained sets were used.

Reversible reactions in the metabolic network can have positive or negative flux values based on the direction of those reactions whereas irreversible reactions always have positive flux values. In the model of the present study, 50 out of 148 reactions are reversible and thus their resulting values can be positive or negative.

3.4.3.2 Optimization Algorithm

In spite of the fact that simplex method is the most commonly used optimization technique in linear programming, the interior point method was used as an optimization algorithm in this study. The main reason of the use of the interior point method is that the unknown flux vector might contain negative fluxes. This is not the case for simplex method which is used as long as all the variables must eventually have nonnegative values (Venkataraman, 2009). However, the iterative algorithm that takes place in the interior point method is similar to the simplex method. Both algorithms start off by identifying a feasible trial solution. At each iteration, the algorithm moves from the current trial solution to a better trial solution in the feasible region. It then continues this process until it reaches a trial solution that is essentially optimal (Hillier *et al.*, 2001).

When these algorithms are compared to each other, the difference originates from the nature of the trial solutions. In the simplex method, the trial solutions consist of corner point feasible (CPF) solutions. In other words, iterations move along the edges on the boundary of feasible region. On the other hand, the interior point method has trial solutions which are the points inside the boundary of feasible region and this is the reason it is referred to as interior point algorithm. The interior point method is alternatively referred to as a barrier algorithm because each constraint boundary is treated as a barrier for trial solutions in the interior points. Figure 3.8-a and b show graphical representation of solution spaces solved by simplex and interior point method, respectively.

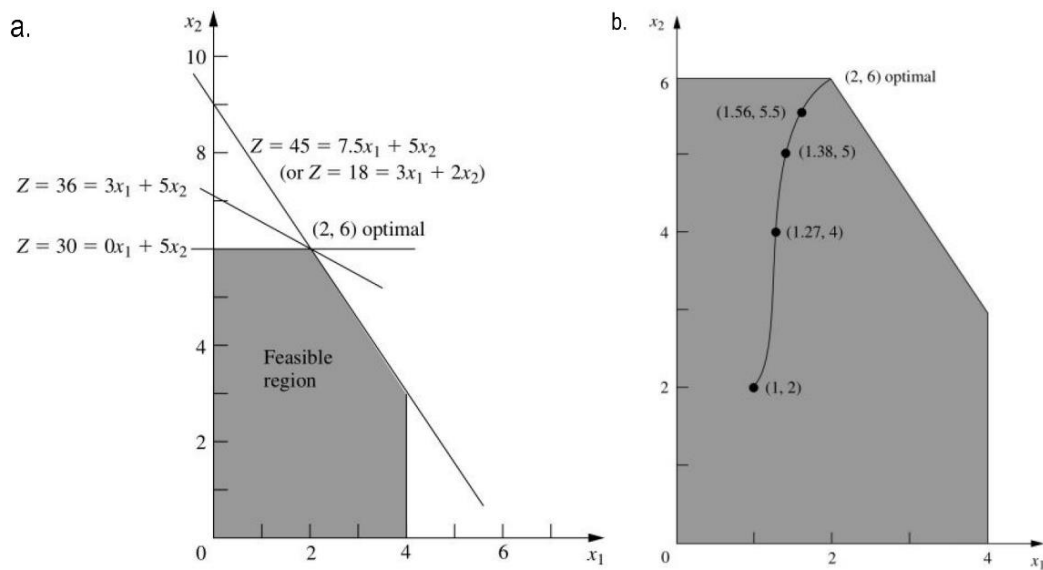


Figure 3.8: Graphical analysis of the iteration approach; a. Simplex method b. Interior point method (Hillier *et al.*, 2001)

Figure 3.8 illustrates the difference of the iteration approach between two algorithms. Interior point algorithm works in three main stages. Firstly it starts off through the interior of the feasible region toward an optimal solution. Then, it moves in a direction that improves the objective function value at the fastest possible rate. Lastly, it transforms the feasible region to place the current trial solution near its center, thereby enabling a large improvement when the previous stage is implemented. This algorithm is designed to solve huge problems efficiently. Considerably more extensive computations are required for each iteration to find the next trial solution.

The simplex method is known to be a more practical and faster algorithm for the routine use of linear programming because the optimum solution can be easily obtained through the corner constraints. However, when the corner or edges are not well defined, the simplex method becomes unreliable.

On the other hand, interior point starts from the interior and propagates to the borders, it has a better chance of reaching a solution. Therefore, an interior point approach is the most suitable algorithm for the linear optimization problem in this study.

3.5 Overall Modeling Procedure

In the present study, a modeling procedure was planned not only to construct the metabolic network but also to implement the network into a Flux Balance model. The modeling methodology followed is summarized in this section. In this procedure, there are mainly four different phases named as initial, preparation, development and result. Figure 3.9 shows these phases.

The initial phase is the investigation of the cellular metabolism in terms of metabolic pathways and their reactions. Growth conditions of *R.palustris* are identified from genome databases to construct the metabolic network. Pathways in the cellular metabolism are listed in standard notation to perform stoichiometric analysis.

For this purpose, the KEGG (Kanehisa *et al.*, 2015) and MetaCyc (Caspi *et al.*, 2014) databases were analyzed. Most reactions were obtained from the KEGG database whereas MetaCyc (Caspi *et al.*, 2014) and BRENDA (Schomburg *et al.*, 2013) databases are used to check the existence of some enzymes/reactions that are not available in KEGG database (Kanehisa *et al.*, 2015).

The preparation phase shows the procedure of stoichiometric analysis which determines the reactions that are included in the metabolic network. After selecting a reaction/enzyme among metabolic reactions in pathway maps, the genome is scanned for the selected enzyme coding reaction. If the enzyme is present in the genomic data of the bacteria, the reaction could be included. If not, literature data is additionally surveyed for that reaction. If the enzyme is reported to be present in literature, then it is also included. The reason of this additional search is that the used databases might not have been updated to include that enzyme.

If no relationship between the enzyme and genomic data is found, the selected reaction must be excluded. The development phase is followed after the iterative preparation phase. A metabolic network is formulated with the selected reactions. The stoichiometric matrix is constructed based on the metabolic network as previously explained. (Section 3.4.1) However, stoichiometric reductions should be made on the formulated network by following a strategy like the one given in 3.4.1. Then, preparation of stoichiometric matrix is finalized and an objective function is set to achieve linear optimization. (Section 3.4.3.1)

The fluxes are assumed to depend on an objective function and as discussed previously, the constraints were either the maximal growth of biomass or maximum hydrogen production.

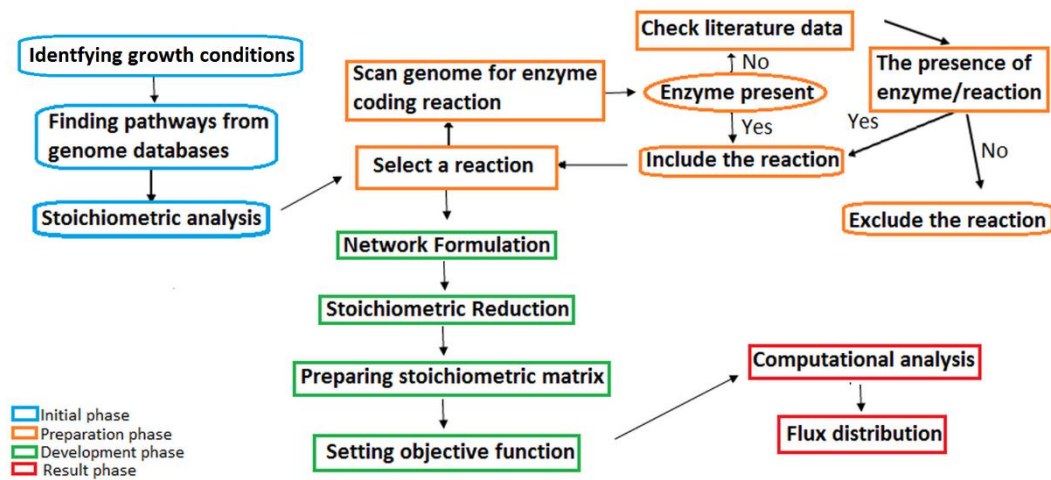


Figure 3.9: Schematic representation of modeling procedure

The result phase starts with a computational analysis where a simulation script is formulated considering principles of linear optimization programming with ‘linprog’ function of MatlabR2014b. Prior to the analysis of flux distribution over the metabolic network of *R.palustris*, a test case having a known flux distribution (Varma *et al.*, 1993b) was adapted into the Matlab script and the script was verified by reproduction of the known results. After that, stoichiometric matrix formed for the metabolism of *R.palustris* is loaded into the simulation in order to obtain a flux distribution which aims to interpret different metabolic phenotypes.

The determined flux distribution can be used to describe experimental results and to predict how cells will respond on their environment. The Matlab scripts used to obtain the resultant flux distributions are given in Appendix F.

CHAPTER 4

RESULTS AND DISCUSSION

4.1 Verification of the Simulation Script

A Matlab script to solve the flux balance analysis problem was written based on the methodology described in Chapter 3. Before applying the script to the *R. palustris* metabolic network, however, a test case was implemented to verify the proper operation of the script. In computational studies, a test case can be defined as a set of conditions with a verifiable solution, which allows validation of the software or model. Once the software program or system passes the test, the actual research case can be implemented with reasonable confidence in the reliability of the algorithm and the accuracy of results. To test the effectiveness and accuracy of the Matlab simulation script, a test case was tried where data from an existing analysis was reproduced. The flux distribution of a simplified network for *E. coli* aerobic respiration, originally computed and published by Varma *et al.* (1993b) was solved with the simulation script used in this study. The values obtained for the fluxes were almost identical to those given in the previously published results. The maximum growth rate was found to have a value of 0.58 g dry weight/h exactly equal to the results of Varma and Palsson (1993b). The results of the test case and comparison of the results with the previous published data are shown in Table 4.1. Accordingly, Figure 4.1 compares these two sets of results, and the graph displays a close match between the data.

Table 4.1: Comparison of flux distribution of test case to published data

Enzyme number	Enzyme abbreviation	Test Fluxes (mmol/h)	Published fluxes (mmol/h)
1	HK	5.55	5.55
2	PGI	0.66	0.38
3	PGIR	0	0
4	G6PDH	4.76	5.05
5	ALD	3.37	3.28
6	FDPASE	0	0
7	TRALD	1.48	1.58
8	TRALDR	0	0
9	TRKET	1.27	1.37
10	TRLETR	0	0
11	PGK	7.94	7.85
12	PGKR	0	0
13	PGM	7.06	6.97
14	PGMR	0	0
15	PYK	5.07	5.09
16	PEPSYN	0	0
17	PEPCK	0	0
18	PEPC	1.68	1.21
19	LACDH	0	0
20	LACDHR	0	0
21	PFLASE	3.45	3.79
22	PFLASER	0	0
23	PTACET	0	0
24	PTACETR	0	0
25	ACCOASN	0	0
26	ALCDH	0	0
27	PYRDH	0	0
28	CITSYN	1.2	1.11
29	MALSYN	0	0
30	ACO	1.2	1.11
31	ACOR	0	0
32	ISODHP	1.2	1.11
33	ISODHPR	0	0
34	ISOLYS	0	0
35	AKGDH	0.56	0.48
36	SCOASN	0.56	0.48
37	SCOASNR	0	0

Table 4.1 (continued):

Enzyme number	Enzyme abbreviation	Test Fluxes (mmol/h)	Published fluxes (mmol/h)
38	SUCCDH	0.56	0.48
39	FUMASE	0.56	0.48
40	FUMASER	0	0
41	MALDH	0.56	0.53
42	MALENZ	0	0
43	TRANSH2	0	0
44	TRANSH2R	0	0
45	NDH1	0	0
46	FDHASE	0.56	0.48
47	FORDH	3.4	3.28
48	CYT	14.6	15.2
49	ATPASE	0	0
50	ATPASER	19.6	19.9
51	VCO2	4.84	4.32
52	Growth Rate	0.58	0.58

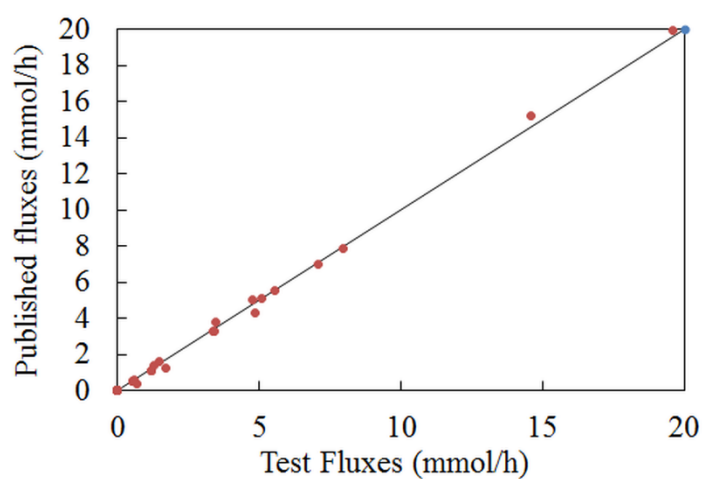


Figure 4.1: Graphical comparison between test fluxes and published fluxes

The schematic representation of the test network is given in Figure 4.2. Enzymes are defined with an abbreviation and the results are summarized in Figure 4.2. Definitions of enzyme abbreviations, coefficients of objective function and Matlab script for the test case are given as Appendix A. Based on the results of test case, the simulation script used in this work can be accepted to work properly.

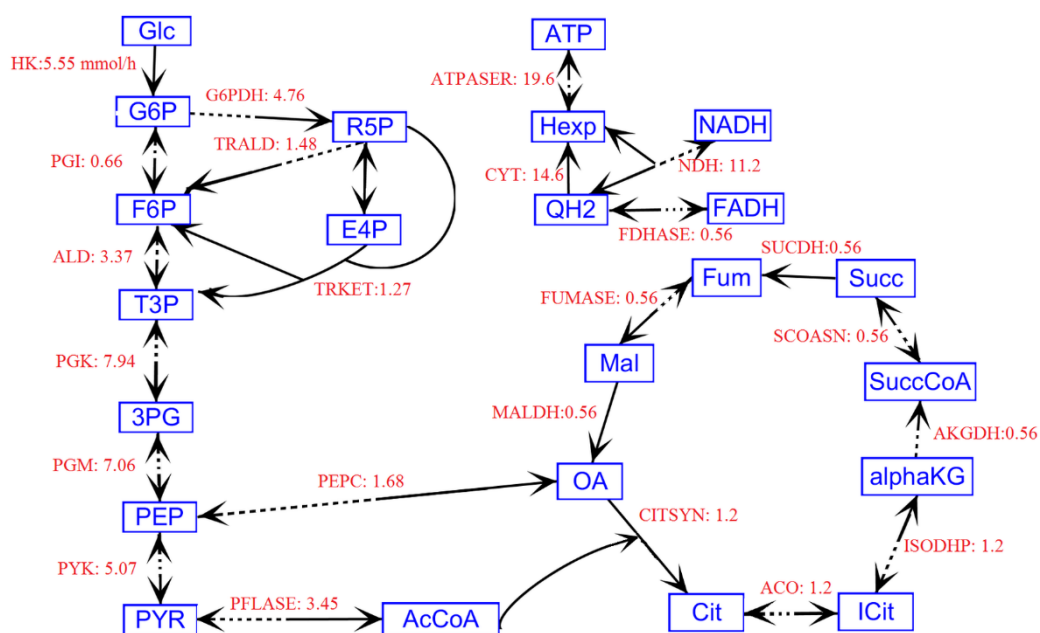


Figure 4.2: Linear optimization results for the test case using network of *E. coli* aerobic respiration (Varma and Palsson, 1993b); partially dashed arrows represent reversible reactions, with the solid portion of the arrow indicating the direction of the calculated flux.

In Figure 4.2, the values of fluxes are in mmol per unit time based on an initial glucose supply flux of 5.55 mmol (1g). Only non-zero fluxes are shown. After this preliminary test case, the case study of this work, namely the flux analysis for the network of *R. palustris* in anaerobic and photoheterotrophic growth modes, was carried out. The results are presented and discussed in the following sections.

4.2 Metabolic Network

The constructed metabolic network is a map showing the carbon utilization pattern of *R. palustris*. It forms the basis of the model on which substrate utilization routes, hydrogen productivities and conversion efficiencies can be evaluated with a mechanistic approach. The metabolic network of *R. palustris* was constructed through the reactions obtained from genome databases and the available literature, following the procedure explained in section 3.5. In this study, the metabolic model contains 148 reconstructed biochemical reactions within the metabolism based on 128 compounds. The list of these compounds and reactions are given in Appendix B. The metabolic network includes sucrose pathway, the pentose phosphate pathway, glycolysis, Calvin cycle, TCA cycle, PHB, synthesis, lumped biosynthetic reactions, photosynthetic reactions and hydrogen production reactions.

The pathways which maltose, pectin and cellulose are consumed and the pathways that require the aerobic respiration were not included in the metabolic network. These pathways are not active in the metabolism of *R. palustris*.

In the central metabolic network, sucrose was considered as the primary carbon source and glutamate the nitrogen source in a growth medium with low nitrogen to carbon ratio, to emulate typical conditions used for hydrogen production. Figure 4.3 represents the constructed carbon flow. Reactions were numbered in the same order of the reaction list given in Appendix B.3.

Metabolites are shown with their names in colored boxes. Black boxes have biosynthetic precursors for biomass growth. Metabolites reacting at different part of the network are shown with different colors to represent the network two dimensional.

In Figure 4.3, each pathway was named with letters A-F to identify its region on the metabolic network. Carbon utilization starts with external sucrose in the 120th reaction. Sucrose is broken down to Glucose-6 phosphate in sucrose pathway (A). Glucose-6 phosphates enter glycolysis (B) and the pentose phosphate pathway (C), which are parallel to each other until producing 3-Phospho D-glycerate. The pentose phosphate pathway (C) is peculiar to *R. palustris* among the PNS bacteria. Following 3-Phospho D-glycerate, carbons are utilized in the Calvin cycle (D) which is a series of biochemical redox reactions to fix the CO₂ evolved. Lastly, organic acids are produced in TCA cycle (E). In the TCA cycle, the 39th and 40th reactions are called the ‘glyoxylate shunt’ which is observed only in the metabolism of *R. palustris*. ATP, CO₂ and electrons are produced and consumed throughout these pathways. Electrons are fed by electron carriers (NAD, FAD) to the reactions on the metabolic network. Residual electrons and ATP are consumed for hydrogen production by nitrogenase and hydrogenase enzymes. In addition, the production of PHB (F) was also observed in the model results. PHB synthesis reduces fluxes in the TCA cycle by sharing electrons. The resulting flux distributions for each case previously defined are listed with the corresponding reaction number in Appendix B.3.

Photosynthetic reactions and hydrogen production reactions are not shown in Figure 4.3 because these reactions are out of the central reaction network. These reactions will be explained in the section of base case results (Section 4.3.2).

4.3 Description of Cases and Results for the Base Case

This section describes input fluxes and different cases applied to the model to understand the effects of changes in the growth conditions of the bacteria on the estimated flux distributions. Additionally, flux distribution of the base case is provided in this section specifically including evaluation of two objective functions used in the model, photosynthetic reactions, hydrogen production reactions and sensitivity analysis.

4.3.1 Inputs and List of Cases

The input and output parameters used for FBA are defined in Table 4.2. An experimental work carried out by Sagir (2012) was used to provide the input parameters (known fluxes). This work inspired the construction of metabolic model in the present study and therefore model inputs were determined based on the experimental conditions. The same work also formed the basis of comparison between the model calculation results which are unknown fluxes estimated by FBA in the present study and their counterparts obtained by Sagir (2012). There are three main input fluxes calculated from the actual values of the bacterial growth medium used in a previous experimental hydrogen production setup with *R. palustris* as the microorganism (Sagir, 2012); the glutamate uptake rate, the initial sucrose consumption rate and the photon flux all in units of mmol/h per culture liter. The calculations of these input parameters are given in Appendix E.

In the present work, the effect of individual parameters (Glutamate uptake rate, initial sucrose consumption rate and photon flux) was evaluated on significant output fluxes shown in Table 4.2.

Table 4.2: Control parameters of stoichiometric model

Parameter name	Units	Type
Glutamate uptake rate	mmol/h	Input (experimental data)
Initial sucrose consumption rate	mmol/h	
Photon flux	mmol/h	
Biomass production rate	gdcw/h	Output (Calculated by the model)
Hydrogen production rate	mmol/h	
CO ₂ production rate	mmol/h	
PHB production rate	mmol/h	
Acetic acid production rate	mmol/h	
Lactic acid production rate	mmol/h	
Formic acid production rate	mmol/h	

Table 4.3 lists different cases studied the effect of changes in input fluxes on the significant outputs. The base case represents the experimental condition of hydrogen production setup with bacterial growth medium of *R. palustris* previously used by Sagir (2012). Therefore, the base case can also be defined as the comparison case.

Table 4.3: List of model cases

Case	Glutamate uptake rate (mmol/h)	Initial sucrose flux (mmol/h)	Photon flux (mmol/h)	Organic acid uptake rate (mmol/h)
0 (Base)	0.1	0.25	5	0
1	varies	0.25	5	0
2	0.1	varies	5	0
3	0.1	0.25	varies	0
4	0.1	0.25	5	varies

In the base case, an initial sucrose consumption flux of 0.25 mmol/h corresponds to 5 mM initial sucrose concentration. The glutamate uptake rate is 0.1 mmol/h, which corresponds to 2 mM initial glutamate concentration. Photon flux is 5 mmol/h assumed as constant from a light source (e.g. a tungsten lamp). The photon flux is calculated considering the experimental illumination (2100 lux) by tungsten lamps. These numbers are based on a culture volume of 50 ml, typically used in the experimental systems of Sagir (2012).

The input fluxes of other cases are similar to base case expect the individual variations in the input fluxes specific to each case. Case 2, 3 and 4 represent the effect of initial glutamate uptake rate, initial sucrose flux, photon fluxes and organic acid fluxes, respectively, on the significant output fluxes previously mentioned in this section. These cases will be discussed in the next sections in detail (Section 4.5.1-4.5.4). The following section will analyze the carbon flow in the metabolism including base case results.

4.3.2 Base Case Results

The fluxes are obtained for an objective function such as maximal growth of biomass or maximum hydrogen production. In the model, these two objective functions were investigated in particular. The resulting flux distributions for both objective functions are shown in Table 4.4 in mmol/h based on 0.25 mmol/h sucrose, 0.1 mmol/h glutamate and 5 mmol/h photon flux (input parameters of base case).

Flux Distribution of the Base Case

The growth rate (147th flux) was the same (0.0118 g dry cell weight/h) for two different objective functions, presumably due to the nitrogen limitations. Bacterial growth is accepted to occur in 3 phases, namely the lag phase, exponential phase and stationary phase. In the lag phase, cell are only increasing their size, therefore, modeling is not appropriate for this growth phase.

In the exponential phase, the presence of carbon and nitrogen sources brings fast bacterial growth. Stationary phase is a period when bacteria consumes the remaining nitrogen sources from the exponential growth rate until their depletion. As objective functions of the model, maximum biomass production rate takes place in the exponential phase whereas maximum hydrogen production rate is observed in both late exponential phase and stationary phase (Waligorska *et al.*, 2009). In the model, it may be speculated that the nitrogen-limited environment causes; short exponential phase and low biomass growth rate. This situation brings the point of maximum biomass growth rate closer to the point of maximum hydrogen production rate. Therefore, having same growth rate for two different objective functions is expected in the case of low nitrogen to carbon ratio.

Table 4.4 shows the flux distributions based on the maximum biomass growth rate (Obj 1) and maximum hydrogen production rate (Obj 2). The bold-italic flux values are results that are exactly the same for both objective functions. Some reactions in the Calvin cycle (3rd, 5th, 8th and 10th), reaction for synthesis of the biomass (62nd - 107th) and sucrose uptake reactions (120th – 122th) were observed to have same flux values. As seen from Table 4.4, 16 fluxes, especially those in the sucrose and pentose phosphate pathways, become zero when the objective function is switched to maximization of hydrogen production. Most of these reactions consume electrons. Furthermore, the direction of the 57th reaction is reversed into consuming formic acid that has been generated intracellularly. Other organic acids (acetic and lactic acids) are also observed to be depleted. Although the fluxes for biosynthetic precursors (62nd -107th) did not change due to nitrogen limitations, the flux of some reactions (i.e. 43th and 44th) supplying electrons increases. Therefore, the number of electrons in the metabolism increases and a higher hydrogen production rate (110th flux) was obtained in the case of objective 2.

Next, as important part of hydrogen production in the bacteria, photosynthetic reactions and hydrogen production reactions are defined and discussed, specifically focusing on their resultant fluxes estimated in the base case.

Table 4.4: The resulting fluxes of all reactions in the metabolic network

(Obj 1: Maximization of biomass growth, Obj 2: Maximization of hydrogen production)

Flux number	Obj 1	Obj 2	Flux number	Obj 1	Obj 2	Flux number	Obj 1	Obj 2
1	71.5	76.9	50	-0.0012	0	99	0.00016	0.00016
2	71.5	76.9	51	0.008	0.007	100	0.00052	0.00052
3	-0.0097	-0.0097	52	-65.9	-66.8	101	0.00026	0.00026
4	71.5	76.9	53	-75.3	-74.6	102	0.0038	0.0038
5	-0.0097	-0.0097	54	-75.3	-74.7	103	0.00014	0.00014
6	71.5	76.9	55	75.3	74.7	104	0.0039	0.0039
7	62.4	65.4	56	0.001	0	105	0.0089	0.0089
8	0.0077	0.0077	57	0.0376	-0.0364	106	0.0089	0.0089
9	-62.4	-65.4	58	0.0012	0	107	0.0027	0.0027
10	0.0075	0.0075	59	0.0006	0.0005	108	0.11	0.53
11	142.9	153.7	60	0.0051	0.0044	109	0.048	0.025
12	-0.117	-0.126	61	0.0123	0.0117	110	0.68	0.82
13	0.118	0.126	62	0.0039	0.0039	111	2.5	2.5
14	194.2	192.2	63	0.0058	0.0058	112	2.5	2.5
15	180.6	180.8	64	0.0043	0.0043	113	-21.5	-21.4

Table 4.4 (continued):

Flux number	Obj 1	Obj 2	Flux number	Obj 1	Obj 2	Flux number	Obj 1	Obj 2
16	71.5	76.9	65	<i>0.0046</i>	<i>0.0046</i>	114	1.217	5.078
17	95.0	96.1	66	<i>0.0025</i>	<i>0.0025</i>	115	-960.6	-958.7
18	38.4	37.7	67	<i>0.029</i>	<i>0.029</i>	116	479.2	478.8
19	32.6	30.7	68	<i>0.0035</i>	<i>0.0035</i>	117	290.8	289.8
20	65.8	61.6	69	<i>0.0016</i>	<i>0.0016</i>	118	-81.4	-90.7
21	-142.9	-153.7	70	<i>0.0056</i>	<i>0.0056</i>	119	1.942	0.0101
22	-62.4	-65.4	71	<i>0.0029</i>	<i>0.0029</i>	120	<i>0.037</i>	<i>0.037</i>
23	-36.5	-35.4	72	<i>0.00097</i>	<i>0.00097</i>	121	<i>0.037</i>	<i>0.037</i>
24	27.5	23.9	73	-0.014	-0.020	122	<i>0.039</i>	<i>0.037</i>
25	71.4	76.8	74	<i>0.016</i>	<i>0.016</i>	123	188.3	188.9
26	-71.5	-76.9	75	<i>-0.00077</i>	<i>-0.00077</i>	124	<i>0.00016</i>	<i>0.00016</i>
27	-116.8	-112.0	76	<i>0.003</i>	<i>0.003</i>	125	0.0015	0
28	36.5	35.4	77	<i>0.00058</i>	<i>0.00058</i>	126	0.0015	0
29	36.5	35.4	78	<i>0.0014</i>	<i>0.0014</i>	127	188.3	188.9
30	79.4	78.2	79	<i>0.0019</i>	<i>0.0019</i>	128	188.3	188.9
31	-34.9	-33.1	80	0.00295	0.00362	129	208.2	207.1
32	-0.188	-0.201	81	<i>0.0025</i>	<i>0.0025</i>	130	188.3	188.9

Table 4.4 (continued):

Flux number	Obj 1	Obj 2	Flux number	Obj 1	Obj 2	Flux number	Obj 1	Obj 2
33	21.4	21.7	82	<i>0.0109</i>	<i>0.0109</i>	131	19.9	18.2
34	65.7	66.6	83	<i>0.0072</i>	<i>0.0072</i>	132	0.0019	0
35	0.18	0.19	84	<i>0.005</i>	<i>0.005</i>	133	0.0019	0
36	57.2	53.6	85	<i>0.0022</i>	<i>0.0022</i>	134	0.00096	0
37	43.4	42.1	86	<i>0.0017</i>	<i>0.0017</i>	135	0.0019	0
38	-0.084	-0.096	87	<i>0.0032</i>	<i>0.0032</i>	136	0.0028	0
39	0.084	0.096	88	<i>0.0002</i>	<i>0.0002</i>	137	-0.0044	0
40	65.7	66.6	89	<i>0.0004</i>	<i>0.0004</i>	138	-0.0019	0
41	-65.6	-66.5	90	<i>0.0006</i>	<i>0.0006</i>	139	24.5	22.2
42	0.028	0.026	91	<i>0.0002</i>	<i>0.0002</i>	140	24.5	22.2
43	292.8	305.0	92	<i>0.0023</i>	<i>0.0023</i>	141	0.21	0.21
44	227.2	238.6	93	<i>0.0054</i>	<i>0.0054</i>	142	0.00053	0
45	67.2	66.5	94	<i>0.00025</i>	<i>0.00025</i>	143	0.00053	0
46	1.68	0.043	95	<i>0.00025</i>	<i>0.00025</i>	144	0.0036	0
47	-304.0	-318.0	96	<i>0.00025</i>	<i>0.00025</i>	145	0.41	0.52
48	304.0	318.0	97	<i>0.00025</i>	<i>0.00025</i>	146	0.0011	0
49	76.8	79.5	98	<i>0.00025</i>	<i>0.00025</i>	147	0.0118	0.0118
						Growth rate:	gdcw/h	gdcw/h

Photosynthetic Reactions

Photosynthetic reactions occur in the membrane between periplasm and central metabolism of the bacteria using external photons. Table 4.5 shows photosynthetic reactions considered in the model and their resulting fluxes with respect to the base case mentioned in section 4.3.1.

Table 4.5: Photosynthetic reactions and their resultant fluxes

Reaction number	Reaction	Flux (mmol/h)
111	$2 \text{ photon} + \text{Q} + 2 \text{ c}_2^{2+} \rightarrow \text{QH}_2 + 2\text{c}_2^{+3}$	2.5
112	$\text{QH}_2 + 2\text{H}_i^+ + 2\text{c}_2^{+3} \rightarrow 2 \text{ c}_2^{2+} + \text{Q} + 4\text{H}_p^+$	2.5
113	$\text{NADH} + \text{Q} + 5\text{H}_i^+ \leftrightarrow \text{QH}_2 + 4\text{H}_p^+ + \text{NAD}^+$	-21.5
114	$\text{ADP}^{3-} + \text{Pi}^{2-} + 3\text{H}_p^+ \rightarrow \text{ATP}^{4-} + \text{H}_2\text{O} + 2\text{H}_i^+$	1.2
35	$\text{Succinate} + \text{Q} \leftrightarrow \text{Fumarate} + \text{QH}_2$	0.18

Photons, with flux 5 mmol/h (for base case), are captured in the reaction center (111th reaction). The 111th and 112th reactions have fluxes in same magnitude and direction because they are sub-sequential. Moreover, the flux of the 113th reaction is higher than other reactions because the reaction binds the central metabolism to the membrane of the bacteria using the electron carrier (NADH). It pumps the protons to the cytoplasm because its sign is negative. Table 4.5 also shows that ATP production rate (1.2 mmol/h) is lower than photon flux. These results were obtained in the case of maximization of biomass growth as objective function. When the objective function is the maximization of hydrogen production, the fluxes had exactly the same values shown in Table 4.5.

Hydrogen Production Reactions

Hydrogen is produced by nitrogenase and hydrogenase enzymes using excess electrons and ATP in the metabolism. As different from other PNS bacteria, the genome sequence of *R. palustris* (wild type) shows genes encoding three nitrogenase isozymes having different metals in their active sites (Mo, V and Fe). The alternative nitrogenase enzymes were also considered in the model because their presence was supported by the Microarray analysis of *R. palustris* cells in the case of nitrogen starvation similar to this modeling case (McKinlay, 2014). All nitrogenase isozymes demand equal number of electrons for H₂ production. The hydrogen production reactions and the resultant fluxes are shown in Table 4.6.

Table 4.6: Reactions for hydrogen production with their resulting fluxes

Enzyme	Reaction	Flux (mmol/h)
Mo-Nitrogenase	$-16\text{ATP} + 8\text{H}^+ + 8\text{e}^- \rightarrow 16\text{ADP} + 4\text{H}_2$	0.048
V- Nitrogenase	$-16\text{ATP} + 8\text{H}^+ + 8\text{e}^- \rightarrow 16\text{ADP} + 4\text{H}_2$	0.048
Fe- Nitrogenase	$-16\text{ATP} + 8\text{H}^+ + 8\text{e}^- \rightarrow 16\text{ADP} + 4\text{H}_2$	0.048
Hydrogenase	$2\text{H}^+ + 2\text{e}^- \rightarrow \text{H}_2$	0.11

R. palustris has an inactive uptake hydrogenase enzyme as different from other PNS bacteria. In other words, the reaction of hydrogenase is expected to irreversibly produce hydrogen similar to the reaction of nitrogenase. As can be seen in Table 4.6, both hydrogenase and nitrogenase fluxes were positive, which means both enzymes are capable of hydrogen production. Thus, the model results confirm this information, producing positive fluxes for hydrogenase.

Moreover, Table 4.6 shows that the hydrogen production rate of one of the nitrogenase isoenzymes (0.047 mmol/h) is lower than the hydrogen production rate of hydrogenase (0.11 mmol/h). This agreed with the literature information stating catalytic rate of nitrogenase is lower than the rate of hydrogenase (Basak *et al.*, 2007).

On the other hand, when the objective function is the maximization of hydrogen production, the rate of nitrogenase was obtained as 0.025 mmol/h, which is lower than its value for the case where the objective function is the maximization of biomass growth. However, the rate of hydrogenase was 0.59 mmol/h, which is higher than the value shown in Table 4.6.

4.3.3 Sensitivity Analysis

Sensitivity analysis is a technique to determine how uncertainty in the output of a model can be attributed to uncertainty in the input to the metabolism (Loucks *et al.*, 2005). In this work for example, one question of sensitivity analysis is how uncertainty in the glutamate uptake rate would affect the specific growth rate and the hydrogen production rate of bacteria, which are target output variables in this model. Glutamate uptake rate is selected as the uncertain input parameter because glutamate is the limiting nutrient due to the low nitrogen to carbon ratio in the bacterial culture.

As with all experimental data, the input fluxes calculated from the data of Sagir (2012) are subject to uncertainty. Therefore it is useful to test the impact of this uncertainty by varying the input fluxes and observing the resulting deviations in the significant output fluxes. In other words, the sensitivity of the results to perturbations in the input needs to be considered.

Sensitivity analysis was performed by slightly changing the initial glutamate uptake rate by +/- 10%. Table 4.7 shows three different values for glutamate uptake rate and their effects on the output values.

The glutamate uptake rates of 0.09, 0.1 and 0.11 mmol/h were chosen to analysis sensitivity of glutamate uptake rate in the growth media to specific growth rate and hydrogen production rate. This analysis was studied by considering both objective functions which are maximum specific growth rate and maximum hydrogen production rate of the bacteria.

Table 4.7: Results of sensitivity analysis based on slight changes in initial glutamate uptake rate (Values in parentheses indicate reduction/increase as a result of the perturbation)

Output fluxes	Glutamate uptake flux		
	0.09 mmol/h	0.1 mmol/h	0.11 mmol/h
Specific growth rate (gdcw/h)	0.0107 (-%9.3)	0.0118	0.013 (+%10.2)
Hydrogen production rate ^a (mmol/h)	0.61 (-%10.3)	0.68	0.75 (+%10.3)
Maximum hydrogen production rate ^b (mmol/h)	0.70 (-%10.3)	0.78	0.86 (+%10.3)

^a Using biomass growth as the objective function

^b Using hydrogen production as the objective function

In Table 4.7, specific growth rate is maximum growth rate of the bacteria obtained when the objective function is maximization of biomass growth with each specific glutamate uptake rate as input parameter. Hydrogen production rates are also obtained in the same manner. Maximum hydrogen production, on the other hand, is the hydrogen produced when the objective function is the maximization of hydrogen production rate with each specific glutamate uptake rate as the input parameter.

The results of the analysis show that output fluxes are affected linearly by 10% changes in the glutamate uptake rate. This is expected due to the linear nature of the optimization procedure. Therefore, the strong dependency of the hydrogen production metabolism of *R. palustris* on glutamate uptake rate is confirmed. To verify the model results, the detailed comparison of experimental and computed production rates will be shown in the next section.

4.4 Comparison with Experimental Results

The performance of the model was tested using the selected output parameters (Table 4.2). For this purpose, experimental data in a recent study (Sagir, 2012) was used to assess and compare to the model results. In the experimental study, biological hydrogen production from sucrose and molasses by PNS bacteria was investigated. *R. palustris* was tested on sucrose and molasses in 50 ml small-scale batch photobioreactors during 200 hours. Sagir reported the time dependent profiles of the medium pH, bacterial growth and hydrogen production. In addition, acetic acid, formic acid and lactic acid were found as end products of the photofermentation of *R. palustris* on sucrose and molasses and their production was also monitored in that study. In the experiments containing sucrose, *R. palustris* was grown for hydrogen production on different sucrose concentrations at 5 mM, 7.5 mM and 10 mM.

In the model, sucrose and glutamate were used as carbon and nitrogen sources to emulate typical conditions for hydrogen production. For comparison with the previously resulted experimental data, the moments of maximum bacterial growth rate (24th hour) and maximum hydrogen production rate (48th hour) for 5 mM sucrose were considered because FBA allows to obtain the fluxes at a single time point subject to the steady-state approximation. Table 4.8 shows the experimental and computed production rates with sucrose concentration and glutamate concentration at 5 mM and 2 mM, respectively.

Table 4.8: Experimental and computed output parameters for the base case

Control parameters	Units	Experimental result	Model result
Biomass production rate	(gdcw/h)	0.0104	0.0118
Hydrogen production rate ^a	(mmol/h)	0.70	0.68
Max H ₂ production ^b	(mmol/h)	0.86	0.83
Acetic acid production	(mmol)	0.004-0.108	0.0128
Lactic acid production	(mmol)	0.008-0.09	0.0127
Formic acid production	(mmol)	0.02-0.12	0.087
Sucrose conversion efficiency	-	53%	56%

^a Using biomass growth as the objective function

^b Using hydrogen production as the objective function

Table 4.8 indicate that the model results agreed well with experimental data. The experimental values of biomass production rate and hydrogen production rate in Table 4.8 are those reported at the 24th hour of the bacterial growth, which corresponds to the maximum biomass production rate. Biomass production rate was calculated using the average cell concentration at 24th hours of the experimental hydrogen production. However, the values of Maximum Hydrogen production are considered when the hydrogen production rate is maximum at the 48th hour for cultures grown in 5mM sucrose media.

In the case of organic acid productions (Acetic acid, Lactic acid and Formic Acid), the 24th hour of the bacterial growth is considered, similar to Biomass production rate and Hydrogen production rate. Rather than single values, ranges are given for experimental organic acid productions because Sagir (2012) measured the concentrations of organic acids at only the 0th, 72nd and 144th hours of bacterial growth.

Therefore, the lower and upper values of the ranges given in the tables correspond to the organic acid fluxes at 0 and 72nd hours of the experimental data, which is the targeted time period for this model.

In Table 4.8, the calculated percent errors between the experimental and model results are 11.8, 2.9, 4.2 % for biomass production rate, hydrogen production rate and maximum hydrogen production rate, respectively. Furthermore, organic acid productions are in the given range of experimental results.

Additionally, sucrose conversion efficiency was calculated from the estimated sucrose uptake flux of the base case and compared with the efficiency resulted by Sagir (2012). The sucrose uptake rate was found to be 0.037 mmol/h as seen from the flux distribution (120th flux) in Table 4.4. For the model, substrate (sucrose) conversion ratio is defined as estimated hydrogen production rate (0.68 mmol/h) divided by theoretical hydrogen production rate (1.2 mmol/h) calculated based on overall reaction of hydrogen production. Therefore, sucrose conversion efficiency was calculated as 56%, which is very close to the experimental efficiency (53 %). The detailed calculation is shown in Appendix E.4.

As a conclusion of this section, the model results revealed good agreement with experimental data previously obtained. This shows that the model is a reliable tool to understand carbon utilization patterns in PNS bacteria.

The distribution of modelled fluxes will help to explain the capability of the hydrogen production on sucrose by *R. palustris* as well as the effects of changes in the growth conditions of the bacteria on biomass production. The following sections are about effects of initial glutamate, sucrose, photon and organic acid fluxes on production rate of output parameters previously defined in Table 4.2.

4.5 Effect of Individual Parameters

This section covers the effect of individual parameters such as glutamate uptake rate, initial sucrose concentration, photon flux and organic acid concentration in the bacterial culture on significant output fluxes previously defined in section 4.3.1.

4.5.1 Glutamate Uptake Rate

Glutamate is one of the essential amino acids of proteins in organisms. Bacterial cells require glutamate for their metabolic processes to multiply. Glutamate is either produced within the metabolism of the bacteria from another nitrogen source (e.g. Ammonium) or directly given to cells through their growth media. In this model, glutamate was externally used as the nitrogen source, which is a typical choice for experimental hydrogen production studies. The range of glutamate uptake rate was found to be 0.065-0.65 mmol/h for a flux distribution based on 0.25 mmol/h initial sucrose flux and 5 mmol/h photon flux. This range corresponds to 1.3 mM – 13 mM initial glutamate concentration. The effect of glutamate uptake rate on the specific growth rate, sucrose uptake rate, H₂ production rate, PHB production rate, CO₂ production rate and the production rates of organic acids (acetic acid, lactic acid and formic acid) have been obtained from simulation results considering both maximum biomass growth and maximum hydrogen production separately as the objective functions.

Figure 4.4 shows the effect of glutamate uptake rate on specific growth rate of biomass at constant sucrose concentration and photon flux. In Figure 4.4, specific growth rate of biomass linearly increases with increasing glutamate uptake rate for both objective functions used.

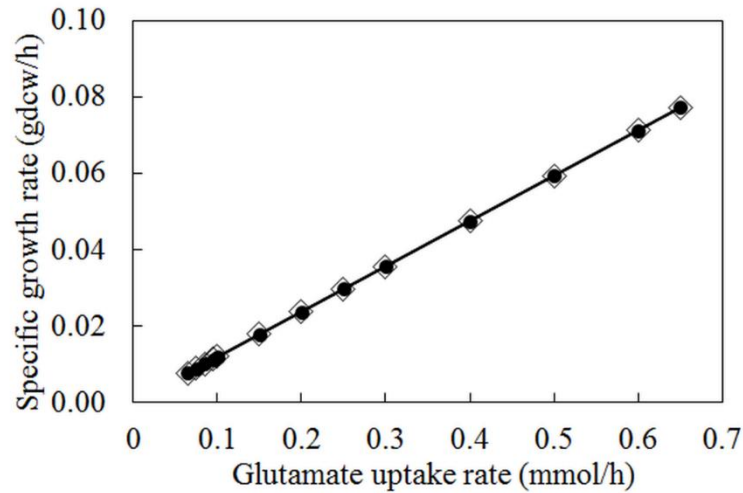


Figure 4.4: Specific growth rate of biomass as a function of glutamate uptake rate for two objective functions (● : Maximum biomass growth, ◊ : Maximum hydrogen production)

When the initial glutamate flux was lower than 0.065 mmol/h, no solution was found because presumably the bacteria could not support growth at these levels of the nitrogen source. There is a minimum threshold amount of nitrogen source to maintain biomass growth with the limited sucrose consumption (Zhang *et al*, 2015). On the other hand, 0.25 mmol/h sucrose was not enough at glutamate uptake rates higher than 0.65 mmol/h. This can be observed in Figure 4.5 where it can be seen that the sucrose uptake rates have to be extrapolated beyond 0.25 mmol/h to supply sufficient carbon when glutamate uptake rates are higher than 0.65 mmol/h. Sucrose uptake rate seems to be close to zero when glutamate uptake rate is 0.065 mmol/h in Figure 4.5. At 0.65 mmol/h of glutamate uptake rate, sucrose uptake rate is approximately 0.25 mmol/h which is the available sucrose flux computed initially. These results indicate that bacteria should have sufficient nitrogen source (glutamate) to use external sucrose, thereby promoting biomass growth.

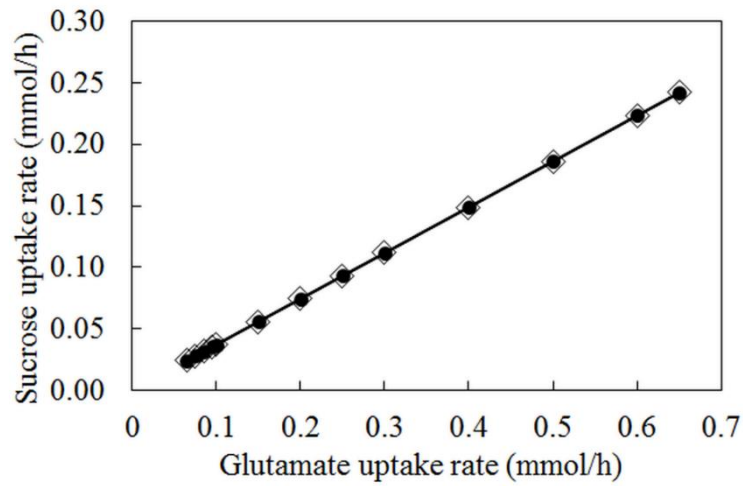


Figure 4.5: Sucrose uptake rate of biomass as a function of glutamate uptake rate for two objective functions (● : Maximum biomass growth, ◇ : Maximum hydrogen production)

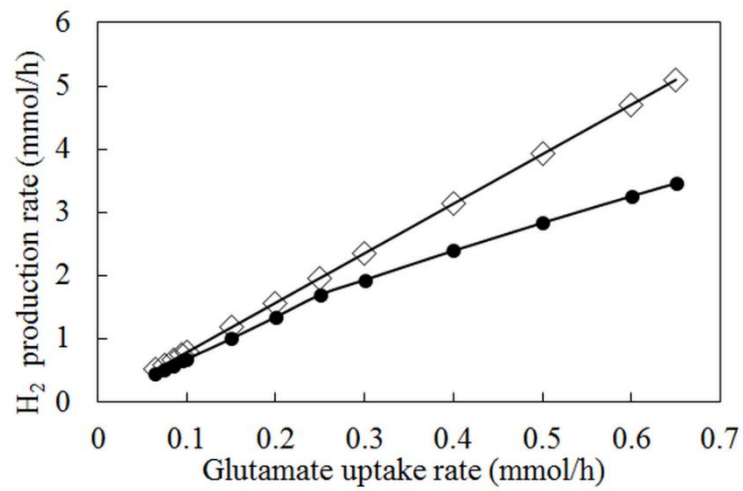


Figure 4.6: Hydrogen production rate as a function of glutamate uptake rate for two objective functions (● : Maximum biomass growth, ◇ : Maximum hydrogen production)

Figure 4.6 shows the changes in hydrogen production rate of biomass when the glutamate uptake rate increases. In general, hydrogen production rate increases linearly with glutamate uptake rate for both objective functions. The deviation in the hydrogen production rate between the two objective functions increases for higher glutamate uptake rates. In addition, the slope of the line for maximum biomass growth exhibits a slight decrease for glutamate uptake rates higher than 0.25 mmol/h. This is because the bacteria also use organic acids obtained as a result of metabolic reactions. This was not observed for the case of maximum hydrogen production because the metabolism uses all available carbon sources including organic acids to produce the maximum hydrogen.

In Figure 4.7, PHB production is plotted with respect to the glutamate uptake rate. For the case of maximum biomass growth, PHB production increases with increasing glutamate uptake rate. PHB production is experimentally observed to increase in the presence of organic acids as additional carbon sources (Wu *et al.*, 2012). However, PHB production is zero in the case of maximum hydrogen production because the organic acids are also used for hydrogen production by bacteria.

Figure 4.8 shows that the CO₂ production rate increases with glutamate uptake rate for two objective functions used. This is because 9 biosynthetic reactions (62th -107th reactions in Figure 4.3) produce CO₂ whereas only 3 of them consume CO₂. Therefore, CO₂ production rate increases with increasing fluxes of biosynthetic reactions resulting from high glutamate uptake rate. However, CO₂ production rate is higher in the case of maximum hydrogen production. The reason of this deviation is that the flux of formic acid production (57th reaction) becomes zero and CO₂ is not consumed to produce formic acid in the case of maximum hydrogen production.

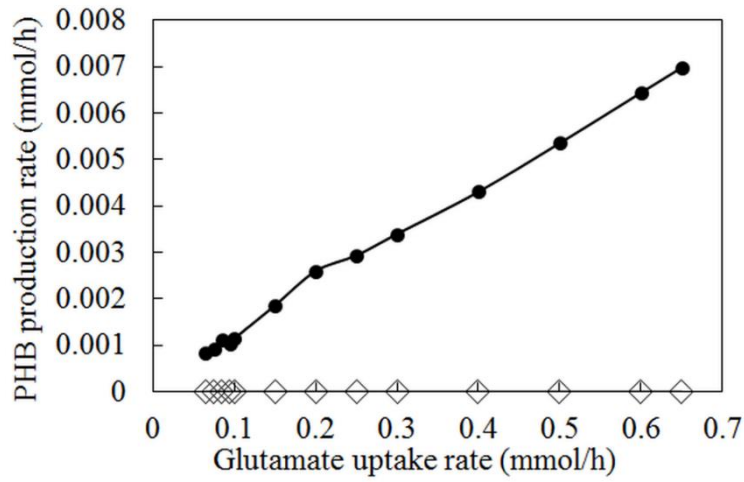


Figure 4.7: PHB production rate as a function of glutamate uptake rate for two objective functions (—● : Maximum biomass growth, —◇ : Maximum hydrogen production)

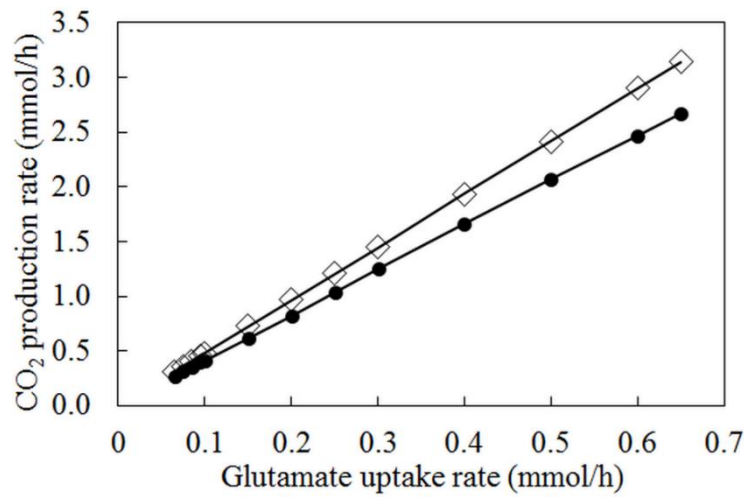


Figure 4.8: CO₂ production rate as a function of glutamate uptake rate for two objective functions (—● : Maximum biomass growth, —◇ : Maximum hydrogen production)

The production rates of organic acids (acetic acid, lactic acid and formic acid) are shown in Figures 4.9-a, b and c. Their production rates increase with glutamate uptake rate in the case of maximum biomass growth whereas organic acid production is not observed in the case of maximum hydrogen production. The fluctuation in Figure 4.9-a after the glutamate uptake of rate 0.2 mmol/h is caused by the increase in acetaldehyde production from acetate (50th reaction). Therefore, acetic acid production rate is slightly reduced.

At high glutamate uptake rates, lactic acid is linearly produced from acetaldehyde via 58th reaction. Lactic acid production rates are lower than acetic acid production rates because lactic acid is produced from the product (Acetaldehyde) of one of the acetic acid reactions (50th reaction). In Figure 4.9-c, the profile of formic acid production is very similar to the CO₂ production rate with respect to the glutamate uptake rate in Figure 4.8. This is because formic acid is produced from CO₂ (57th reaction).

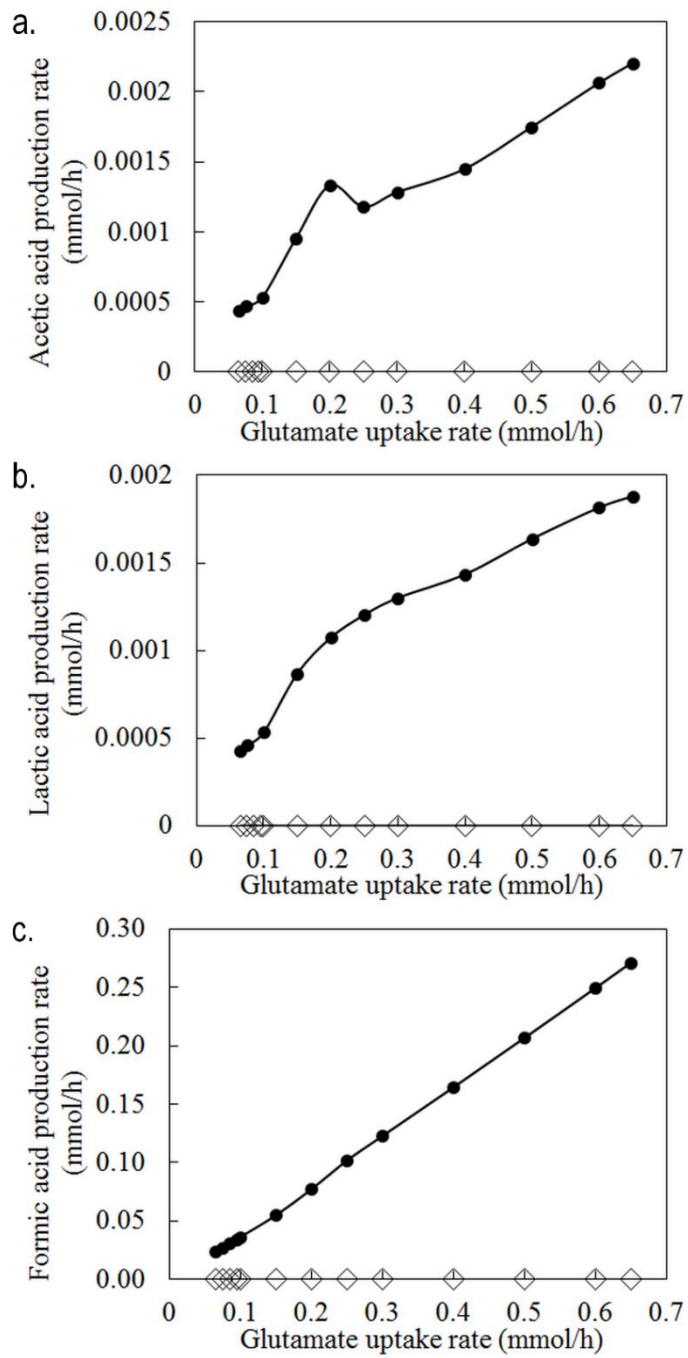


Figure 4.9: Organic acid production rates as a function of glutamate uptake rate for two objective functions (● : Maximum biomass growth, ◇ : Maximum hydrogen production)

4.5.2 Initial Sucrose Concentration

Sucrose was used as a carbon source in this model. Flux analyses with various sucrose concentrations (1mM- 20 mM) were carried out on the metabolic network. In this case, the glutamate uptake rate was kept constant as 0.1 mmol/h. In addition, 5 mmol/h photon flux was computed for the energy source. The effect of initial sucrose concentration on specific growth rate, sucrose uptake rate, H₂ production rate, PHB production rate, CO₂ production rate and production rates of organic acids (acetic acid, lactic acid and formic acid) were obtained from simulation results considering both maximum biomass growth and maximum hydrogen production individually as the objective function.

The specific growth rate and sucrose uptake rate are shown in Figure 4.10 as a function of initial sucrose concentration for the two objective functions. The specific growth rate is same at each every sucrose concentration. This result shows that biomass growth is not affected by sucrose concentration. The ultimate reason of this result lies behind the fact that sucrose uptake rate is observed as constant although different sucrose concentrations are computed (Figure 4.10-b). Therefore, biomass growth becomes a strong function of glutamate concentration where glutamate uptake rate is constant.

The sucrose uptake rate was found to be 0.037 mmol/h for both objective functions at each initial sucrose concentration (1 mM - 20 mM). This is because sucrose uptake is dictated by the limiting nutrient, i.e. glutamate. Since the glutamate flux is constant, the sucrose uptake remains the same. This is the reason of using the term of 'initial sucrose concentration' rather than initial sucrose uptake, since all of the available sucrose in the growth media is not consumed by bacteria. Similar trends were obtained for H₂ production, PHB production and CO₂ production in the following illustrations because of same reason.

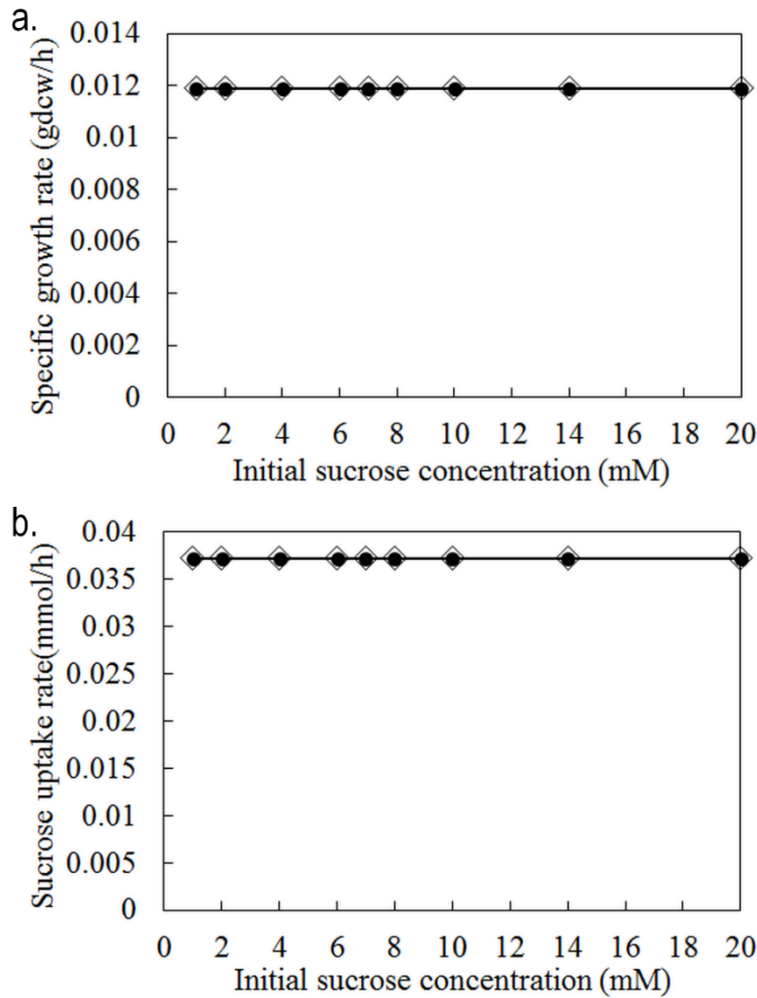


Figure 4.10: Specific growth rate (a) and Sucrose uptake rate (b) as a function of initial sucrose concentration for two objective functions (● : Maximum biomass growth, ◊ : Maximum hydrogen production)

At 5 mmol/h photon flux, a constant glutamate uptake rate and sucrose uptake rate result in the profile in Figure 4.11 for hydrogen production. The hydrogen production rate in the case of maximum hydrogen production is higher than the rate profile in the other case. This is because bacteria also consumes organic acids produced after reaching maximum biomass growth for hydrogen production.

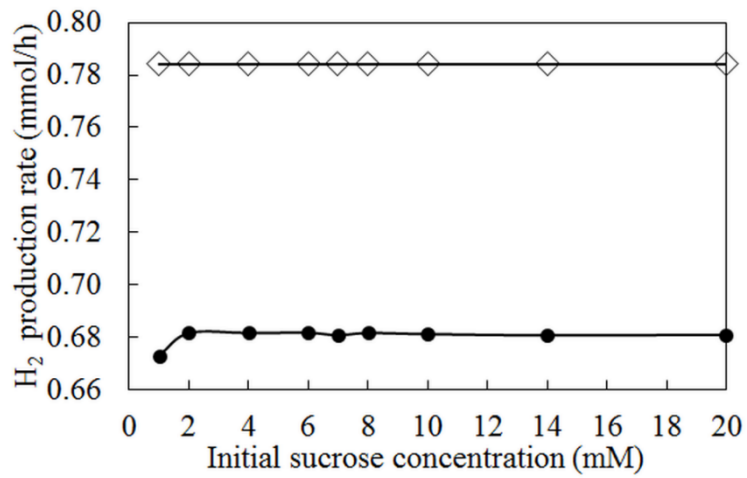


Figure 4.11: H₂ production rate as a function of initial sucrose concentration for two objective functions (● : Maximum biomass growth, ◇ : Maximum hydrogen production)

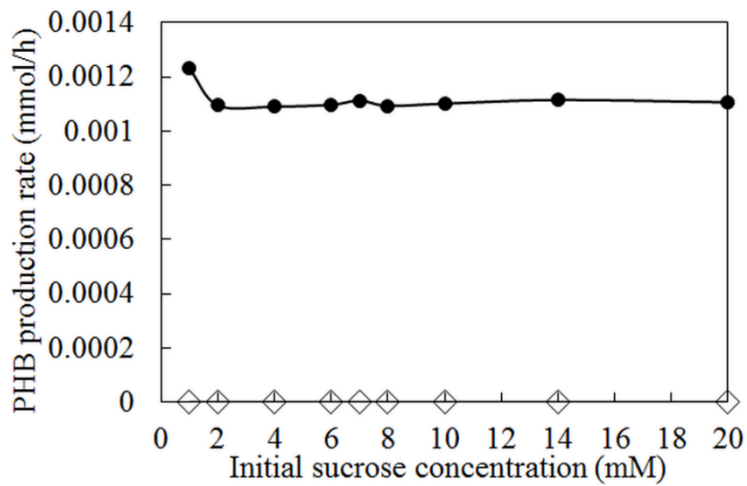


Figure 4.12: PHB production rate as a function of initial sucrose concentration for two objective functions (● : Maximum biomass growth, ◇ : Maximum hydrogen production)

In Figure 4.12, the PHB production rate is zero in the case of maximum hydrogen production whereas it has a constant profile for maximum biomass growth. This case is the opposite of Figure 4.11 because PHB production is a competitive pathway with H₂ production in terms of sharing available electrons and ATP in the metabolic network.

CO₂ production rate is illustrated as a function of initial sucrose concentration for two objective functions in Figure 4.13. Similar to H₂ production rate, CO₂ production rate is higher for maximum hydrogen production.

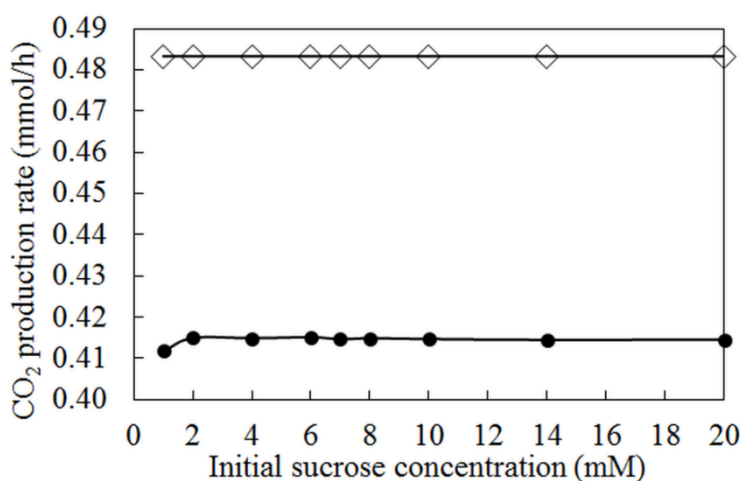


Figure 4.13: CO₂ production rate as a function of initial sucrose concentration for two objective functions (● : Maximum biomass growth, ◊ : Maximum hydrogen production)

Organic acid profiles with respect to initial sucrose concentration are seen in Figure 4.14. Since lactic acid production is affected by acetic acid production via the 58th reaction, their profile (Figure 4.14-a and b) are similar. However, formic acid production is only affected by CO₂ production via 57th reaction.

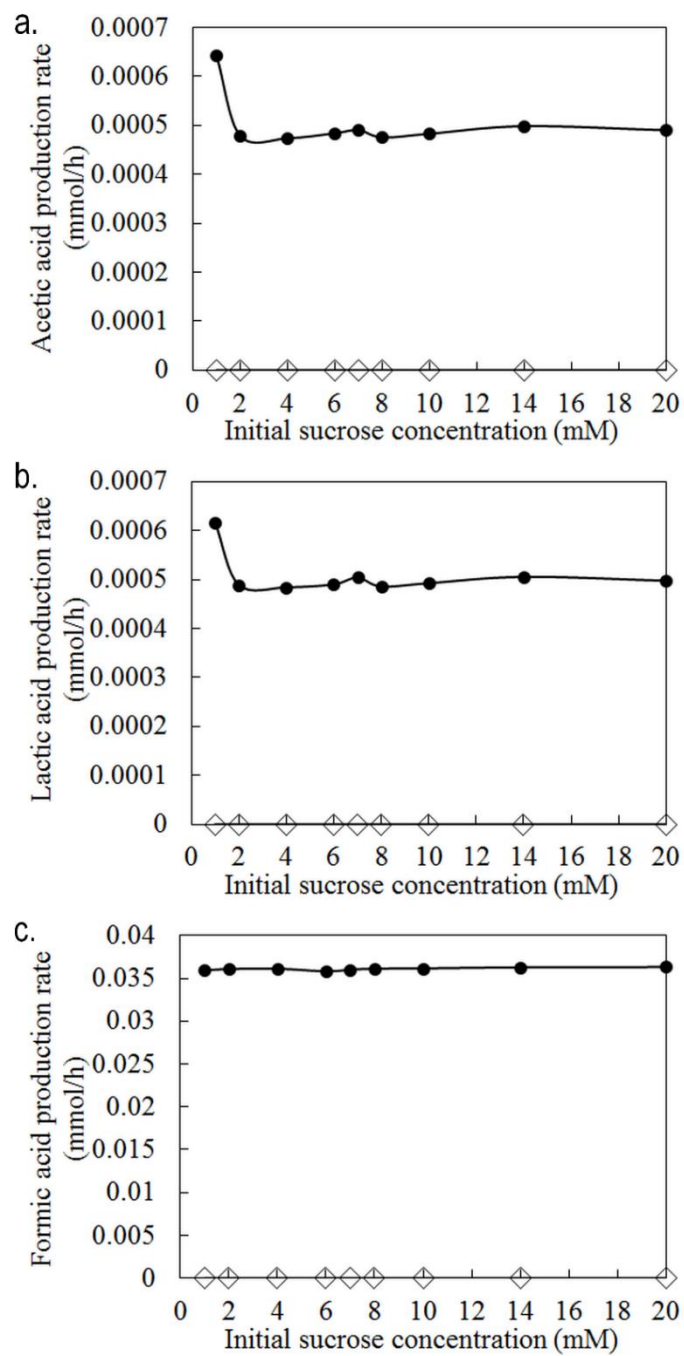


Figure 4.14: Production rate of acetic acid (a), lactic acid (b) and formic acid (c) as a function of initial sucrose concentration for two objective functions (—● : Maximum biomass growth, —◇ : Maximum hydrogen production)

4.5.3 Effect of Illumination

In this work, *R. palustris* is assumed to adopt a photoheterotrophic growth mode using energy from light and carbon from organic compounds. For this reason, the incoming photon flux from a light source plays a significant role on the resulting flux distribution of the metabolic network. The experimental photon flux based on the work of Sagir (2012) was calculated to be 5 mmol/h as shown in Appendix E.3. A range of photon fluxes (0 – 150 mmol/h) was utilized to observe the effect of photon flux on the specific growth rate, sucrose uptake rate, H₂ production rate, PHB production rate, CO₂ production rate and production rates of organic acids (acetic acid, lactic acid and formic acid) considering both maximum biomass growth and maximum hydrogen production as the objective functions. In this case, glutamate uptake rate and initial sucrose concentration were kept constant as 0.1 mmol/h and 5 mM, respectively.

Specific growth rate was obtained constant at each photon flux computed for both objective functions as seen in Figure 4.15. Growth rate is a strong function of glutamate uptake rate (nitrogen source) instead of the photon flux. This is because, *R. palustris* was considered in nitrogen starving condition where nitrogen source is very low (2 mM) in the growth media. The nitrogen limitation is also seen in Figure 4.16 showing constant sucrose uptake rate with respect to increasing photon flux. Constant glutamate uptake rate leads to constant sucrose uptake rate of bacteria.

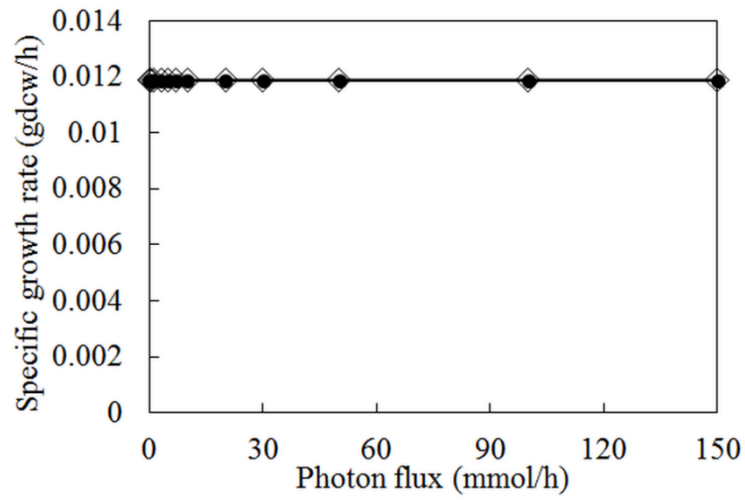


Figure 4.15: Specific growth rate as a function of photon flux for two objective functions (● : Maximum biomass growth, ◇ : Maximum hydrogen production)

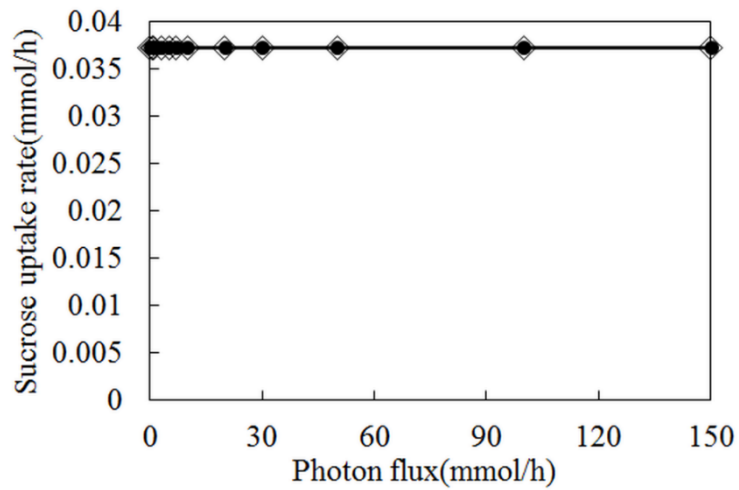


Figure 4.16: Sucrose uptake rate as a function of photon flux for two objective functions (● : Maximum biomass growth, ◇ : Maximum hydrogen production)

In Figure 4.17, maximum hydrogen production was obtained when 10 mmol/h photon flux was provided with 5 mM sucrose and 2 mM glutamate initially used in the case of maximum biomass growth. Sasikala *et al.* (1995) stated that saturated hydrogen production was obtained at around 5000 lux corresponding to 13 mmol/h which is close to the value found in this work. At higher photon fluxes, H₂ production rate decreases because of the inhibitory effect of high intensity light to H₂ production. The highest irradiation of the day (0.9 kW/m²) which approximately corresponds to photon flux of 30 mmol/h was experimentally observed to deteriorate H₂ production (Miyake *et al.*, 1999). Figure 4.17 agrees with this observation because a significant decrease in hydrogen production was resulted at photon fluxes of 10-30 mmol/h. In the model results, however, H₂ production rate is not affected by photon flux in the case of maximum hydrogen production.

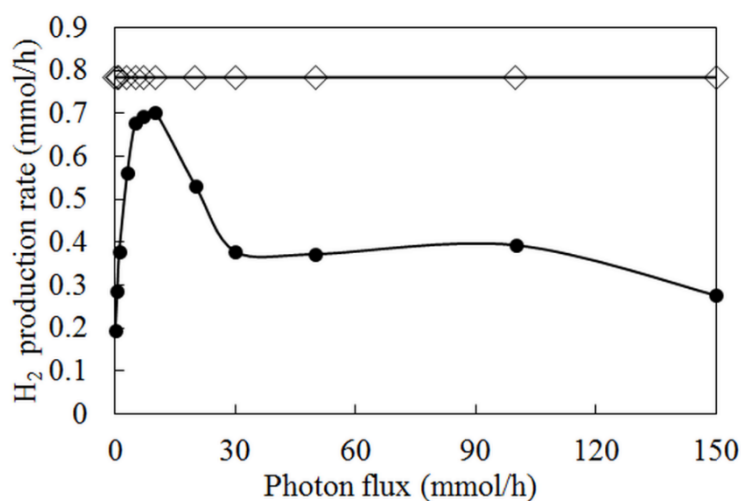


Figure 4.17: H₂ production rate as a function of photon flux for two objective functions (● : Maximum biomass growth, ◇ : Maximum hydrogen production)

PHB production was seen antagonistic to H₂ production for both objective functions in Figure 4.18. This is because PHB production pathway near TCA cycle competes with H₂ production for reducing equivalents and ATP. In the flux distribution, when photon flux increases, more ATP is produced by the enzyme of ATP synthase. However, H₂ production decreases after a certain photon flux (10 mmol/h) because of increase in PHB production triggered by the accumulation of organic acids that has been produced intracellularly. Nitrogenase cannot utilize excess ATP converted from high intense light (McKinlay *et al.*, 2010) and, therefore ATP is used for organic acid productions (Figure 4.20). With the accumulated organic acids, PHB synthesis becomes favorable and decreases hydrogen production.

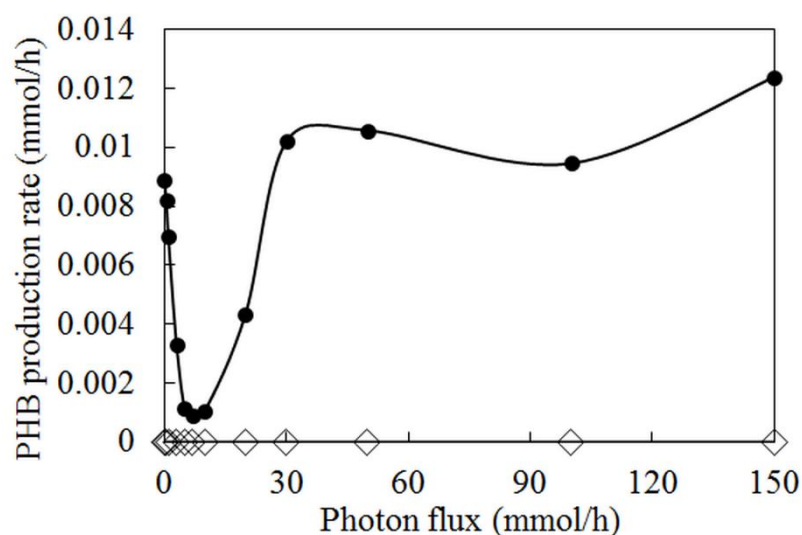


Figure 4.18: PHB production rate as a function of photon flux for two objective functions (● : Maximum biomass growth, ◇ : Maximum hydrogen production)

In Figure 4.19, the CO₂ production rate was found lower than H₂ production in the case of maximum biomass growth as expected due to stoichiometric relation between H₂ and CO₂ in the overall H₂ production reaction shown below.

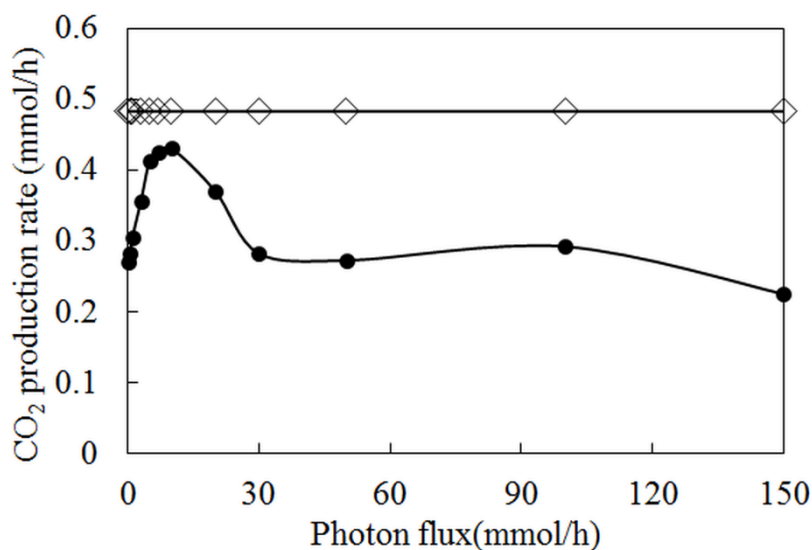


Figure 4.19: CO₂ production rate as a function of photon flux for two objective functions (● : Maximum biomass growth, ◇ : Maximum hydrogen production)

Moreover, in Figure 4.19, the CO₂ production rate was found to slightly decrease and reach a constant value unlike hydrogen production rate at higher photon fluxes because of constant growth rate of the biomass. In the case of maximum hydrogen production, CO₂ production rate was found constant at 0.48 mmol/h.

Even when the photon flux is zero, the simulation results in growth and H₂ production. The reason is that bacteria uses energy from organic sources in the growth media. As seen from the estimated fluxes, sucrose is broken down into beta-D-Fructose and alpha-D-Glucose 6-phosphate via 120th and 121th reactions. Similarly, 27th, 123-128th, 16th, 6th, 2nd, 1th, 4th, 12nd and 13th reactions occur without ATP consumption, respectively. In 15th reaction, phosphoenolpyruvate from 13th reaction is used to produce ATP. Therefore, growth and hydrogen production are observed at zero photon flux. Additionally, organic acid production rates are higher initially as seen in Figure 4.20.

When H₂ production rate is found maximum, organic acid production rates reach minimum values. This shows that bacteria consumes also organic acids for H₂ production at a given photon flux.

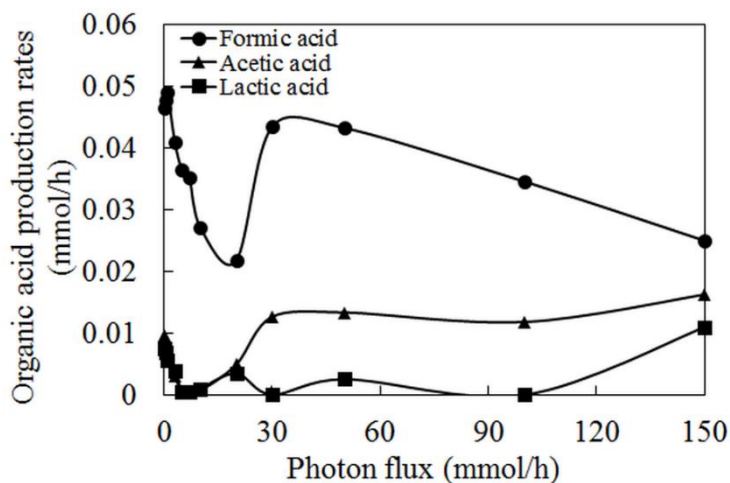


Figure 4.20: Organic acid production rates as a function of photon flux

At lower photon fluxes, a decrease was observed for all organic acid production rates in Figure 4.20. This might be because maximum hydrogen production was observed at photon flux of 10 mmol/h and organic acids are also used to produce hydrogen up to this flux value.

Organic acid production rates start to increase after this point until photon flux of 30 mmol/h where lower rates in hydrogen production were observed in Figure 4.17. This is because excess electrons and ATP are accumulated within the metabolism at high photon flux and the fluxes of some reactions in TCA cycle increases. For example, 37th, 30th, 41th and 46th reactions in TCA cycle produces more CO₂ when photon flux is increased from 20 to 30 mmol/h. However, a decrease was seen in CO₂ production rate rather than increase in this range of Figure 4.19 because excess CO₂ is converted to formic acid via 57th reaction. Therefore formic acid production rate increases in this range of photon flux (20-30 mmol/h).

However, an increase in acetic acid production was not found as higher as increase in formic acid production because electron are directed from acetic acid to PHB synthesis through 51th-56th reactions.

Even CO₂ production rate was resulted constant between photon fluxes of 30 and 100 mmol/h, formic acid production decreases because lactic acid is produced from formic acid (58th reaction) to balance the electron flow at higher photon fluxes. However, lactic acid production does not significantly change until photon flux of 100 mmol/h. This is because, lactic acid is converted to pyruvate in TCA cycle via 59th reaction when stationary phases were observed for both hydrogen production rate and CO₂ production rate in Figure 4.17 and 4.19, respectively. At the higher photon fluxes, lactic acid is accumulated rather than completing the TCA cycle because hydrogen production was deteriorated between photon fluxes of 100 and 150 mmol/h.

4.5.4 Organic Acids in the Growth Media

At high organic acid production rates, the pH of growth media decreases resulting lower the biomass growth and H₂ production. Therefore, understanding effects of organic acid production is important for H₂ production. In this work, acetic acid, lactic acid and formic acid production rates were considered. Input fluxes were given for the organic acids formate, acetate and lactate. Table 4.9 presents the individual effects of organic acids on H₂ production in the case of maximum biomass growth as the objective function.

Table 4.9: Individual effects of organic acids on H₂ production

Initial flux of	Hydrogen production rate (mmol/h)		
	Acetate	Lactate	Formate
No acid	0.6783	0.6783	0.6783
0.001 mmol/h	0.6846	0.6826	0.6825
0.004 mmol/h	0.6952	0.6935	0.6851
0.01 mmol/h	0.715	0.713	0.6901

When no organic acids were present initially, hydrogen production rate was found to be 0.6783 mmol/h. In general, H₂ production rate increases with increasing initial flux of the organic acids because bacteria can also consume organic acids as substrates. H₂ production rates are higher in the initial presence of only acetic acid compared to the other organic acids at each initial flux used in Table 4.9. In addition, H₂ production rates when only lactic acid is used are higher than rates when only formic acid is used at each flux computed. Therefore, the most and least effective organic acid for H₂ production is found acetic acid and formic acid, respectively.

This result seems reasonable because Uyar *et al.* (2009) obtained highest hydrogen productivities using acetic and lactic acid as substrates to PNSB (*R. capsulatus*) for photo fermentation compared to other organic acids (butyrate, propionate and malate).

4.6 Applicability of the Model

The capabilities of metabolic networks is a complex problem and a fascinating topic of study for biologists and biotechnologists. Mathematical models were developed to reveal important results helping to create new hypotheses and to optimize metabolic pathways in an organism. In this work, FBA was used to model metabolic network of *R. palustris*. However, FBA resulted a range of solutions instead of a precise solution. This model can be improved by incorporating additional interactions between the genotype and phenotype of the organism. In other words, the range of solutions can be narrowed further by introducing new data sources. This model has a stable basis depending on the stoichiometry of the organism. In addition, this model sheds light to obtain new hypotheses to be tested *in vivo*. For example, the sucrose pathway hypothesized in this model attracts the attention to study sucrose metabolism of *R. palustris*.

The objective of modeling metabolic networks is to have a maximum product synthesis which is maximum hydrogen production for this work. Models can be used by industrial companies to create their products at desired form. Understanding utilization manner of substrates through the metabolism of the organism provides to optimize the desired product.

CHAPTER 5

CONCLUSIONS AND RECOMMENDATIONS

A metabolic framework was formulated in this study with the aim of understanding carbon utilization patterns in purple non-sulfur bacteria (PNSB) producing hydrogen. For this purpose, *R. palustris* was selected as a model bacteria with the utilization of sucrose and glutamate as carbon and nitrogen sources for hydrogen producing conditions, respectively. In a previous experimental work (Sagir, 2012), maximum hydrogen productivity was obtained using *R. palustris* grown on sucrose and glutamate, compared to the other PNS species *R. sphaeriodes*, *R. capsulatus* and *R. capsulatus* YO3 (hup-). This work enabled the determination of model inputs, and provided a basis for verification of the model.

Flux Balance Analysis (FBA) was used as a mathematical tool to formulate the network of biochemical reactions. 148 reconstructed biochemical reactions and 128 compounds were considered within the reaction network from substrate to product. Flux distributions were obtained based on different cases defined for the model. These distributions were obtained as optimal solutions depending on an objective function considered in the study. Maximal growth of biomass or maximum hydrogen production were either used as an objective function. The entire reaction network was assumed at pseudo steady state condition. A pathway of the network was visualized to differentiate metabolic pathways used to construct the metabolic model and to evaluate the resulting flux distribution. Model results were found to agree well with the experimental literature. Hydrogen production rate was estimated 0.68 mmol/h whereas the experimental hydrogen production rate was 0.7 mmol/h.

Substrate conversion efficiency of the model was calculated 56% as close to the experimental efficiency (53%). Both hydrogenase and nitrogenase fluxes were positive, which means both enzymes are capable of providing hydrogen production. Hydrogen production rate of hydrogenase (0.11 mmol/h) was found to be higher than the rate of nitrogenase (0.048 mmol/h). The growth rate was the same for two different objective functions, presumably due to the nitrogen limitations.

The capability of the hydrogen production on sucrose by *R. palustris* was assessed with the results of the metabolic model. The effects of changes in the growth conditions of the bacteria such as glutamate uptake rate, sucrose concentration, photon flux and organic acid concentrations were observed on biomass production and hydrogen production, in particular.

Specific growth rate of biomass linearly increases with increasing glutamate uptake rate for both objective functions used. The initial glutamate flux of 0.065 mmol/h was observed as the minimum threshold glutamate uptake rate for maintenance of biomass growth. The biomass growth is not affected by sucrose concentration, because biomass growth is controlled by the glutamate uptake rate, which is limiting in the medium.

Maximum hydrogen production was obtained with 10 mmol/h photon flux as the input along with 5 mM sucrose and 2 mM glutamate for the case of maximum biomass growth. At higher photon fluxes, H₂ production rate decreases and PHB production was observed antagonistic to H₂ production for both objective functions. In addition, the most and least effective organic acid for H₂ production was found as acetic acid and formic acid, respectively.

The results can be evaluated for metabolic engineering studies to enhance yields of hydrogen production. For example, the pathways for organic acid productions can be examined by genetic studies to contribute the higher H₂ yield.

This is because the flux distribution obtained in this work shows that organic acids which are produced intracellularly triggers the PHB synthesis against the H₂ production. However, it should be taken into account that the same distribution results an increase in the H₂ production when the extracellular organic acids are available in the growth media of the bacteria. In addition, investigation of the sucrose metabolism of PNSB offers the potential to obtain insight into a low cost hydrogen production system because sucrose is a cheap feedstock compared to other organic substrates.

As recommendation for future works, the model in the present study can be applied to other PNSB as long as significant changes in their metabolic pathways are considered. In addition, it can be used to evaluate the effect of possible gene knockouts on the biomass growth or hydrogen production (Orth *et al.*, 2010). Moreover, further developments might be required such as adding new metabolic pathways, using different carbon or nitrogen sources, combining some kinetic parameters, including more experimental data and creating a user interface to identify the resulting flux distributions easily.

It should be emphasized that the model, and the procedure employed to analyze hydrogen production in this study, provides insight into the theoretical limits of the biological hydrogen production process. On the experimental and practical side, cost analysis of the enhanced hydrogen production from the bacteria can be performed to assess the worth and potential utility of metabolic engineering studies in the future.

REFERENCES

- Adessi, A., Torzillo, G., Baccetti, E., & De Philippis, R. (2012). Sustained outdoor H₂ production with *Rhodospseudomonas palustris* cultures in a 50 L tubular photobioreactor. *International Journal of Hydrogen Energy*, 37(10), 8840–8849.
- Androga, D.D., Özgür, E., Eroglu, I., Gündüz, U., & Yücel, M. (2012). Photofermentative Hydrogen Production in Outdoor Conditions. In D. Minic (Ed.), *Hydrogen Energy - Challenges and Perspectives*. InTech.
- Argun, H., Kargi, F., Kapdan, I.K., & Oztekin, R. (2008). Bio-hydrogen production by dark fermentation of wheat powder solution: Effects of C/N and C/P ratio on hydrogen yield and formation rate. *International Journal of Hydrogen Energy*, 33(7), 1813–1819.
- Azwar, M.Y., Hussain, M.A., & Abdul-Wahab, A.K. (2013). Development of biohydrogen production by photobiological, fermentation and electrochemical processes: A review. *Renewable and Sustainable Energy Reviews*, 31, 158-173.
- Basak, N., & Das, D. (2007). The prospect of purple non-sulfur (PNS) photosynthetic bacteria for hydrogen production: the present state of the art, *World Journal of Microbiology and Biotechnology*, 23, 31–42.
- Boran, E., Özgür, E., Yücel, M., Gündüz, U., & Eroglu, I. (2012a). Biohydrogen production by *Rhodobacter capsulatus* Hup⁻ mutant in pilot solar tubular photobioreactor. *International Journal of Hydrogen Energy*, 37(21), 16437–16445.
- Brentner, L.B., Peccia, J., & Zimmerman, J.B. (2010). Challenges in developing biohydrogen as a sustainable energy source: implications for a research agenda. *Environmental Science & Technology*, 44(7), 2243–2254.
- Cai, G., Jin, B., Monis, P., & Saint, C. (2010). Metabolic flux network and analysis of fermentative hydrogen production. *Biotechnology Advances*, 29, 375-387. doi:10.1016/j.biotechadv.2011.02.001
- Cameron, D.C., & Tong, I.T. Cellular and metabolic engineering: An overview. *Applied Biochemistry and Biotechnology*, 38(1-2), 105-140.

Cammack, R. (1999). Bioinorganic chemistry: Hydrogenase sophistication. *Nature*, 397(6716), 214–215.

Caspi, R., Altman, T., Billington, R., Dreher, K., Foerster, H., Fulcher, C.A., Holland, T.A., Keseler, I.M., Kothari, A., Kubo, A., Krummenacker, M., Latendresse, M., Mueller, L.A., Ong, Q., Paley, S., Subhraveti, P., Weaver, D.S., Weerasinghe, D., Zhang, P., & Karp, P.D. (2013). The MetaCyc database of metabolic pathways and enzymes and the BioCyc collection of Pathway/ Genome Databases. *Nucleic Acids Research*, 42(1), 459-471. doi: 10.1093/nar/gkt1103

Chen, Y.T., Wu, S.C., & Lee, C.M. (2012). Relationship between cell growth, hydrogen production and poly- β -hydroxybutyrate (PHB) accumulation by *Rhodospseudomonas palustris* WP3-5. *International Journal of Hydrogen Energy*, 37, 13887–13894. doi:10.1016/j.ijhydene.2012.06.024

Crown, S.B. & M.R. Antoniewicz. (2013). Publishing metabolic flux analysis studies: A review and future perspectives. *Metabolic Engineering*, 20, 42-48.

Das, D., & Veziroglu, T.N. (2001). Hydrogen production by biological processes: a survey of literature. *International Journal of Hydrogen Energy*, 26(1), 13–28.

Doman, L., Singer, L., Zaretskaya, V., Jones, A. & Huetteman, T. (2016). International Energy Outlook, *U.S. Energy Information Administration*. Retrieved July 22, 2016, from www.eia.gov/forecasts/ieo

Durot, M., Bourguignon, P.Y., & Schachter V. (2009). Genome-scale models of bacterial metabolism: reconstruction and applications. *FEMS Microbiology Reviews*, 33(1), 164-190.

Edwards, J.S., & Palsson, B.O. (2000). The *Escherichia coli* MG1655 in silico metabolic genotype: Its definition, characteristics, and capabilities. *Proceedings of the National Academy of Sciences*, 97(10), 5528-5533.

Eroglu, I., Özgür, E., Eroglu, E., Yücel, M., & Gündüz, U. (2014). Applications of photofermentative hydrogen production. In D. Zannoni & R. De Philippis (Eds.), *Microbial Bioenergy: Hydrogen Production* (pp. 237–267). Springer.

Feist, A.M., & Palsson, B.O. (2010). The biomass objective function. *Current Opinion in Microbiology*, 13(3), 344 -349. doi:10.1016/j.mib.2010.03.003

Gao, J., Gorenflo, V.M., Scharer, J.M., & Budman, H.M. (2007). Dynamic metabolic modeling for a MAB bioprocess. *Biotechnology Progress*, 23,168–181.

- Ghosh, D., & Hallenbeck, P.C. (2014). Cyanobacteria and photosynthetic bacteria: metabolic engineering of hydrogen production. *Advances in Enzymatic Conversion of Biomass to Biofuels* (pp.112-124). Future Science Ltd.
- Golomysova, A., Gomelsky, M., & Ivanov, P.S. (2010). Flux balance analysis of photoheterotrophic growth of purple non-sulfur bacteria relevant to biohydrogen production. *International Journal of Hydrogen Energy*, 35(23), 12751-12760.
- Goyal, Y., Kumar, M., & Gayen, K. (2013). Metabolic engineering for enhanced hydrogen production: a review. *Canadian Journal of Microbiology*. 59, 59-78, doi: 10.1139/cjm-2012-0494
- Hädicke, O., Grammel, H., & Klamt, S. (2011). Metabolic network modeling of redox balancing and biohydrogen production in purple nonsulfur bacteria. *BMC Systems Biology*. 5(150). doi:10.1186/1752-0509-5-150
- Hallenbeck, P.C., & Benemann, J.R. (2002). Biological hydrogen production; Fundamentals and limiting processes. *International Journal of Hydrogen Energy*, 27(11-12), 1185–1193.
- Hallenbeck, P.C., & Ghosh, D. (2009). Advances in fermentative biohydrogen production: the way forward? *Trends in Biotechnology*, 27(5), 287–297.
- Hallenbeck, P.C. (2014). Bioenergy from Microorganisms: An Overview. In D. Zannoni & R. De Philips (Eds.), *Microbial Bioenergy: Hydrogen Production* (pp. 3–21). Springer.
- Hallenbeck, P.C., & Liu, Y. (2014). Recent advances in hydrogen production by photosynthetic bacteria. *International Journal of Hydrogen Energy*, 41(7), 4446–4454. doi:10.1016/j.ijhydene.2015.11.090
- Haryanto, A., Fernando, S., Murali, N., & Adhikari, S. (2005). Current Status of Hydrogen Production Techniques by Steam Reforming of Ethanol: A review. *Energy & Fuels*, 19(5), 2098-2106.
- Hillier, F.S., & Lieberman, G.J. (1997). Introduction to operations research, 7th edition. Newyork, NY: McGraw-Hill.
- Imam, S., Yilmaz, S., Sohmen, U., Gorzalski, A.S., Reed, J.L., Noguera, D.R., & Donohue, T.J. (2011). iRsp1095: a genome-scale reconstruction of the *Rhodobacter sphaeroides* metabolic network. *BMC Systems Biology*, 5(116). doi:10.1186/1752-0509-5-116

- Kanehisa, M., Sato, Y., Kawashima, M., Furumichi, M., & Tanabe, M. (2015). KEGG as a reference resource for gene and protein annotation. *Nucleic Acids Research*, *44*, 457-462. doi: 10.1093/nar/gkv1070
- Kapdan, I.K., & Kargi, F., (2006), Bio-hydrogen production from waste materials. *Enzyme and Microbial Technology*, *38*,569–582.
- Keskin, T., Abo-Hashesh, M. & Hallenbeck, P.C. (2011). Photofermentative hydrogen production from wastes. *Bioresource Technology*, *102*, 8557-8568. doi:10.1016/j.biortech.2011.04.004
- Keskin, T., & Hallenbeck, P.C. (2012). Hydrogen production from sugar industry wastes using single-stage photofermentation. *Bioresource Technology*, *112*, 131–136.
- Klamt, S., Schuster, S., & Gilles, E.D. (2002). Calculability analysis in underdetermined metabolic networks illustrated by a model of the central metabolism in purple non-sulfur bacteria. *Biotechnology and Bioengineering*, *77*(7), 734-751.
- Klamt, S., Grammel, H., Straube, R., Ghosh, R., & Gilles, E.D. (2008). Modeling the electron transport chain of purple non-sulfur bacteria. *Molecular Systems Biology*, *4*,156–174.
- Koffas, M., Roberge, C., Lee, K., & Stephanopoulos, G. (1999). Metabolic engineering. *Annual Review of Biomedical Engineering*, *1*, 535-557.
- Koku, H., Eroğlu, I., Gunduz, U., Yucel, & M., Turker, L. (2002). Aspects of the Metabolism of Hydrogen Production by *Rhodobacter sphaeroides*. *International Journal of Hydrogen Energy*, *2*, 1325-1329.
- Kotay, S.M., & Das, D. (2008). Biohydrogen as a renewable energy resource-prospects and potential. *International Journal of Hydrogen Energy*, *33*(1), 258-263.
- Larimer, F.W., Chain, P., Hauser, L., Lamerdin, J., Malfatti, S., Do, L., Land, M.L., Pelletier, D.A., Beatty, J.T., Lang, A.S., Tabita, F.R., Gibson, J.L., Hanson, T.E., Bobst, C., Torres, J.L.T.Y., Peres, C., Harrison, F.H., Gibson, J., & Harwood, C.S. (2003). Complete genome sequence of the metabolically versatile photosynthetic bacterium *Rhodospseudomonas palustris*. *Nature Biotechnology* *22*, 55 – 61.
- Levin, D.B., Lawrence, P., & Love, Murray. (2004). Biohydrogen production: prospects and limitations to practical application. *International Journal of Hydrogen Energy*, *29*, 173-185. doi:10.1016/S0360-3199(03)00094-6

Lipman, T. (2011). An overview of hydrogen production and storage systems with renewable hydrogen case studies. *Clean Energy States Alliance*. US DOE Grant DE-FC3608GO18111 A000, Office of Energy Efficiency and Renewable Energy Fuel Cell Technologies Program.

Lo, Y.C., Chen, C.Y., Lee, C.M., & Chang, J. (2010). Sequential dark-photo fermentation and autotrophic microalgal growth for high-yield and CO₂-free biohydrogen production. *International Journal of Hydrogen Energy*, 35, 10944–10953. doi:10.1016/j.ijhydene.2010.07.090

Loucks, D.P., & Beek, E.V. (2005). Water resources systems planning and management: an introduction to methods, models and applications. Paris, France: UNESCO Publishing.

Madigan M.T., & Jung D.O. (2009). An overview of purple bacteria: systematics, physiology, and habitats. In C.N. Hunter, F. Daldal, M.C. Thurnauer & J.T. Beatty (Eds.), *The Purple Phototrophic Bacteria*, (pp. 1-15). Dordrecht: Springer Netherlands.

Marbán, G., & Valdés-Solís, T. (2007). Towards the hydrogen economy? *International Journal of Hydrogen Energy*, 32(12), 1625–1637. doi:10.1016/j.ijhydene.2006.12.017

McKinlay, J.B., & Harwood, C.S. (2010). Carbon dioxide fixation as a central redox cofactor recycling mechanism in bacteria. *Proceedings of the National Academy of Sciences*, 107, 11669–11675.

McKinlay, J.B., & Harwood, C.S. (2011). Calvin cycle flux, pathway constraints, and substrate oxidation state together determine the H₂ biofuel yield in photoheterotrophic bacteria. *mBio* 2(2):e00323-10. doi:10.1128/mBio.00323-10

McKinlay, J.B. (2014). Systems Biology of Photobiological Hydrogen Production by Purple Non-Sulfur Bacteria. In D. Zannoni & R. De Philippis (Eds.), *Microbial Bioenergy: Hydrogen Production* (pp. 155-176). Springer.

Miller, G.Q., Penner, D.W. (2004) Possibilities and Challenges for a Transition to a Hydrogen Economy, Technical Program, Pisa, Italy.

Miyake, J., Wakayama, T., Schnackenberg, J., Arai, T., & Asada, Y. (1999). Simulation of the daily sunlight illumination pattern for bacterial photo-hydrogen production. *Journal of Bioscience and Bioengineering*, 88, 659–663.

- Ni, M., Dennis, Y.C., Michael, K.H., & Leung, K.S. (2006). An overview of hydrogen production from biomass. *Fuel Processing Technology*, 87, 461-472. doi:10.1016/j.fuproc.2005.11.003
- Oda, Y., Samanta, S.K., Rey, F.E., Wu, L., Liu, X., Yan, T., Zhou, J., & Harwood, C.S. (2005). Functional genomic analysis of three nitrogenase isozymes in the photosynthetic bacterium *Rhodospseudomonas palustris*. *Journal of Bacteriology*, 187, 7784–7794. doi:10.1128/JB.187.22.7784–7794.2005
- Oh, Y., Raj, S.M., Jung, G.Y., & Park, S. (2011). Current status of the metabolic engineering of microorganisms for biohydrogen production. *Bioresource Technology*, 102(18), 8357-8367. doi:10.1016/j.biortech.2011.04.054
- Ooshima, H., Takakuwa, S., Katsuda, T., Okuda, M., Shirasawa, T., Azuma, M., & Kato, J. (1998). Production of hydrogen by a hydrogenase-deficient mutant of *Rhodobacter capsulatus*. *Journal of Fermentation and Bioengineering*, 85(5), 470–5.
- Orth, J.D., Thiele, I., & Palsson, B. (2010). What is flux balance analysis? *Nature Biotechnology*, 28(3), 245-247.
- Öztürk, Y., Yücel, M., Daldal, F., Mandaci, S., Gündüz, U., Türker, L., & Eroğlu, I. (2006). Hydrogen production by using *Rhodobacter capsulatus* mutants with genetically modified electron transfer chains. *International Journal of Hydrogen Energy*, 31(11), 1545–1552. doi:10.1016/j.ijhydene.2006.06.042
- Papin, J.A., Stelling, J., Price, N.D., Klamt, S., Schuster, S., & Palsson, B.O. (2004). Comparison of network-based pathway analysis methods. *Trends in Biotechnology*, 22(8), 400-405. doi:10.1016/j.tibtech.2004.06.010
- Rey, F.E., Heiniger, E.K., & Harwood, C.S. (2007). Redirection of metabolism for biological hydrogen production. *Applied and Environmental Microbiology*, 73, 1665–1671.
- Riis, T., & Hagen, E.F. (2006). Hydrogen Production R&D Priorities and Gaps. *International Energy Agency*, pp (6-16).
- Sagir, E. (2012). Photobiological hydrogen production from sugar beet molasses. M.Sc. Thesis submitted to the Department of Biochemistry of Middle East Technical University.
- Sasikala, K., Ramama, C.V., & Rao, P.R. (1991). Environmental regulation for optimal biomass yield and photoproduction of hydrogen by *Rhodobacter sphaeroides* O.U.001. *Biotechnology*, 16(9), 597–601.

Sasikala, C., Ramana, C.V., & Rao, P.R. (1995). Regulation of simultaneous hydrogen photoproduction during growth by pH and glutamate in *Rhodobacter sphaeroides* O.U. 001. *International Journal of Hydrogen Energy*, 20(2), 123–6.

Schomburg, I., Chang, A., Placzek, S., Söhngen, C., Rother, M., Lang, M., Munaretto, C., Ulas, S., Stelzer, M., Grote, A., Scheer, M., & Schomburg, D. (2013). BRENDA in 2013: integrated reactions, kinetic data, enzyme function data, improved disease classification: new options and contents in BRENDA. *Nucleic Acids Research*, 41(Database issue), 764-772. doi: 10.1093/nar/gks1049

Shin, H., Youn, J., & Kim, S. (2004). Hydrogen production from food waste in anaerobic mesophilic and thermophilic acidogenesis. *International Journal of Hydrogen Energy*, 29(13), 1355–1363.

Sparling, R., Carere, R.C., Rydzak, T., Schellenberg, J., & Levin, D.B. (2012). Thermodynamic and Biochemical Aspect of Hydrogen Production by Dark Fermentation. In N. Azbar & D.B. Levin (Eds.), *State of the Art and Progress in Production of Biohydrogen* (pp. 160-187). Bentham Science.

Stephanopoulos, G.N., Aristidou, A.A., & Nielsen, J. (1998). *Metabolic Engineering Principles and Methodologies*. California: Academic Press.

Tanis, J. (2006). *Metabolic Engineering: Flux Balance Analysis*. *Information and Communication Theory Group*, TU Delft.

Tao, Y., Chen, Y., Wu, Y., He, Y., & Zhou, Z. (2007). High hydrogen yield from a two-step process of dark- and photo-fermentation of sucrose. *International Journal of Hydrogen Energy*, 32(2), 200–206. doi:10.1016/j.ijhydene.2006.06.034

Tao, Y., Liu, D., Yan, X., Zhou, Z., Lee, J.K., & Yang, C. (2011). Network identification and flux quantification of glucose metabolism in *Rhodobacter sphaeroides* under photoheterotrophic H₂-Producing conditions. *Journal of Bacteriology*, 194(2), 274–283. doi:10.1128/JB.05624-11

Urbaniec, K., & Grabarczyk, R. (2014). Hydrogen production from sugar beet molasses -A techno-economic study. *Journal of Cleaner Production*, 65, 324–329. <http://doi.org/10.1016/j.jclepro.2013.08.027>

U.S. Energy Information Administration (EIA).(2008). The Impact of Increased Use of Hydrogen on Petroleum Consumption and Carbon Dioxide Emissions, Report #: SR-OIAF-CNEAF/2008-04

- Uyar, B., Eroglu, I., Yücel, M., & Gündüz, U. (2009). Photofermentative hydrogen production from volatile fatty acids present in dark fermentation effluents. *International Journal of Hydrogen Energy* 34, 4517-4523. doi:10.1016/j.ijhydene.2008.07.057
- Varma, A., & Palsson, B.O. (1993b). Metabolic capabilities of *Escherichia coli*: II. Optimal growth patterns. *Journal of Theoretical Biology*, 165, 503-522.
- Varma A., & Palsson B.O. (1994). Metabolic flux balancing: basic concepts, scientific and practical use. *Nature Biotechnology*, 12(10), 994-998. doi:10.1038/nbt1094-994
- Venkata, M.S. Vijaya, B.Y., Murali, K.T., Rao, N.C., Lalit, V., & Sarma, P.N. (2007). Biohydrogen production from chemical wastewater as substrate by selectively enriched anaerobic mixed consortia: influence of fermentation pH and substrate composition. *International Journal of Hydrogen Energy*, 32(13), 2286–95.
- Venkataraman, P. (2009). Applied Optimization with MATLAB Programming, 2nd Edition. Hoboken, NJ: Wiley.
- Vignais, P.M., Colbeau, A., Willison, J.C., & Jouanneau, Y. (1985). Hydrogenase, nitrogenase and hydrogen metabolism in the photosynthetic bacteria. In *Advances in Microbial Physiology*, 26, pp (154–234). Academic Press.
- Vincenzini, M., Marchini, A., Ena, A., & De Philippis, R. (1997). H₂ and poly-β-hydroxybutyrate, two alternative chemicals from purple non sulfur bacteria. *Biotechnology Letters*, 197, 759-762.
- Waligorska, M., Seifert, K., Gorecki, K., Moritz, M., & Laniecki, M. (2009). Kinetic model of hydrogen generation by *Rhodobacter sphaeroides* in the presence of NH₄⁺ ions. *Journal of Applied Microbiology*, 107(4), 1308-1318.
- Wu, S.C., Liou, S.Z., & Lee, C.M. (2012). Correlation between bio-hydrogen production and poly-β-hydroxybutyrate (PHB) synthesis by *Rhodospseudomonas palustris* WP3-5. *Bioresource Technology*, 113, 44-50.
- Zhang, D., Xiao, N., Mahbubani, K.T., Rio-Chanona, E.A., Slater, N.K.H., & Vassiliadis, V.S. (2015). Bioprocess modelling of biohydrogen production by *Rhodospseudomonas palustris*: Model development and effects of operating conditions on hydrogen yield and glycerol conversion efficiency. *Chemical Engineering Science*, 130, 68-78.

APPENDIX A

TEST CASE

A.1 Test Case Details

Table A.1: Definitions of enzymes used in the test case with the related reaction number

Enzyme number	Enzyme abbreviation	Definition
1	HK	Hexokinase
2	PGI	Phosphoglucose isomerase
3	PGIR	Reverse phosphoglucose isomerase
4	G6PDH	Glucose-6-phosphate dehydrogenase
5	ALD	Aldolase
6	FDPASE	Fructose 1,6 - Diphosphatase
7	TRALD	Transaldolase
8	TRALDR	Reverse transaldolase
9	TRKET	Transketolase
10	TRLETR	Reverse transketolase
11	PGK	Phosphoglycerate kinase
12	PGKR	Reverse phosphoglycerate kinase
13	PGM	Phosphoglycerate mutase
14	PGMR	Reverse phosphoglycerate mutase
15	PYK	Pyruvate kinase
16	PEPSYN	Phosphoenolpyruvate synthase
17	PEPCK	Phosphoenolpyruvate carboxykinase
18	PEPC	Phosphoenolpyruvate carboxylase
19	LACDH	Lactate dehydrogenase
20	LACDHR	Reverse lactate dehydrogenase
21	PFLASE	Pyruvate formate-lyase
22	PFLASER	Reverse pyruvate formate-lyase
23	PTACET	Acetate thiokinase
24	PTACETR	Reverse acetate thiokinase

Table A.1 (continued):

Enzyme number	Enzyme abbreviation	Definition
25	ACCOASN	Acetyl CoA synthase
26	ALCDH	Aldehyde dehydrogenase
27	PYRDH	Pyruvate dehydrogenase
28	CITSYN	Citrate synthase
29	MALSYN	Malate synthase
30	ACO	Aconitase
31	ACOR	Reverse aconitase
32	ISODHP	Isocitrate dehydrogenase
33	ISODHR	Reverse isocitrate dehydrogenase
34	ISOLYS	Isocitrate lyase
35	AKGDH	Alpha-ketoglutarate dehydrogenase
36	SCOASN	Succinyl CoA synthase
37	SCOASNR	Reverse succinyl CoA synthase
38	SUCCDH	Succinate dehydrogenase
39	FUMASE	Fumarate hydratase
40	FUMASER	Reverse fumarate hydratase
41	MALDH	Malate dehydrogenase
42	MALENZ	Malic Enzyme
43	TRANSH	Transhydrogenase
44	TRANSHR	Reverse transhydrogenase
45	NDH	NADH dehydrogenase
46	FDHASE	FADdiphosphatase
47	FORDH	Formate dehydrogenase
48	CYT	Cytochrome reductase
49	ATPASE	ATP synthase
50	ATPASER	Reverse ATP synthase
51	VCO2	Net CO ₂ production

Table A.2: List of metabolites used in reactions of the test case

Metabolites	Definition
GLC	Glucose
PEP	Phosphoenolpyruvate
PYR	Pyruvate
G6P	Glucose-6-phosphate
F6P	Fructose-6-phosphate
ATP	Adenozin 3'-trifosfat
CO ₂	Carbondioxide
R5P	Ribose-5-phosphate
T3P	Glyceraldehyde-3-phosphate
E4P	Erythrose-4-phosphate
3PG	3-phosphoglyceric acid
OA	Oxaloacetate
Lac	Lactate
AcCoA	Acetyl CoA
Form	Formate
AC	Acetate
Eth	Ethanol
Cit	Citrate
Glx	Glyoxylate
Mal	Malate
Icit	Isocitrate
alphaKG	Alpha-ketoglutarate
Succ	Succinate
SucCoA	Succinyl CoA
Fum	Fumarate
Hexp	Protons (H ⁺)
QH ₂	Quinol

Table A.3: Coefficients of metabolites in the objective function used in the test case
(Table A.2 can be referred for definitions of the metabolite abbreviations)

Metabolites	Coefficients (mmol/g dry cell weight)
ATP	41.3
NAD	3.55
NADP	18.2
G6P	0.205
F6P	0.0709
R5P	0.898
E4P	0.361
T3P	0.129
3PG	1.50
PEP	0.519
PYR	2.83
AcCoA	3.75
OA	1.79
AKG	1.08

A.2 Matlab Script for the Test Case

```
%%%START%%%  
clc;  
% simplex is used as optimization method for 'linprog' function  
options = optimoptions('linprog','Algorithm','dual-  
simplex','TolFun',1e-6);  
  
% stoichiometric matrix of the test case is loaded to the workspace  
S_struct = load('palsonmatrix.mat');  
sm = S_struct.palsonmatrix;  
  
% dependent rows of the stoichiometric matrix are eliminated with  
'licols'  
% function  
sto_transpose = sm';  
reduced_sto_tranpose = licols(sm',1e-8);  
  
% reduced stoichiometric is defined as 'S'  
S = reduced_sto_tranpose';  
  
%S is stoichiometric matrix giving mass balances  
l = size(S,2); % number of columns of raw matrix (# of fluxes-  
enzymes)  
w = size(S,1); % number of rows of raw matrix (# of metabolites)  
demandcolumn = S(:,l-1); % Growth reaction coefficients of biomass  
supplycolumn = S(:,1); % Coefficients of inputs  
  
% Objective function is set  
% Note that linprog minimizes function by default so we will minimize  
%-obj as equivalent to maximizing obj  
obj = zeros(l-1,1); % initializing objective function vector  
obj(l-1) = sum(demandcolumn); % max biomass growth as objective function
```

```

%INEQUALITIES
% To make the growth reaction nonzero, A and b are described as vector.
A = zeros(l-1,l-1);
A(1,l-1) = -1;
b = zeros(l-1,1);
b(1)=-0.01;

% EQUALITIES
S(:,l) =[]; % remove input fluxes from stoichiometric matrix
           % where the input(supply) fluxes are constant
% for S.v=0, Aeq.x-beq=0 is defined as below
Aeq = S;
beq = -1*supplycolumn; % the supply flux constant from right
                        hand side

ub = 200;
UB = ub*ones(l-1,1); %upper bound as a constraint
LB =zeros(l-1,1);    %lower bound as another constraint

x0=zeros(l-1,1);     %initial guess for simplex algorithm

%'linprog' funtion is called to solve this optimization problem
[x, objectivevalue, exitflag,output] = linprog(obj, A, b, Aeq, beq, LB,
UB,x0,options );

%%%%END%%

```

APPENDIX B

METABOLIC NETWORK OF THE MODEL

B.1 List of Metabolites

	<u>Abbreviation</u>	<u>Definition</u>
1	RL5P	D-Ribulose 5-phosphate
2	R15P	D-Ribulose 1,5-bisphosphate
3	6PG	6-Phospho-D-gluconate
4	X5P	D-Xylulose 5-phosphate
5	3PG	3-Phospho-D-glycerate
6	GL6P	D-Glucono-1,5-lactone 6-phosphate
7	F6P	D-Fructose 6-phosphate
8	GAld3P	D-Glyceraldehyde 3-phosphate
9	E4P	D-Erythrose 4-phosphate
10	S7P	Sedoheptulose 7-phosphate
11	R5P	D-Ribose 5-phosphate
12	beta-F6P	beta-D-Fructose 6-phosphate
13	5PR1DP	5-Phospho-alpha-D-ribose 1-diphosphate
14	3PGP	3-Phospho-D-glyceroyl phosphate
15	2PG	2-Phospho-D-glycerate
16	PEP	Phosphoenolpyruvate
17	PYR	Pyruvate
18	Pi	Orthophosphate
19	PPi	Diphosphate
20	beta-G6P	beta-D-Glucose 6-phosphate
21	F16P	D-Fructose 1,6-bisphosphate
22	beta-F16P	beta-D-Fructose 1,6-bisphosphate
23	GP	Glycerone phosphate
24	S17P	Sedoheptulose 1,7-bisphosphate
25	alpha-G6P	alpha-D-Glucose 6-phosphate
26	Mal	(S)-Malate
27	OA	Oxaloacetate

28	Fum	Fumarate
29	AcCoA	Acetyl-CoA
30	Glx	Glyoxylate
31	CoA	CoA
32	Succ	Succinate
33	Cit	Citrate
34	Icit	Isocitrate
35	2OG	2-Oxoglutarate
36	Glu	Glutamate
37	Gly	Glycine
38	SuccCoA	Succinyl-CoA
39	Ac	Acetate
40	AcP	Acetyl phosphate
41	AcAl	Acetaldehyde
42	AcAlCoA	Acetoacetyl-CoA
43	3-Hbut(S)	(S)-3-Hydroxybutanoyl-CoA
44	3-Hbut(R)	(R)-3-Hydroxybutanoyl-CoA
45	PHB	Poly-beta-hydroxybutyrate
46	Form	Formate
47	Lac	Lactate
48	MTHF	5,10-Methylenetetrahydrofolate
49	THF	Tetrahydrofolate
50	Ser	Serine
51	NH3	Ammonia
52	Shiki	Shikimate
53	Chor	Chorismate
54	Ala	Alanine
55	Valerate	3-Methyl-2-Oxobutanoate
56	Val	Valine
57	Leu	Leucine
58	Asp	Aspartate
59	Asn	Asparagine
60	Lys	Lysine
61	Cys	Cysteine
62	HSer	Homoserine
63	Met	Methionine
64	Thr	Threonine
65	Ile	Isoleucine
66	His	Histidine
67	Gln	Glutamine
68	Pro	Proline
69	Trp	Tryptophan
70	Arg	Arginine

71	Tyr	Tyrosine
72	Phe	Phenylalanine
73	Asp-Sald	Aspartae-Semialdehyde
74	IMP	Inosinmonophosphate
75	r ATP	r ATP
76	r GTP	r GTP
77	r UTP	r UTP
78	r CTP	r CTP
79	d ATP	d ATP
80	d GTP	d GTP
81	d CTP	d CTP
82	d TTP	d TTP
83	G3P	Glycerol-3-phosphate
84	FAs	Fatty Acids
85	CPD-Ea	CDP-Ethanolamine
86	MA	Myristic Acid
87	LS	Lipid Synthesis
88	NDPHep	NDP-Heptose
89	CMP-KDO	CMP-3-deoxy-D-manno-octulosonate
90	TDP-Glu	TDP-Glucosamine
91	UDP-Ag	UDP-Acetylglucosamine
92	UDP Ama	UDP-N-Acetylmuramic-acid
93	Dap	Diaminopimelate
94	Bchla	bachteriochlorophyll_a
95	AcLac	Acetolactate
96	H ₂	Hydrogen
97	Suext	External Sucrose
98	Suc	Produced sucrose
99	Suc6P	Sucrose 6'-phosphate
100	beta-Fruc	beta-D-Fructose
101	G1P	D-Glucose 1-phosphate
102	UDP-Glc	UDP-Glucose
103	aaT6P	alpha,alpha'-Trehalose 6-phosphate
104	aaT	alpha,alpha-Trehalose
105	betaG1P	beta-D-Glucose 1-phosphate
106	Glc	Glucose
107	ADP-Glc	ADP-glucose
108	Fruc	Fructose
109	alpha-Glu	alpha D-Glucose
110	Pho	Photon
111	NAD ⁺	Oxidized nicotinamide adenine dinucleotide
112	NADH	Reduced NAD ⁺

113	NADP ⁺	Nicotinamide adenine dinucleotide phosphate
114	NADPH	Reduced NADP ⁺
115	UDP	Uridine Diphosphate
116	ATP	Adenosine triphosphate
117	ADP	Adenosine diphosphate
118	AMP	Adenosine monophosphate
119	Q	Quinone
120	QH ₂	Hydroquinone
121	CO ₂	Carbon dioxide
122	Fd-Rd	Reduced Ferredoxin
123	Fd-Ox	Oxidized Ferredoxin
124	c ₂ -red	Ferro cytochrome c
125	c ₂ -ox	Ferri cytochrome c
126	H ⁺	Protons in cytoplasm
127	H _p	Protons in periplasm
128	H ₂ O	Water

B.2 List of Enzymes

Table B.1: Definitions of enzymes used in the construction of the metabolic network of *R. palustris*

EC number	Enzyme name
EC 2.7.1.19	ribulose phosphate kinase
EC 1.1.1.44	phosphogluconate dehydrogenase
EC 5.1.3.1	phosphoribulose epimerase
EC 4.1.1.39	ribulose-bisphosphate carboxylase;
EC 5.3.1.6	ribose-5-phosphate isomerase
EC 3.1.1.31	6-phosphogluconolactonase
EC 2.2.1.1	transketolase
EC 2.7.6.1	ribose-phosphate diphosphokinase
EC 2.7.2.3	phosphoglycerate kinase
EC 5.4.2.12	phosphoglycerate mutase
EC 4.2.1.11	phosphopyruvate hydratase
EC 2.7.9.1	pyruvate, phosphate dikinase
EC 2.7.1.40	pyruvate kinase
EC 1.1.1.49	glucose-6-phosphate dehydrogenase
EC 3.1.3.11	fructose-bisphosphatase
EC 2.7.1.11	6-phosphofructokinase
EC 1.2.1.12	glyceraldehyde-3-phosphate dehydrogenase
EC 4.1.2.13	fructose-bisphosphate aldolase
EC 5.3.1.1	triose-phosphate isomerase
EC 5.3.1.9	glucose-6-phosphate isomerase
EC 3.1.3.37	sedoheptulose-bisphosphatase
EC 2.2.1.2	transaldolase
EC 1.1.1.40	malate dehydrogenase
EC 1.1.1.37	malate dehydrogenase
EC 4.2.1.2	fumarate hydratase
EC 1.1.5.4	malate:quinone oxidoreductase
EC 2.3.3.9	malate synthase
EC 1.3.5.4	fumarate reductase
EC 4.1.1.31	phosphoenolpyruvate carboxylase
EC 4.1.1.49	phosphoenolpyruvate carboxykinase
EC 2.3.3.1	(R)-citric synthase
EC 4.2.1.3	aconitate hydratase

Table B.1 (continued):

EC number	Enzyme name
EC 4.1.3.1	isocitrate lyase
EC 1.1.1.42	isocitrate dehydrogenase
EC 2.6.1.44	alanine---glyoxylate transaminase
EC 6.2.1.5	succinyl-CoA synthetase
EC 2.8.3.18	succinyl-CoA:acetate CoA-transferase
EC 1.2.7.3	2-oxoglutarate synthase
EC 2.7.2.1	acetate kinase
EC 2.3.1.8	phosphate acetyltransferase
EC 6.2.1.1	acetyl-CoA synthetase
EC 1.2.1.3	aldehyde dehydrogenase
EC 2.3.1.9	acetyl-CoA C-acetyltransferase
EC 1.2.7.1	pyruvate synthase
EC 1.1.1.35	3-hydroxyacyl-CoA dehydrogenase
EC 1.1.1.36	D-3-hydroxyacyl-CoA reductase
EC 5.1.2.3	3-hydroxybutyryl-CoA epimerase
EC 1.2.1.43	formate dehydrogenase
EC 4.1.2.36	lactate synthase
EC 1.1.2.3	L-lactate dehydrogenase
EC 2.7.1.69	sucrose phosphotransferase system
EC 3.2.1.26	beta-fructofuranosidase
EC 2.7.1.4	D-fructokinase
EC 5.4.2.2	phosphoglucomutase
EC 2.7.7.9	UDP glucose pyrophosphorylase
EC 2.4.1.15	trehalose phosphate synthase
EC 3.1.3.12	trehalose-phosphatase
EC 2.4.1.64	alpha,alpha-trehalose phosphorylase
EC 5.4.2.6	beta-phosphoglucomutase
EC 2.7.7.27	ADP-glucose synthase
EC 2.4.1.245	alpha,alpha-trehalose synthase
EC 3.6.1.21	ADP-sugar diphosphatase
EC 2.4.1.14	sucrose-phosphate synthase
EC 3.1.3.24	sucrose-phosphate phosphatase

Table B.1 (continued):

EC number	Enzyme name
EC 2.4.1.13	sucrose synthase
EC 3.2.1.20	alpha-glucosidase
EC 2.4.1.4	amylsucrase(invertase)
EC 2.4.1.7	sucrose phosphorylase
EC 2.7.1.2	glucokinase
EC 3.1.3.9	glucose-6-phosphatase
EC 1.12.7.2	hydrogenase
EC 1.18.6.1	nitrogenase
EC 3.6.3.14	ATP synthase
EC 1.16.1.2	diferric-transferrin reductase
EC 2.7.1.23	NAD ⁺ kinase
EC 2.7.4.3	adenylate kinase
EC 1.6.1.2	transhydrogenase

B.3 List of Reactions with their Enzymes

The reactions with an asterisks represent lumped reactions for biosynthetic precursors whereas ME is the abbreviation of multiple enzymes.

R: Reversible reaction

I: Irreversible reaction

Table B.2: Definitions of the reactions on the metabolic network

Flux #	Reaction Type	Enzyme	Reaction
1	I	EC 2.7.1.19	ATP + D-Ribulose 5-phosphate \rightarrow ADP + D-Ribulose 1,5-bisphosphate
2	I	EC 1.1.1.44	6-Phospho-D-gluconate + NADP ⁺ \rightarrow D-Ribulose 5-phosphate + CO ₂ + NADPH + H ⁺
3	R	EC 5.1.3.1	D-Ribulose 5-phosphate \leftrightarrow D-Xylulose 5-phosphate
4	I	EC 4.1.1.39	D-Ribulose 1,5-bisphosphate + CO ₂ + H ₂ O \rightarrow 2 (3-Phospho-D-glycerate)
5	R	EC 5.3.1.6	D-Ribulose 5-phosphate \leftrightarrow D-Ribose 5-phosphate
6	I	EC 3.1.1.31	D-Glucono-1,5-lactone 6-phosphate + H ₂ O \rightarrow 6-Phospho-D-gluconate
7	I	EC 2.2.1.1	D-Fructose 6-phosphate + D-Glyceraldehyde 3-phosphate \rightarrow D-Erythrose 4-phosphate + D-Xylulose 5-phosphate
8	R	EC 2.2.1.1	Sedoheptulose 7-phosphate + D-Glyceraldehyde 3-phosphate \leftrightarrow D-Ribose 5-phosphate + D-Xylulose 5-phosphate
9	R	EC 2.2.1.1	beta-D-Fructose 6-phosphate + D-Glyceraldehyde 3-phosphate \leftrightarrow D-Erythrose 4-phosphate + D-Xylulose 5-phosphate
10	R	EC 2.7.6.1	ATP + D-Ribose 5-phosphate \leftrightarrow AMP + 5-Phospho-alpha-D-ribose 1-diphosphate
11	R	EC 2.7.2.3	ATP + 3-Phospho-D-glycerate \leftrightarrow ADP + 3-Phospho-D-glyceroyl phosphate
12	R	EC 5.4.2.12	2-Phospho-D-glycerate \leftrightarrow 3-Phospho-D-glycerate
13	R	EC 4.2.1.11	2-Phospho-D-glycerate \leftrightarrow Phosphoenolpyruvate + H ₂ O
14	I	EC 2.7.9.1	ATP + Pyruvate + Orthophosphate \rightarrow AMP + Phosphoenolpyruvate + Diphosphate
15	I	EC 2.7.1.40	ADP + Phosphoenolpyruvate \rightarrow ATP + Pyruvate
16	I	EC 1.1.1.49	beta-D-Glucose 6-phosphate + NADP ⁺ \rightarrow D-Glucono-1,5-lactone 6-phosphate + NADPH + H ⁺
17	I	EC 3.1.3.11	D-Fructose 1,6-bisphosphate + H ₂ O \rightarrow D-Fructose 6-phosphate + Orthophosphate

Table B.2 (continued):

Flux #	Reaction Type	Enzyme	Reaction
18	I	EC 3.1.3.11	beta-D-Fructose 1,6-bisphosphate + H ₂ O → beta-D-Fructose 6-phosphate + Orthophosphate
19	I	EC 2.7.1.11	ATP + D-Fructose 6-phosphate → ADP + D-Fructose 1,6-bisphosphate
20	I	EC 2.7.1.11	ATP + beta-D-Fructose 6-phosphate → ADP + beta-D-Fructose 1,6-bisphosphate
21	R	EC 1.2.1.12	D-Glyceraldehyde 3-phosphate + Orthophosphate + NAD ⁺ ↔ 3-Phospho-D-glyceroyl phosphate + NADH + H ⁺
22	R	EC 4.1.2.13	D-Fructose 1,6-bisphosphate ↔ Glycerone phosphate + D-Glyceraldehyde 3-phosphate
23	R	EC 4.1.2.13	Sedoheptulose 1,7-bisphosphate ↔ Glycerone phosphate + D-Erythrose 4-phosphate
24	R	EC 4.1.2.13	beta-D-Fructose 1,6-bisphosphate ↔ Glycerone phosphate + D-Glyceraldehyde 3-phosphate
25	R	EC 5.3.1.1	D-Glyceraldehyde 3-phosphate ↔ Glycerone phosphate
26	R	EC 5.3.1.9	alpha-D-Glucose 6-phosphate ↔ beta-D-Fructose 6-phosphate
27	R	EC 5.3.1.9	alpha-D-Glucose 6-phosphate ↔ beta-D-Glucose 6-phosphate
28	I	EC 3.1.3.37	Sedoheptulose 1,7-bisphosphate + H ₂ O → Sedoheptulose 7-phosphate + Orthophosphate
29	R	EC 2.2.1.2	Sedoheptulose 7-phosphate + D-Glyceraldehyde 3-phosphate ↔ D-Erythrose 4-phosphate + beta-D-Fructose 6-phosphate
30	I	EC 1.1.1.40	(S)-Malate + NADP ⁺ → Pyruvate + CO ₂ + NADPH + H ⁺
31	R	EC 1.1.1.37	(S)-Malate + NAD ⁺ ↔ Oxaloacetate + NADH + H ⁺
32	R	EC 4.2.1.2	(S)-Malate ↔ Fumarate + H ₂ O
33	I	EC 1.1.5.4	(S)-Malate + Quinone → Oxaloacetate + Hydroquinone
34	I	EC 2.3.3.9	Acetyl-CoA + H ₂ O + Glyoxylate → (S)-Malate + CoA

Table B.2 (continued):

Flux #	Reaction Type	Enzyme	Reaction
35	R	EC 1.3.5.4	Quinone + Succinate \leftrightarrow Hydroquinone + Fumarate
36	I	EC 4.1.1.31	H ₂ O + Phosphoenolpyruvate + CO ₂ \rightarrow Orthophosphate + Oxaloacetate
37	I	EC 4.1.1.49	ATP + Oxaloacetate \rightarrow ADP + Phosphoenolpyruvate + CO ₂
38	R	EC 2.3.3.1	Citrate + CoA \leftrightarrow Acetyl-CoA + H ₂ O + Oxaloacetate
39	I	EC 4.2.1.3	Citrate \rightarrow Isocitrate
40	I	EC 4.1.3.1	Isocitrate \rightarrow Succinate + Glyoxylate
41	R	EC 1.1.1.42	Isocitrate + NADP ⁺ \leftrightarrow 2-Oxoglutarate + CO ₂ + NADPH + H ⁺
42	I	EC 2.6.1.44	Glyoxylate + L-Glutamate \leftrightarrow Glycine + 2-Oxoglutarate
43	R	EC 6.2.1.5	ATP + Succinate + CoA \leftrightarrow ADP + Orthophosphate + Succinyl-CoA
44	I	EC 2.8.3.18	Succinyl-CoA + Acetate \rightarrow Acetyl-CoA + Succinate
45	R	EC 1.2.7.3	2 Reduced ferredoxin + Succinyl-CoA + CO ₂ + 2 H ⁺ \leftrightarrow 2 Oxidized ferredoxin + 2-Oxoglutarate + CoA
46	I	ME	2-Oxoglutarate + CoA + NAD ⁺ \rightarrow Succinyl-CoA + CO ₂ + NADH + H ⁺
47	R	EC 2.7.2.1	ATP + Acetate \leftrightarrow ADP + Acetyl phosphate
48	R	EC 2.3.1.8	Acetyl-CoA + Orthophosphate \leftrightarrow CoA + Acetyl phosphate
49	I	EC 6.2.1.1	ATP + Acetate + CoA \rightarrow AMP + Diphosphate + Acetyl-CoA
50	R	EC 1.2.1.3	Acetaldehyde + NAD ⁺ + H ₂ O \leftrightarrow Acetate + NADH + H ⁺
51	R	EC 2.3.1.9	2 Acetyl-CoA \leftrightarrow CoA + Acetoacetyl-CoA
52	R	EC 1.2.7.1	2 Reduced ferredoxin + Acetyl-CoA + CO ₂ + 2 H ⁺ \leftrightarrow 2 Oxidized ferredoxin + Pyruvate + CoA

Table B.2 (continued):

Flux #	Reaction Type	Enzyme	Reaction
53	R	EC 1.1.1.35	Acetoacetyl-CoA + NADH + H ⁺ \leftrightarrow (S)-3-Hydroxybutanoyl-CoA + NAD ⁺
54	R	EC 1.1.1.36	(R)-3-Hydroxybutanoyl-CoA + NADP ⁺ \leftrightarrow Acetoacetyl-CoA + NADPH + H ⁺
55	I	EC 5.1.2.3	(R)-3-Hydroxybutanoyl-CoA \rightarrow (S)-3-Hydroxybutanoyl-CoA
56	I	EC 2.3.1-	(R)-3-Hydroxybutanoyl-CoA \rightarrow Poly-beta-hydroxybutyrate + CoA
57	R	EC 1.2.1.43	CO ₂ + NADPH + H ⁺ \leftrightarrow Formate + NADP ⁺
58	I	EC 4.1.2.36	Formate + Acetaldehyde \rightarrow (S)-Lactate
59	I	EC 1.1.2.3	(S)-lactate + 2 ferricytochrome c \rightarrow pyruvate + 2 ferrocytochrome c + 2 H ⁺
60	R	MTHF to THF*	5,10-Methylenetetrahydrofolate + Glycine + H ₂ O \leftrightarrow Tetrahydrofolate + L-Serine
61	I	THF to MTHF*	Glycine + Tetrahydrofolate + NAD ⁺ \leftrightarrow 5,10-Methylenetetrahydrofolate + Ammonia + CO ₂ + NADH + H ⁺
62	I	Chor syn*	PEP + ATP + Shiki \rightarrow Chorismate + ADP + 2 Pi
63	I	Ala syn*	Pyruvate + Ammonium + NADH \rightarrow Alanine + NAD ⁺
64	I	Val syn*	Glutamate + 3-Methyl-2-Oxobutanoate \rightarrow alpha-Ketoglutarate(2-Oxoglutarate) + Valine
65	I	Leu syn*	Acetyl-CoA + Ammonium + 3-Methyl-2-Oxobutanoate \rightarrow CO ₂ + Leucine + CoA
66	R	Asn syn*	Ammonium + Aspartate \leftrightarrow Asparagine
67	I	Asp syn*	Oxaloacetate + Glutamate \rightarrow 2-Oxoglutarate + Aspartate
68	I	Lys syn*	Diaminopimelate \rightarrow CO ₂ + Lysine
69	I	Met syn*	Acetyl-CoA + NADPH + 5,10-Methylenetetrahydrofolate + Cysteine + Homoserine \rightarrow Pyruvate + Acetate + Ammonium + Methionine + CoA + NADP ⁺ + Tetrahydrofolate
70	I	Thr syn*	ATP + Homoserine \rightarrow Threonine + ADP + Phosphate

Table B.2 (continued):

Flux #	Reaction Type	Enzyme	Reaction
71	I	Ile syn*	Pyruvate + NADPH + Glutamate + Threonine \rightarrow 2-Oxoglutarate + CO ₂ + Ammonium + Isoleucine + NADP ⁺
72	I	His syn*	ATP + CO ₂ + 5-Phosphoribosyl-1-Pyrophosphate + Glutamine + 2NAD ⁺ \rightarrow 2-Oxoglutarate + 2NADH + Histidine + 2Pyrophosphate + AMP
73	I	Glu syn*	2-Oxoglutarate + Ammonium + NADH \rightarrow Glutamate + NAD ⁺
74	I	Gln syn*	ATP + Ammonium + Glutamate \rightarrow Glutamine + ADP + Phosphate
75	I	Pro syn*	ATP + 2NADPH + Glutamate \rightarrow Proline + ADP + Phosphate + 2NADP ⁺
76	I	Arg syn*	ATP + CO ₂ + 2 Ammonium + Aspartate + Proline \rightarrow Fumarate + Arginine + Pyrophosphate + AMP
77	I	Trp syn*	Chorismate + 5-Phosphoribosyl-1-Pyrophosphate + Glutamine + Serine \rightarrow Pyruvate + Glyceraldehyde-3-Phosphate + CO ₂ + Glutamate + Tryptophan + Pyrophosphate
78	I	Tyr syn*	Chorismate + Glutamate + NAD ⁺ \rightarrow 2-Oxoglutarate + CO ₂ + NADH + Tyrosine
79	I	Phe syn*	Chorismate + Glutamate \rightarrow 2-Oxoglutarate + CO ₂ + Phenylalanine
80	I	Ser syn*	3-Phosphoglycerate + Glutamate + NAD ⁺ \rightarrow 2-Oxoglutarate + NADH + Serine + Phosphate
81	I	Cys syn*	Acetyl-CoA + Sulfide + Serine \rightarrow Acetate + Cysteine + CoA
82	I	Asp-Sald syn*	ATP + NADPH + Aspartate \rightarrow Aspartate-Semialdehyde + ADP + Phosphate + NADP ⁺
83	I	HSer syn*	NADPH + Aspartate-Semialdehyde \rightarrow Homoserine + NADP ⁺
84	I	rATP Syn*	3ATP + Aspartate + Inosimonophosphate \rightarrow Fumarate + rATP + 3ADP + Phosphate
85	I	rGTP*	3ATP + Glutamine + NAD ⁺ + Inosimonophosphate \rightarrow NADH + Glutamate + rGTP + 2ADP + Pyrophosphate + AMP
86	I	rCTP*	ATP + Ammonium + rUTP \rightarrow rCTP + ADP + Phosphate
87	I	rUTP*	4ATP + 5-Phosphoribosyl-1-Pyrophosphate + Aspartate + Glutamine \rightarrow Glutamate + rUTP + 4ADP + Phosphate + Pyrophosphate

Table B.2 (continued):

Flux #	Reaction Type	Enzyme	Reaction
88	I	dATP*	NADPH + rATP → dATP + NADP ⁺
89	I	dGTP*	NADPH + rGTP → dGTP + NADP ⁺
90	I	dCTP*	NADPH + rCTP → dCTP + NADP ⁺
91	I	dTTP*	NADPH + 5-10-Methylenetetrahydrofolate + dCTP → dTTP + NADP ⁺ + Tetrahydrofolate
92	I	G3P	NADH + D-Glyceraldehyde 3-phosphate → Glycerol-3-Phosphate + NAD ⁺
93	I	FAs syn*	8.481 Acetyl-CoA + 7.481 ATP + 14.21 NADPH → Fatty Acids + 7.481 ADP + 7.481 Pi + 8.481 CoA + 14.21 NADP ⁺
94	I	CDP-Ea syn*	ATP + Acetate + Ammonium + rATP + NAD ⁺ → NADH + CDP-Ethanolamine + ADP + Pyrophosphate
95	I	MA syn*	7 Acetyl-CoA + 6 ATP + 11 NADPH → Myristic Acid + 6 ADP + 6 Pi + 7 CoA + 11 NADP ⁺
96	I	Lipid syn*	7 Acetyl-CoA + 6 ATP + 12 NADPH → C14_0_FS + 6 ADP + 6 Pi + 7 CoA + 12 NADP ⁺
97	I	CMP_KDO syn*	Ribose-5-Phosphate + Phosphoenolpyruvate + 2 ATP → CMP_KDO + 2 ADP + Phosphate
98	I	NDPHep syn*	1.5 Glucose-6-Phosphate + ATP + 4 NADP ⁺ → 4 NADPH + NDP-Heptose + ADP + Pi
99	I	TDPGlc syn*	Fructose-6-Phosphate + 2 ATP + Ammonium → TDP-Glucosamine + 2 ADP + 2 Phosphate
100	I	UDPag syn*	Fructose-6-Phosphate + Acetyl-CoA + ATP + Glutamine → Glutamate + UDP-Acetylglucosamine + ADP + Phosphate + CoA
101	I	UDPAma syn*	Phosphoenolpyruvate + NADPH + UDP-Acetylglucosamine → UDP-N-Acetylmuramic-acid + NADP ⁺
102	I	Dam syn*	Pyruvate + Succinyl-CoA + NADPH + Glutamate + Aspartate-Semialdehyde → 2-Oxoglutarate + Succinate + Diaminopimelate + CoA + NADP ⁺
103	I	bchla syn*	4 Pyruvate + 4 Glycerol-3-Phosphate + 8 Succinyl-CoA + 3 NADPH + 8 Glycine + ADP + Pi → ATP + 18 CO ₂ + 4 Ammonium + bacteriochlorophyll a + 8 CoA + 3 NADP ⁺
104	I	Shiki syn*	Phosphoenolpyruvate + Erythrose-4-Phosphate + NADPH → 2 Phosphate + NADP ⁺ + Shikimate

Table B.2 (continued):

Flux #	Reaction Type	Enzyme	Reaction
105	I	EC 2.3.1.9	2 Pyruvate \rightarrow CO ₂ + Acetolactate
106	I	Valerate syn*	NADPH + Acetolactate \rightarrow NADP ⁺ + 3-Methyl-2-Oxobutanoate
107	I	IMP syn*	5 ATP + CO ₂ + 5-Phosphoribosyl-1-Pyrophosphate + 2 5-10-Methylenetetrahydrofolate + Aspartate + Glycine + 2 Glutamine + 2 NADP ⁺ \rightarrow Fumarate + 2 NADPH + 2 Glutamate + 5 ADP + 5 Phosphate + Pyrophosphate + 2 Tetrahydrofolate + Inosinmonophosphate
108	I	EC 1.12.7.2	QH2 \rightarrow Q + H ₂
109	I	EC 1.18.6.1	16 ATP + 8Fd_red \rightarrow 16 ADP + 16 Pi + 4H ₂ + 8Fd_ox
110	I	Transporter	H ₂ \rightarrow out
111	I	Reaction Center	2 Ferrocytochrome c + Ubiquinone + 2 photons \rightarrow Ubiquinol + 2 Ferricytochrome c
112	I	EC 1.6.1.2	Ubiquinol + 2 Ferricytochrome c \rightarrow Ubiquinone + 2 Ferrocytochrome c + 2 H ⁺
113	R	EC 1.6.5.3	Ubiquinone + NADH + H ⁺ \leftrightarrow Ubiquinol + NAD ⁺
114	I	EC 3.6.3.14	3H ⁺ + ADP + Pi \rightarrow ATP + H ₂ O + 2H _p
115	R	EC 2.7.1.23	ATP \leftrightarrow ADP + Orthophosphate
116	R	EC 3.6.1.1	Diphosphate \leftrightarrow H ₂ O + 2 Phosphate
117	I	EC 2.7.4.3	ATP + AMP \rightarrow 2 ADP
118	R	EC 1.6.1.2	NADH + NADP ⁺ + H ⁺ \leftrightarrow NADPH + NAD ⁺ + H _p
119	R	EC 1.6.1.2	NADH + 2Fd_ox + H ⁺ \leftrightarrow NAD ⁺ + 2 Fd_red
120	I	EC 2.7.1.69	Sucrose + Protein N(pi)-phospho-L-histidine \rightarrow Sucrose 6-phosphate + Protein histidine
121	I	EC 3.2.1.26	Sucrose 6-phosphate + H ₂ O \rightarrow beta-D-Fructose + alpha-D-Glucose 6-phosphate
122	R	EC 2.7.1.4	ATP + beta-D-Fructose \leftrightarrow ADP + beta-D-Fructose 6-phosphate

Table B.2 (continued):

Flux #	Reaction Type	Enzyme	Reaction
123	R	EC 5.4.2.2	alpha-D-Glucose 6-phosphate \leftrightarrow D-Glucose 1-phosphate
124	I	EC 2.7.7.9	UTP + D-Glucose 1-phosphate \rightarrow Diphosphate + UDP-glucose
125	I	EC 2.4.1.15	UDP-glucose + alpha-D-Glucose 6-phosphate \rightarrow UDP + alpha,alpha'-Trehalose 6-phosphate
126	I	EC 3.1.3.12	alpha,alpha'-Trehalose 6-phosphate + H ₂ O \rightarrow alpha,alpha'-Trehalose + Orthophosphate
127	I	EC 2.4.1.64	alpha,alpha'-Trehalose + Orthophosphate \rightarrow D-Glucose + beta-D-Glucose 1-phosphate
128	R	EC 5.4.2.6	beta-D-Glucose 1-phosphate \leftrightarrow beta-D-Glucose 6-phosphate
129	I	EC 2.7.7.27	ATP + D-Glucose 1-phosphate \rightarrow Diphosphate + ADP-glucose
130	I	EC 2.4.1.245	ADP-glucose + D-Glucose \rightarrow alpha,alpha'-Trehalose + ADP
131	I	EC 3.6.1.21	ADP-glucose + H ₂ O \rightarrow AMP + D-Glucose 1-phosphate
132	I	EC 2.4.1.14	UDP-glucose + D-Fructose 6-phosphate \rightarrow UDP + Sucrose 6'-phosphate
133	I	EC 3.1.3.24	Sucrose 6'-phosphate + H ₂ O \rightarrow Sucrose + Orthophosphate
134	I	EC 2.4.1.13	UDP-glucose + D-Fructose \rightarrow UDP + Sucrose
135	I	EC 3.2.1.20	Sucrose + H ₂ O \rightarrow beta D-Fructose + alpha D-Glucose
136	I	EC 2.4.1.4	Sucrose \rightarrow D-Fructose + D-Glucose
137	R	ME	UDP-glucose + 2 H ₂ O \leftrightarrow UDP + D-Glucose + alpha-D-Glucose
138	R	EC 2.4.1.7	Sucrose + Orthophosphate \leftrightarrow D-Fructose + D-Glucose 1-phosphate
139	I	EC 2.7.1.2	ATP + alpha-D-Glucose \rightarrow ADP + alpha-D-Glucose 6-phosphate
140	R	EC 3.1.3.9	alpha-D-Glucose 6-phosphate + H ₂ O \leftrightarrow alpha-D-Glucose + Orthophosphate

Table B.2 (continued):

Flux #	Reaction Type	Enzyme	Reaction
141	I	Transporter	Sucrose → out
142	I	Transporter	Acetate → out
143	I	Transporter	Lactate → out
144	I	Transporter	Formate → out
145	I	Transporter	CO ₂ → out
146	I	Transporter	PHB (Poly-beta-hydroxybutyrate) → out

APPENDIX C

PART OF THE STOICHIOMETRIC MATRIX

This matrix is part of the stoichiometric matrix including 148 columns (reactions) and 128 rows (metabolites) considered in the model.

Table C.1: Partly tabulated form of the stoichiometric matrix

	1	2	3	4	5	6
	EC 2.7.1.19	EC 1.1.1.44	EC 5.1.3.1	EC 4.1.1.39	EC 5.3.1.6	EC 3.1.1.31
ATP	-1	0	0	0	0	0
ADP	1	0	0	0	0	0
R5P	-1	1	-1	0	-1	0
R15P	1	0	0	-1	0	0
6PG	0	-1	0	0	0	1
NADP+	0	-1	0	0	0	0
NADPH	0	1	0	0	0	0
CO2	0	1	0	-1	0	0
H+	0	1	0	0	0	0
Hpp	0	0	0	0	0	0
X5P	0	0	1	0	1	0
3PG	0	0	0	2	0	0
H2O	0	0	0	-1	0	-1
GL6P	0	0	0	0	0	-1
F6P	0	0	0	0	0	0
GAld3P	0	0	0	0	0	0
E4P	0	0	0	0	0	0
S7P	0	0	0	0	0	0
R5P	0	0	0	0	0	0
F6P	0	0	0	0	0	0
PEP	0	0	0	0	0	0

APPENDIX D

GROWTH REACTION COEFFICIENTS OF *R. palustris*

Table D.1: Coefficients of biomass growth reaction (148th reaction) per g dry cell weight (Appendix B1 can be referred for abbreviations of the metabolites)

Metabolites	mmol metabolite/ g dry cell weight
ATP	20.87
Ala	0.488
Cys	0.079
Asp	0.208
Glu	0.249
Phe	0.160
Gly	0.529
His	0.082
Ile	0.250
Lys	0.296
Leu	0.389
Met	0.133
Asn	0.208
Pro	0.190
Gln	0.227
Arg	0.255
Ser	0.413
Thr	0.219
Val	0.365
Trp	0.049
Tyr	0.119
ADP	-20.87

Table D.1 (continued):

Pi	-20.87
rATP	0.382
rGTP	0.158
rCTP	0.098
rUTP	0.106
dATP	0.018
dGTP	0.030
dCTP	0.030
dTTP	0.018
G3P	0.227
FA	0.454
UDP-Glc	0.014
CDP-Ea	0.021
MA	0.021
Lipid syn	0.021
CMP-KDO	0.021
NDPHep	0.021
TDP-Glu	0.014
UDPAg	0.022
UDP Ama	0.022
Dam	0.022
ADP-Glu	0.123
3-Hbut(S)	0.581
CoA	-0.581
Bchla	0.011

APPENDIX E

SAMPLE CALCULATIONS

E.1 Calculation of Initial Sucrose Flux

The small scale photobioreactor used in the experiments of Sagir (2012) is 50 ml. 5 mM sucrose in the growth medium can be calculated in the unit of mmol as seen in (E.1)

$$5 (mM) \frac{mmol}{l} \times \frac{l}{1000ml} \times 50ml = 0.25mmol \quad (E.1)$$

Therefore, 0.25 mmol sucrose is given to the system per hour and per culture liter.

E.2 Calculation of Initial Glutamate Flux

In experimental conditions, 2 mM glutamate in the growth medium used in 50 ml of the small scale photobioreactor. The initial glutamate flux can be calculated as seen E.2.

$$2 (mM) \frac{mmol}{l} \times \frac{l}{1000ml} \times 50ml = 0.1mmol \quad (E.2)$$

Therefore, 0.1 mmol glutamate is given to system per hour and per culture liter.

E.3 Calculation of Photon Flux

In the experiments, 2000-2200 lux illumination is used for photosynthesis. In order to obtain the photon flux in terms of mmol, 2100 lux is converted as $140 \frac{W}{m^2}$ by using conversion factor of lux to W/m^2 (0.065) based on the tungsten lamps (60-100 W). Also, Sagir (2012) used 50 ml small lab scale photobioreactor corresponding 0.002 m^2 surface area.

$$\text{Power of the light on the surface} = 136 \frac{W}{m^2} \times 0.002 m^2 = 0.27 \frac{J}{s} \quad (E.3)$$

The energy content of one photon at 660 nm can be calculated by (E.4) where h is Planck constant, c is speed of light and λ is the wavelength.

$$E = \frac{h \times c}{\lambda} = \frac{(6.626 \times 10^{-34} J.s) \times (3 \times 10^8 \frac{m}{s})}{660 \times 10^{-9} m} = 3 \times 10^{-19} \frac{J}{\text{photon}} \quad (E.4)$$

The number of photons directed to the surface of the photobioreactor can be calculated.

$$\begin{aligned} \# \text{ of photons} &= \frac{\text{energy of the light}}{\text{energy of one photon}} = \frac{0.27 \frac{J}{s}}{3 \times 10^{-19} \frac{J}{\text{photon}}} \times 3600 \frac{s}{h} \\ &= 3.24 \times 10^{21} \frac{\text{photons}}{h} \end{aligned}$$

Using Avogadro number, photon flux in the unit of mmol/h is calculated.

$$\text{Photon flux} = \frac{\# \text{ of photons}}{\text{mole of photons}} = \frac{3.24 \times 10^{21} \frac{\text{photons}}{h}}{6.023 \times 10^{23} \frac{\text{photons}}{\text{mole}}} \times 1000 \frac{\text{mmole}}{\text{mole}} = 5 \frac{\text{mmol}}{h}$$

E.4 Calculation of Sucrose Conversion Efficiency

The overall hydrogen production reaction on sucrose is given below.



The metabolic model results 0.037 mmol/h of sucrose uptake rate in the base case. Based on this uptake rate, theoretical hydrogen production rate can be calculated using the stoichiometry in the overall reaction.

$$\textit{Theoretical hydrogen production} = 33 \times 0.037 = 1.2 \text{ mmol/h}$$

Hydrogen production flux of the base case is 0.68 mmol/h which is estimated hydrogen production rate of the model. The calculation of the substrate conversion efficiency of the model is shown below.

$$\textit{Substrate conversion efficiency} = \frac{\textit{Estimated hydrogen production rate}}{\textit{Theoretical production rate}} \times 100$$

$$\textit{Substrate conversion efficiency} = \frac{0.68 \text{ mmol/h}}{1.2 \text{ mmol/h}} \times 100 = 56\%$$

APPENDIX F

MATLAB SCRIPTS

F.1 Objective Function: Maximum Biomass Growth Rate

```
clc;
% interior point is used as optimization method for 'linprog'
function
options = optimoptions('linprog','Algorithm','interior-
point','Display','iter','TolFun',1e-
10,'MaxIter',10000,'TolCon',1e-5);

% stoichiometric matrix of the test case is loaded to the
workspace
S_struct = load('sm.mat');
sm_r = S_struct.sm;

% dependent rows of the stoichiometric matrix are eliminated
with 'licols'
% functions
sto_transpose = sm_r';
reduced_sto_tranpose = licols(sm_r',1e-10);

% reduced stoichiometric is defined as 'S'
S = reduced_sto_tranpose';
l = size(S,2); % number of columns of raw matrix (# of
fluxes-enzymes)
```

```

w = size(S,1); % number of rows of raw matrix (# of
metabolites)
d_c = S(:,l-1); % Growth reaction (demand) coefficients of
biomass
s_c = S(:,1); % Coefficients of inputs

% Objective function is set
% Note that linprog minimizes function by default so we will
minimize -obj as equivalent to maximizing obj
obj = zeros(l-1,1); % initializing objective function vector
obj(l-1)= sum(d_c); % maximum biomass growth

%INEQUALITY
% To make the demand reaction nonzero, A and b are described
as vector.
A = zeros(l-1,l-1);
A(1,l-1) = -1;
b = zeros(l-1,1);
b(1)=-0.0001;

% EQUALITIES
S(:,1) = []; % remove supply flux from variable matrix
% the supply flux is constant
Aeq = S;
beq =s_c; % the supply flux constant from right hand side
ub = 1000;
UB = ub*ones(l-1,1); %upper bound as a constraint
LB = -1000+zeros(l-1,1); %lower bound as another constraint

% CONSTRAINTS
LB(1:2)=0;
LB(4)=0;
LB(6:7)=0;

```

```
LB(14:20)=0;
LB(28)=0;
LB(30)=0;
LB(33:34)=0;
LB(36:37)=0;
LB(39:40)=0;
LB(42)=0;
LB(44)=0;
LB(46)=0;
LB(49)=0;
LB(55:56)=0;
LB(58:59)=0;
LB(61:65)=0;
LB(80)=0;
LB(108:110)=0;
LB(114)=0;
LB(117)=0;
LB(120:121)=0;
LB(124:127)=0;
LB(129:136)=0;
LB(139)=0;
LB(141:end)=0;
```

```
%'linprog' funtion is called to solve this optimization
problem
```

```
x0=ones(l-1,1);
```

```
[x, objectivevalue, exitflag,output] = linprog(obj, A, b,
Aeq, beq, LB,UB,x0,options );
```

F.2 Objective Function: Maximum Hydrogen Production Rate

```
clc;
% interior point is used as optimization method for 'linprog'
function
options = optimoptions('linprog','Algorithm','interior-
point','TolFun',1e-10,'MaxIter',10000,'TolCon',1e-3);

% stoichiometric matrix of the test case is loaded to the
workspace
S_struct = load('sm.mat');
sm_r = S_struct.sm;

% dependent rows of the stoichiometric matrix are eliminated
with 'licols'
% functions
sto_transpose = sm_r';
reduced_sto_tranpose = licols(sm_r',1e-10);

% reduced stoichiometric is defined as 'S'
S = reduced_sto_tranpose';
l = size(S,2); % number of columns of raw matrix (# of
fluxes-enzymes)
w = size(S,1); % number of rows of raw matrix (# of
metabolites)
d_c = S(:,l-1); % Growth reaction (demand) coefficients of
biomass
s_c = S(:,1); % Coefficients of inputs

% Objective function is set
% Note that linprog minimizes function by default so we will
%minimize -obj as equivalent to maximizing obj
```

```

obj = zeros(1-1,1); % initializing objective function vector
obj(110)= -1; % maximum hydrogen production rate

%INEQUALITY
% To make the demand reaction nonzero, A and b are described
as vector.
A = zeros(1-1,1-1);
A(1,1-1) = -1;
b = zeros(1-1,1);
b(1)=-0.0001;

% EQUALITIES
S(:,1) =[]; % remove supply flux from variable matrix
           % the supply flux is constant
Aeq = S;
beq = s_c; % the supply flux constant from right hand side
ub = 1000;
UB = ub*ones(1-1,1); %upper bound as a constraint
LB = -1000+zeros(1-1,1); %lower bound as another constraint

% CONSTRAINTS
LB(1:2)=0;
LB(4)=0;
LB(6:7)=0;
LB(14:20)=0;
LB(28)=0;
LB(30)=0;
LB(33:34)=0;
LB(36:37)=0;
LB(39:40)=0;
LB(42)=0;
LB(44)=0;
LB(46)=0;

```

```
LB(49)=0;
LB(55:56)=0;
LB(58:59)=0;
LB(61:65)=0;
LB(80)=0;
LB(108:110)=0;
LB(114)=0;
LB(117)=0;
LB(120:121)=0;
LB(124:127)=0;
LB(129:136)=0;
LB(139)=0;
LB(141:end)=0;

%'linprog' funtion is called to solve this optimization
problem
x0=0.001*ones(1-1,1);

[x, objectivevalue, exitflag,output] = linprog(obj, A, b,
Aeq, beq, LB, UB,x0,options );
```

APPENDIX G

FLUX DISTRIBUTIONS

Only one representative flux distribution is shown for each case and objective function.

Table G.1: Flux distribution of different cases for the objective function of maximum biomass growth rate

Fluxes (mmol/h)	The cases at maximum biomass growth rate				
	Base Case	Case 1	Case 2	Case 3	Case 4
Glutamate flux	0.1	0.3	0.1	0.1	0.1
Sucrose flux	0.25	0.25	0.1	0.25	0.25
Photon flux	5	5	5	30	5
Acetic acid	0	0	0	0	0.01
1	71.52	78.11	71.53	77.66	71.69
2	71.50	78.06	71.51	77.64	71.67
3	-0.0097	-0.0290	-0.0097	-0.0097	-0.0097
4	71.52	78.11	71.53	77.66	71.69
5	-0.0097	-0.0290	-0.0097	-0.0097	-0.0097
6	71.50	78.06	71.51	77.64	71.67
7	62.45	66.35	62.71	67.70	62.80
8	0.0077	0.0232	0.0077	0.0077	0.0077
9	-62.43	-66.32	-62.70	-67.69	-62.79
10	0.0075	0.0224	0.0075	0.0075	0.0075
11	142.91	155.86	142.94	155.23	143.26
12	-0.118	-0.360	-0.118	-0.094	-0.117
13	0.118	0.360	0.118	0.094	0.117
14	194.16	197.64	196.01	193.39	195.85
15	180.55	185.94	181.05	187.49	181.02
16	71.50	78.06	71.51	77.64	71.67
17	95.07	96.58	95.20	98.98	95.23
18	38.36	38.19	38.22	38.48	38.23
19	32.63	30.22	32.48	31.27	32.42
20	65.81	59.14	65.53	62.65	65.38
21	-142.91	-155.86	-142.94	-155.23	-143.26

Table G.1 (continued):

Fluxes (mmol/h)	The cases at maximum biomass growth rate				
	Base Case	Case 1	Case 2	Case 3	Case 4
Glutamate flux	0.1	0.3	0.1	0.1	0.1
Sucrose flux	0.25	0.25	0.1	0.25	0.25
Photon flux	5	5	5	30	5
Acetic acid	0	0	0	0	0.01
22	-62.45	-66.36	-62.71	-67.71	-62.80
23	-36.46	-32.50	-36.06	-34.07	-35.97
24	27.46	20.96	27.31	24.17	27.15
25	71.45	77.91	71.46	77.61	71.62
26	-71.47	-77.96	-71.48	-77.62	-71.64
27	-116.82	-112.28	-117.02	-114.31	-116.88
28	36.46	32.50	36.06	34.07	35.97
29	36.45	32.48	36.06	34.06	35.96
30	79.50	76.72	80.47	75.96	80.36
31	-34.98	-35.21	-36.75	-30.57	-36.63
32	-0.188	-0.573	-0.189	-0.136	-0.198
33	21.38	23.52	21.80	24.64	21.81
34	65.71	64.45	65.33	69.89	65.35
35	0.18	0.54	0.18	0.12	0.19
36	57.16	53.17	58.13	50.66	58.00
37	43.45	41.13	43.06	44.67	43.06
38	-0.084	-0.259	-0.084	-0.031	-0.093
39	0.084	0.259	0.084	0.031	0.093
40	65.74	64.54	65.36	69.92	65.38
41	-65.65	-64.28	-65.27	-69.89	-65.29
42	0.028	0.083	0.027	0.025	0.027
43	292.82	280.98	287.37	297.60	287.80
44	227.26	216.98	222.19	227.80	222.60
45	67.23	65.76	67.09	81.22	67.07
46	1.68	1.77	1.91	11.43	1.87
47	-304.05	-290.97	-297.50	-304.45	-298.06
48	304.05	290.97	297.50	304.45	298.06
49	76.79	73.93	75.31	76.62	75.47
50	-0.0012	-0.0712	-0.0009	-0.0186	-0.0009
51	0.0080	0.0241	0.0080	0.0171	0.0081
52	-65.86	-65.00	-65.48	-70.04	-65.51
53	-75.29	-78.56	-76.18	-89.27	-76.21

Table G.1 (continued):

Fluxes (mmol/h)	The cases at maximum biomass growth rate				
	Base Case	Case 1	Case 2	Case 3	Case 4
Glutamate flux	0.1	0.3	0.1	0.1	0.1
Sucrose flux	0.25	0.25	0.1	0.25	0.25
Photon flux	5	5	5	30	5
Acetic acid	0	0	0	0	0.01
54	-75.30	-78.59	-76.19	-89.28	-76.21
55	75.30	78.58	76.19	89.27	76.21
56	0.0011	0.0034	0.0011	0.0102	0.0012
57	0.0377	0.1940	0.0370	0.0621	0.0387
58	0.0012	0.0712	0.0009	0.0186	0.0009
59	0.0007	0.0699	0.0004	0.0185	0.0004
60	0.0051	0.0152	0.0049	0.0036	0.0050
61	0.0124	0.0371	0.0122	0.0109	0.0123
62	0.0039	0.0117	0.0039	0.0039	0.0039
63	0.0058	0.0174	0.0058	0.0058	0.0058
64	0.0043	0.0130	0.0043	0.0043	0.0043
65	0.0046	0.0139	0.0046	0.0046	0.0046
66	0.0025	0.0074	0.0025	0.0025	0.0025
67	0.0299	0.0896	0.0299	0.0299	0.0299
68	0.0035	0.0106	0.0035	0.0035	0.0035
69	0.0016	0.0047	0.0016	0.0016	0.0016
70	0.0056	0.0168	0.0056	0.0056	0.0056
71	0.0030	0.0089	0.0030	0.0030	0.0030
72	0.0010	0.0029	0.0010	0.0010	0.0010
73	-0.0194	-0.0581	-0.0195	-0.0209	-0.0194
74	0.0157	0.0471	0.0157	0.0157	0.0157
75	-0.0008	-0.0023	-0.0008	-0.0008	-0.0008
76	0.0030	0.0091	0.0030	0.0030	0.0030
77	0.0006	0.0018	0.0006	0.0006	0.0006
78	0.0014	0.0042	0.0014	0.0014	0.0014
79	0.0019	0.0057	0.0019	0.0019	0.0019
80	0.0029	0.0088	0.0031	0.0044	0.0030
81	0.0025	0.0076	0.0025	0.0025	0.0025
82	0.0109	0.0328	0.0109	0.0109	0.0109
83	0.0072	0.0215	0.0072	0.0072	0.0072
84	0.0050	0.0150	0.0050	0.0050	0.0050
85	0.0022	0.0067	0.0022	0.0022	0.0022

Table G.1 (continued):

Fluxes (mmol/h)	The cases at maximum biomass growth rate				
	Base Case	Case 1	Case 2	Case 3	Case 4
Glutamate flux	0.1	0.3	0.1	0.1	0.1
Sucrose flux	0.25	0.25	0.1	0.25	0.25
Photon flux	5	5	5	30	5
Acetic acid	0	0	0	0	0.01
86	0.0017	0.0052	0.0017	0.0017	0.0017
87	0.0032	0.0095	0.0032	0.0032	0.0032
88	0.0002	0.0006	0.0002	0.0002	0.0002
89	0.0004	0.0011	0.0004	0.0004	0.0004
90	0.0006	0.0017	0.0006	0.0006	0.0006
91	0.0002	0.0006	0.0002	0.0002	0.0002
92	0.0027	0.0081	0.0027	0.0027	0.0027
93	0.0054	0.0162	0.0054	0.0054	0.0054
94	0.0002	0.0007	0.0002	0.0002	0.0002
95	0.0002	0.0007	0.0002	0.0002	0.0002
96	0.0002	0.0007	0.0002	0.0002	0.0002
97	0.0002	0.0007	0.0002	0.0002	0.0002
98	0.0002	0.0007	0.0002	0.0002	0.0002
99	0.0002	0.0005	0.0002	0.0002	0.0002
100	0.0005	0.0016	0.0005	0.0005	0.0005
101	0.0003	0.0008	0.0003	0.0003	0.0003
102	0.0038	0.0114	0.0038	0.0038	0.0038
103	0.0001	0.0004	0.0001	0.0001	0.0001
104	0.0039	0.0117	0.0039	0.0039	0.0039
105	0.0090	0.0269	0.0090	0.0090	0.0090
106	0.0090	0.0269	0.0090	0.0090	0.0090
107	0.0028	0.0083	0.0028	0.0028	0.0028
108	0.11	0.29	0.10	0.22	0.11
109	0.05	0.14	0.05	0.01	0.05
110 H ₂ production rate	0.68	1.93	0.68	0.38	0.72
111	2.5	2.5	2.5	15	2.5
112	2.5	2.5	2.5	15	2.5
113	-21.45	-23.77	-21.87	-24.54	-21.89
114	1.22	0.62	0.74	7.46	0.77
115	-960.57	-962.37	-960.85	-958.80	-960.86
116	479.17	477.99	479.30	479.02	479.25

Table G.1 (continued):

Fluxes (mmol/h)	The cases at maximum biomass growth rate				
	Base Case	Case 1	Case 2	Case 3	Case 4
Glutamate flux	0.1	0.3	0.1	0.1	0.1
Sucrose flux	0.25	0.25	0.1	0.25	0.25
Photon flux	5	5	5	30	5
Acetic acid	0	0	0	0	0.01
117	290.85	287.66	290.76	287.08	290.70
118	-81.39	-89.42	-81.88	-71.90	-82.04
119	1.94	2.48	2.18	11.36	2.16
120	0.037	0.112	0.037	0.037	0.037
121	0.037	0.112	0.037	0.037	0.037
122	0.039	0.115	0.039	0.044	0.039
123	188.32	190.34	188.54	191.95	188.56
124	0.0002	0.0005	0.0002	0.0002	0.0002
125	0.0015	0.0046	0.0015	0.0056	0.0015
126	0.0015	0.0046	0.0015	0.0056	0.0015
127	188.32	190.34	188.54	191.95	188.55
128	188.32	190.34	188.54	191.95	188.55
129	208.21	206.38	207.96	208.99	207.92
130	188.32	190.33	188.53	191.94	188.55
131	19.88	16.04	19.42	17.05	19.36
132	0.0019	0.0036	0.0018	0.0072	0.0020
133	0.0019	0.0036	0.0018	0.0072	0.0020
134	0.0010	0.0015	0.0009	0.0023	0.0010
135	0.0019	0.0036	0.0018	0.0072	0.0020
136	0.0029	0.0051	0.0028	0.0096	0.0030
137	-0.0044	-0.0097	-0.0042	-0.0152	-0.0046
138	-0.0019	-0.0036	-0.0018	-0.0072	-0.0020
139	24.54	20.98	24.43	21.95	24.31
140	24.54	20.98	24.44	21.95	24.31
141	0.213	0.138	0.063	0.213	0.213
142	0.0005	0.0013	0.0005	0.0127	0.0005
143	0.0005	0.0013	0.0005	0.0000	0.0005
144	0.04	0.12	0.04	0.04	0.04
145	0.41	1.25	0.41	0.28	0.43
146	0.0011	0.0034	0.0011	0.0102	0.0012
147 Biomass growth rate	0.0119	0.0356	0.0119	0.0119	0.0119

Table G.2: Flux distribution of different cases for the objective function of maximum hydrogen production rate

Fluxes (mmol/h)	The cases at maximum Hydrogen Production				
	Base Case	Case 1	Case 2	Case 3	Case 4
Glutamate flux	0.1	0.3	0.1	0.1	0.1
Sucrose flux	0.25	0.25	0.1	0.25	0.25
Photon flux	5	5	5	30	5
Acetic acid	0	0	0	0	0.01
1	76.69	77.14	76.65	72.18	77.49
2	76.67	77.08	76.63	72.16	77.47
3	-0.0097	-0.0290	-0.0097	-0.0097	-0.0097
4	76.69	77.14	76.65	72.18	77.49
5	-0.0097	-0.0290	-0.0097	-0.0097	-0.0097
6	76.67	77.08	76.63	72.16	77.47
7	65.70	65.84	65.67	63.19	66.22
8	0.0077	0.0232	0.0077	0.0077	0.0077
9	-65.68	-65.81	-65.66	-63.17	-66.21
10	0.0075	0.0224	0.0075	0.0075	0.0075
11	153.24	153.89	153.17	144.23	154.85
12	-0.126	-0.379	-0.126	-0.117	-0.126
13	0.126	0.379	0.126	0.117	0.126
14	192.46	192.79	192.43	182.36	193.39
15	183.04	183.06	183.03	178.51	183.42
16	76.67	77.08	76.63	72.16	77.47
17	96.03	95.67	96.03	97.52	96.29
18	37.35	36.98	37.36	39.81	37.28
19	30.33	29.83	30.36	34.33	30.07
20	61.25	60.19	61.28	70.12	60.62
21	-153.24	-153.89	-153.17	-144.23	-154.85
22	-65.70	-65.84	-65.67	-63.19	-66.22
23	-34.81	-34.29	-34.83	-39.23	-34.54
24	23.89	23.21	23.92	30.31	23.35
25	76.61	76.92	76.58	72.11	77.42
26	-76.63	-76.97	-76.60	-72.12	-77.43
27	-112.99	-112.11	-113.02	-115.32	-112.40
28	34.81	34.29	34.83	39.23	34.54
29	34.80	34.27	34.82	39.22	34.53
30	76.44	76.52	76.44	75.54	76.83

Table G.2 (continued):

Fluxes (mmol/h)	The cases at maximum Hydrogen Production				
	Base Case	Case 1	Case 2	Case 3	Case 4
Glutamate flux	0.1	0.3	0.1	0.1	0.1
Sucrose flux	0.25	0.25	0.1	0.25	0.25
Photon flux	5	5	5	30	5
Acetic acid	0	0	0	0	0.01
31	-32.31	-33.06	-32.28	-24.07	-33.00
32	-0.200	-0.601	-0.200	-0.192	-0.210
33	22.90	23.35	22.89	20.22	23.04
34	66.83	66.21	66.84	71.50	66.67
35	0.19	0.57	0.19	0.18	0.20
36	51.89	51.69	51.90	52.71	52.01
37	42.36	41.60	42.37	48.75	41.92
38	-0.095	-0.287	-0.095	-0.087	-0.105
39	0.095	0.287	0.095	0.087	0.105
40	66.85	66.30	66.86	71.51	66.69
41	-66.76	-66.01	-66.77	-71.43	-66.59
42	0.026	0.082	0.026	0.010	0.026
43	302.84	298.38	302.90	334.01	300.26
44	236.17	232.64	236.22	262.67	233.76
45	68.88	67.59	68.89	79.25	68.39
46	2.21	1.87	2.22	7.92	1.89
47	-315.35	-310.57	-315.42	-349.04	-312.26
48	315.35	310.57	315.42	349.04	312.26
49	79.19	77.95	79.21	86.37	78.51
50	0	0	0	0	0
51	0.0069	0.0207	0.0069	0.0069	0.0069
52	-66.99	-66.71	-67.00	-71.66	-66.83
53	-77.98	-77.81	-77.96	-77.54	-78.00
54	-77.99	-77.83	-77.97	-77.55	-78.01
55	77.99	77.83	77.97	77.55	78.01
56	1.46E-27	2.91E-20	4.51E-28	8.19E-28	9.19E-28
57	0	0	0	0	0
58	0	0	0	0	0
59	0	0	0	0	0
60	0.0044	0.0147	0.0045	-0.0038	0.0045
61	0.0117	0.0366	0.0118	0.0035	0.0118
62	0.0039	0.0117	0.0039	0.0039	0.0039

Table G.2 (continued):

Fluxes (mmol/h)	The cases at maximum Hydrogen Production				
	Base Case	Case 1	Case 2	Case 3	Case 4
Glutamate flux	0.1	0.3	0.1	0.1	0.1
Sucrose flux	0.25	0.25	0.1	0.25	0.25
Photon flux	5	5	5	30	5
Acetic acid	0	0	0	0	0.01
63	0.0058	0.0174	0.0058	0.0058	0.0058
64	0.0043	0.0130	0.0043	0.0043	0.0043
65	0.0046	0.0139	0.0046	0.0046	0.0046
66	0.0025	0.0074	0.0025	0.0025	0.0025
67	0.0299	0.0896	0.0299	0.0299	0.0299
68	0.0035	0.0106	0.0035	0.0035	0.0035
69	0.0016	0.0047	0.0016	0.0016	0.0016
70	0.0056	0.0168	0.0056	0.0056	0.0056
71	0.0030	0.0089	0.0030	0.0030	0.0030
72	0.0010	0.0029	0.0010	0.0010	0.0010
73	-0.0200	-0.0586	-0.0199	-0.0282	-0.0199
74	0.0157	0.0471	0.0157	0.0157	0.0157
75	-0.0008	-0.0023	-0.0008	-0.0008	-0.0008
76	0.0030	0.0091	0.0030	0.0030	0.0030
77	0.0006	0.0018	0.0006	0.0006	0.0006
78	0.0014	0.0042	0.0014	0.0014	0.0014
79	0.0019	0.0057	0.0019	0.0019	0.0019
80	0.0036	0.0094	0.0035	0.0118	0.0035
81	0.0025	0.0076	0.0025	0.0025	0.0025
82	0.0109	0.0328	0.0109	0.0109	0.0109
83	0.0072	0.0215	0.0072	0.0072	0.0072
84	0.0050	0.0150	0.0050	0.0050	0.0050
85	0.0022	0.0067	0.0022	0.0022	0.0022
86	0.0017	0.0052	0.0017	0.0017	0.0017
87	0.0032	0.0095	0.0032	0.0032	0.0032
88	0.0002	0.0006	0.0002	0.0002	0.0002
89	0.0004	0.0011	0.0004	0.0004	0.0004
90	0.0006	0.0017	0.0006	0.0006	0.0006
91	0.0002	0.0006	0.0002	0.0002	0.0002
92	0.0027	0.0081	0.0027	0.0027	0.0027
93	0.0054	0.0162	0.0054	0.0054	0.0054
94	0.0002	0.0007	0.0002	0.0002	0.0002

Table G.2 (continued):

Fluxes (mmol/h)	The cases at maximum Hydrogen Production				
	Base Case	Case 1	Case 2	Case 3	Case 4
Glutamate flux	0.1	0.3	0.1	0.1	0.1
Sucrose flux	0.25	0.25	0.1	0.25	0.25
Photon flux	5	5	5	30	5
Acetic acid	0	0	0	0	0.01
95	0.0002	0.0007	0.0002	0.0002	0.0002
96	0.0002	0.0007	0.0002	0.0002	0.0002
97	0.0002	0.0007	0.0002	0.0002	0.0002
98	0.0002	0.0007	0.0002	0.0002	0.0002
99	0.0002	0.0005	0.0002	0.0002	0.0002
100	0.0005	0.0016	0.0005	0.0005	0.0005
101	0.0003	0.0008	0.0003	0.0003	0.0003
102	0.0038	0.0114	0.0038	0.0038	0.0038
103	0.0001	0.0004	0.0001	0.0001	0.0001
104	0.0039	0.0117	0.0039	0.0039	0.0039
105	0.0090	0.0269	0.0090	0.0090	0.0090
106	0.0090	0.0269	0.0090	0.0090	0.0090
107	0.0028	0.0083	0.0028	0.0028	0.0028
108	0.61	1.14	0.62	0.77	0.70
109	0.01	0.10	0.01	0.00	0.01
110 H ₂ production rate	0.78	2.35	0.78	0.78	0.82
111	2.5	2.5	2.5	15	2.5
112	2.5	2.5	2.5	15	2.5
113	-22.47	-22.78	-22.46	-19.63	-22.55
114	0.99	1.08	0.99	14.87	1.73
115	-958.66	-958.87	-958.66	-957.34	-958.62
116	479.04	477.14	479.05	478.68	479.11
117	289.38	287.95	289.40	291.20	289.24
118	-84.90	-86.50	-84.84	-70.76	-87.05
119	2.05	2.10	2.05	7.60	1.68
120	0.037	0.112	0.037	0.037	0.037
121	0.037	0.112	0.037	0.037	0.037
122	0.037	0.112	0.037	0.037	0.037
123	189.66	189.20	189.65	187.48	189.87
124	0.0002	0.0005	0.0002	0.0002	0.0002
125	1.32E-27	2.69E-20	5.11E-28	2.87E-28	2.45E-27

Table G.2 (continued):

Fluxes (mmol/h)	The cases at maximum Hydrogen Production				
	Base Case	Case 1	Case 2	Case 3	Case 4
Glutamate flux	0.1	0.3	0.1	0.1	0.1
Sucrose flux	0.25	0.25	0.1	0.25	0.25
Photon flux	5	5	5	30	5
Acetic acid	0	0	0	0	0.01
126	8.46E-28	2.68E-20	1.61E-28	1.05E-27	3.64E-56
127	189.66	189.19	189.65	187.48	189.87
128	189.66	189.19	189.65	187.48	189.87
129	207.38	206.37	207.39	209.93	207.20
130	189.66	189.19	189.65	187.48	189.87
131	17.72	17.17	17.74	22.45	17.33
132	2.31E-27	3.45E-20	4.43E-28	7.15E-37	3.61E-27
133	1.73E-27	3.45E-20	3.85E-28	8.67E-28	9.36E-28
134	8.93E-28	1.70E-20	5.76E-29	1.34E-28	1.61E-30
135	5.50E-36	7.16E-20	1.91E-28	3.38E-28	9.11E-28
136	1.02E-26	6.38E-20	1.34E-26	4.03E-27	4.66E-28
137	0	0	0	0	0
138	0	0	0	0	0
139	21.83	21.37	21.85	25.80	21.54
140	21.83	21.37	21.85	25.80	21.54
141	0.213	0.138	0.063	0.213	0.213
142	1.37E-27	3.03E-20	2.55E-28	8.74E-28	1.07E-27
143	6.53E-28	2.32E-20	2.54E-28	4.15E-28	7.35E-28
144	1.38E-27	2.27E-19	8.48E-28	2.61E-27	4.14E-27
145	0.48	1.45	0.48	0.48	0.50
146	7.17E-28	2.91E-20	2.9E-28	4.34E-28	8.84E-28
147 Biomass growth rate	0.0119	0.0356	0.0119	0.0119	0.0119

APPENDIX H

TABULATED RAW DATA OF THE PLOTS

Table H.1: Effect of initial glutamate flux in the case of maximum biomass growth rate
(Raw data of Figure 4.3-4.8)

Uptake rates (mmol/h)		Production rates (mmol/h)							
Glutamate	Sucrose	Biomass	H ₂	PHB	CO ₂	Acetic acid	Lactic Acid	Formic Acid	
0.065	0.0242	0.0077	0.4420	0.0008	0.2698	0.0004	0.0004	0.0239	
0.075	0.0279	0.0089	0.5105	0.0009	0.3114	0.0005	0.0005	0.0272	
0.1	0.0372	0.0119	0.6783	0.0011	0.4134	0.0005	0.0005	0.0364	
0.15	0.0559	0.0178	0.9994	0.0019	0.6113	0.0010	0.0009	0.0550	
0.2	0.0745	0.0238	1.3415	0.0026	0.8176	0.0013	0.0011	0.0773	
0.25	0.0931	0.0297	1.6941	0.0029	1.0410	0.0012	0.0012	0.1018	
0.3	0.1117	0.0356	1.9301	0.0034	1.2489	0.0013	0.0013	0.1228	
0.4	0.1490	0.0475	2.3925	0.0043	1.6620	0.0014	0.0014	0.1645	
0.5	0.1862	0.0594	2.8334	0.0054	2.0679	0.0017	0.0016	0.2068	
0.6	0.2234	0.0713	3.2547	0.0064	2.4681	0.0021	0.0018	0.2495	
0.65	0.2421	0.0772	3.4586	0.0070	2.6665	0.0022	0.0019	0.2710	

Table H.2: Effect of initial glutamate flux in the case of maximum hydrogen production rate

(Raw data of Figure 4.3-4.8)

Uptake rates (mmol/h)		Production rates (mmol/h)						
Glutamate	Sucrose	Biomass	H ₂	PHB	CO ₂	Acetic acid	Lactic Acid	Formic Acid
0.075	0.0279	0.0089	0.5881	0	0.3625	0	0	0
0.1	0.0372	0.0119	0.7841	0	0.4833	0	0	0
0.15	0.0559	0.0178	1.1762	0	0.7249	0	0	0
0.2	0.0745	0.0238	1.5683	0	0.9666	0	0	0
0.25	0.0931	0.0297	1.9603	0	1.2082	0	0	0
0.3	0.1117	0.0356	2.3524	0	1.4499	0	0	0
0.4	0.1490	0.0475	3.1365	0	1.9331	0	0	0
0.5	0.1862	0.0594	3.9207	0	2.4164	0	0	0
0.6	0.2234	0.0713	4.7048	0	2.8997	0	0	0
0.65	0.2421	0.0772	5.0969	0	3.1413	0	0	0

Table H.3: Effect of initial sucrose flux in the case of maximum biomass growth rate

(Raw data of Figure 4.9-4.13)

Initial Sucrose Concentration (mM)	Sucrose uptake rate (mmol/h)	Production rates (mmol/h)						
		Biomass	H ₂	PHB	CO ₂	Acetic acid	Lactic Acid	Formic Acid
1	0.0372	0.0119	0.6730	0.0012	0.4117	0.0006	0.0006	0.0359
2	0.0372	0.0119	0.6816	0.0011	0.4149	0.0005	0.0005	0.0361
4	0.0372	0.0119	0.6816	0.0011	0.4149	0.0005	0.0005	0.0361
6	0.0372	0.0119	0.6817	0.0011	0.4151	0.0005	0.0005	0.0358
7	0.0372	0.0119	0.6808	0.0011	0.4146	0.0005	0.0005	0.0360
8	0.0372	0.0119	0.6816	0.0011	0.4149	0.0005	0.0005	0.0361
10	0.0372	0.0119	0.6812	0.0011	0.4147	0.0005	0.0005	0.0362
14	0.0372	0.0119	0.6808	0.0011	0.4145	0.0005	0.0005	0.0363
20	0.0372	0.0119	0.6810	0.0011	0.4145	0.0005	0.0005	0.0363

Table H.4: Effect of initial sucrose flux in the case of maximum hydrogen production rate

(Raw data of Figure 4.9-4.13)

Initial Sucrose Concentration (mM)	Sucrose uptake rate (mmol/h)	Production rates (mmol/h)						
		Biomass	H ₂	PHB	CO ₂	Acetic acid	Lactic Acid	Formic Acid
1	0.0372	0.0119	0.7841	0	0.4833	0	0	0
2	0.0372	0.0119	0.7841	0	0.4833	0	0	0
4	0.0372	0.0119	0.7841	0	0.4833	0	0	0
6	0.0372	0.0119	0.7841	0	0.4833	0	0	0
7	0.0372	0.0119	0.7841	0	0.4833	0	0	0
8	0.0372	0.0119	0.7841	0	0.4833	0	0	0
10	0.0372	0.0119	0.7841	0	0.4833	0	0	0
14	0.0372	0.0119	0.7841	0	0.4833	0	0	0
20	0.0372	0.0119	0.7841	0	0.4833	0	0	0

Table H.5: Effect of photon flux in the case of maximum biomass growth rate

(Raw data of Figure 4.14-4.19)

Photon flux (mmol/h)	Sucrose uptake rate (mmol/h)	Production rates (mmol/h)						
		Biomass	H ₂	PHB	CO ₂	Acetic acid	Lactic Acid	Formic Acid
0	0.0372	0.0119	0.1956	0.0089	0.2702	0.0097	0.0075	0.0465
0.5	0.0372	0.0119	0.2879	0.0082	0.2824	0.0089	0.0069	0.0479
1	0.0372	0.0119	0.3795	0.0070	0.3041	0.0073	0.0056	0.0490
3	0.0372	0.0119	0.5615	0.0033	0.3568	0.0030	0.0038	0.0409
5	0.0372	0.0119	0.6783	0.0011	0.4134	0.0005	0.0005	0.0364
7	0.0372	0.0119	0.6939	0.0009	0.4246	0.0003	0.0006	0.0353
10	0.0372	0.0119	0.7025	0.0011	0.4307	0.0007	0.0010	0.0272
20	0.0372	0.0119	0.5317	0.0043	0.3703	0.0049	0.0035	0.0218
30	0.0372	0.0119	0.3782	0.0102	0.2822	0.0127	0.0000	0.0435
50	0.0372	0.0119	0.3726	0.0106	0.2725	0.0134	0.0026	0.0433
100	0.0372	0.0119	0.3933	0.0095	0.2920	0.0118	0.0000	0.0346
150	0.0372	0.0119	0.2765	0.0124	0.2251	0.0163	0.0110	0.0251

Table H.6: Effect of photon flux in the case of maximum hydrogen production rate

(Raw data of Figure 4.14-4.19)

Photon flux (mmol/h)	Sucrose uptake rate (mmol/h)	Production rates (mmol/h)						
		Biomass	H ₂	PHB	CO ₂	Acetic acid	Lactic Acid	Formic Acid
0	0.0372	0.0119	0.7841	0	0.4833	0	0	0
0.5	0.0372	0.0119	0.7841	0	0.4833	0	0	0
1	0.0372	0.0119	0.7841	0	0.4833	0	0	0
3	0.0372	0.0119	0.7841	0	0.4833	0	0	0
5	0.0372	0.0119	0.7841	0	0.4833	0	0	0
7	0.0372	0.0119	0.7841	0	0.4833	0	0	0
10	0.0372	0.0119	0.7841	0	0.4833	0	0	0
20	0.0372	0.0119	0.7841	0	0.4833	0	0	0
30	0.0372	0.0119	0.7841	0	0.4833	0	0	0
50	0.0372	0.0119	0.7841	0	0.4833	0	0	0
100	0.0372	0.0119	0.7841	0	0.4833	0	0	0
150	0.0372	0.0119	0.7841	0	0.4833	0	0	0